# Functional Microparticles and Microcapsules for Advanced Applications

by

**Prashant NeerajKumar Yadav**

AcSIR Registration Number: 10CC16J26003

A thesis submitted to the
Academy of Scientific & Innovative Research
for the award of the degree of
**DOCTOR OF PHILOSOPHY**
in
**Science**

Under the supervision of

**Dr. Kadhiravan Shanmuganathan**
**Dr. Ashootosh V. Ambade**



**CSIR-National Chemical Laboratory, Pune**
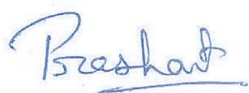


**Academy of Scientific and Innovative Research**
AcSIR Headquarters, CSIR-HRDC campus
Ghaziabad, U.P. – 201 002, India

**January 2023**

# Certificate

This is to certify that the work incorporated in this Ph.D. thesis entitled, "**Functional Microparticles and Microcapsules for Advanced Applications**", submitted by **Prashant NeerajKumar Yadav** to the Academy of Scientific and Innovative Research (AcSIR), in partial fulfilment of the requirements for the award of the Degree of **Doctor of Philosophy in Science**, embodies original research work carried out by the student. We, further certify that this work has not been submitted to any other University or Institution in part or full for the award of any degree or diploma. Research material obtained from other sources and used in this research work has been duly acknowledged in the thesis. Images, illustrations, figures, tables, etc., used in the thesis from other sources, have also been duly cited and acknowledged.

| | | |
|---|---|---|
| Signature of Student | Signature of Co-Supervisor | Signature of Supervisor |
| **Prashant N. Yadav** | **Dr. Ashootosh V. Ambade** | **Dr. Kadhiravan Shanmuganathan** |
| Date: 05th Jan 2023 | Date: 05th Jan 2023 | Date: 05th Jan 2023 |
| Place: Pune | Place: Pune | Place: Pune |
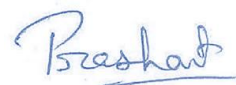
# Statement of Academic Integrity

I, **Prashant NeerajKumar Yadav**, a Ph.D. student of the Academy of Scientific and Innovative Research (AcSIR) with Registration No. **10CC16J26003** hereby undertake that, the thesis entitled "Functional Microparticles and Microcapsules for Advanced Applications" has been prepared by me and that the document reports original work carried out by me and is free of any plagiarism in compliance with the  UGC Regulations on "*Promotion of Academic Integrity and Prevention of Plagiarism in Higher Educational Institutions (2018)*" and the CSIR Guidelines for "*Ethics in Research and in Governance (2020)*".

Signature of the Student

Date: 05th Jan 2023

Place: Pune

---

It is hereby certified that the work done by the student, under my/our supervision, is plagiarism free in accordance with the UGC Regulations on "*Promotion of Academic Integrity and Prevention of Plagiarism in Higher Educational Institutions (2018)*" and the CSIR Guidelines for "*Ethics in Research and in Governance (2020)*".

Signature of the Co-supervisor

Name: Dr. Ashootosh V. Ambade

Date:  05th Jan 2023

Place:  Pune

Signature of the Supervisor

Name: Dr. Kadhiravan Shanmuganathan

Date:  05th Jan 2023

Place:  Pune

*Dedicated to*

> *My parents*
>
> *Teachers*
>
> *Soldiers*
>
> *Research Scholars*

# Acknowledgement

# Table of Contents

# Abbreviation

- HME: Hot-melt extrusion

- BCP: Block copolymer

- SEC: Scanning Electron Microscopy

- DSC: Differential Scanning Calorimetry

- TGA: Thermogravimetric Analysis

- UV: Ultraviolet

- SEC: Size Exclusion Chromatography

- SIONPs: Superparamagnetic iron oxide nanoparticles

- PLGA: Poly(lactic-co-glycolic acid)

- PLA: Poly(lactic acid)

- PAA: Poly(acrylic acid)

- EO: Essential oils

- μ-CT: x-ray micro-computed tomography

- BET: Brunauer-Emmett-Teller

- MIC: Microcapsules

- MIS: Microspheres

- HPLC: High performance liquid chromatography

- PDA: Polydopamine

- $Fe_3O_4$ NPs: iron oxide nanoparticles

- PBA: 1-pyrenebutyric acid

- PUU: Polyurea-urethane

- PCL: Poly(caprolactone)

- PGA: Poly(glycolic acid)

- TBAH: Tetrabutylammonium hydroxide

- XPS: X-ray photoelectron spectroscopy

- VSM: Vibrating sample magnetometer

- FTIR: Fourier transform infra-red spectroscopy

- NMR: Nuclear magnetic resonance

- DMP: Dimethyl phthalate

- EG: Ethylene glycol

- PCPO: Polycarbonate polyol

- DGE: Diglycidyl ether

- DMAc: Dimethylacetamide

- NMMO: N-Methylmorpholine N-oxide

- DMSO: Dimethyl sulfoxide

- Cuoxam: Cuprammonium hydroxide

- TBPH: Tetrabutylphosphonium hydroxide

- QDs: Quantum dots

- CNF: Cellulose nanofibers

- MCC: Microcrystalline cellulose

- DMAP: 4-dimethylaminopyridine

- DCC: N, N'-Dicyclohexylcarbodiimide

- DMF: Dimethylformamide

- MB: Micro beads

- FMB: Fluorescence magnetic cellulose microbeads

- RT: Room temperature

- RPM: Rotation per minute

- CP/MAS: Cross polarization/magic angle spinning

- UV-VIS: Ultraviolet-visible

- NPs: Nanoparticles

- EDX: Energy dispersive X-ray spectroscopy

- A. U.: Arbitrary unit

- OPV: Oligo(p-phenylenevinylene)

- L-B-L: Layer-by-layer

- U-F: Urea-formaldehyde

- M-F: Melamine-formaldehyde

- PS: Polystyrene

- W/O: Water-in-oil

- O/W: Oil-in-water

- O/O: Oil-in-oil

- MDI: Methylene diphenyl diisocyanate

- TDI: Tolylene-2,4-diisocyanate

- IPDI: Isophorone diisocyanate

- HMDI: Hexamethylene diisocyanate

- DEG: Diethylene glycol

- PG: Propylene glycol

- BDO: Butane-1,4-diol

- PEG: Polyethylene glycol

- HDO: Hexane-1,6-diol

- BDM: Benzene-1,4-dimethanol

- DABCO: 1,4-diazabicyclo[2.2.2]octane

- PVA: Polyvinyl alcohol

- PVP: Polyvinylpyrrolidone

- FE-SEM: Field emission scanning electron microscopy

- $T_g$: Glass transition temperature

- Ppm: Parts per million

- PBS: Polybutylene succinate

- DEET: N, N-Diethyl-m-toluamide

- DBTDL: Dibutyltin dilaurate

- PDI: Polydispersity index

- ATR: Attenuated total reflectance

- PHA: Poly(hydroxy alkanoates)

- DCM: Dichloromethane

- HMDA: Hexamethylenediamine

- EDA: Ethylene diamine

- PEI: Polyethyleneimine

- PLQY: Photoluminescence quantum yield

# List of Figures

# List of Schemes

# List of Tables

# Chapter 1

# Introduction

### 1.1. Microparticles

Generally, microparticles can be classified according to their size, i.e., in the range of 1 to 1,000 microns.[1] The size-based definition is usually unclear because microspheres are also widely used to define particles with a diameter greater than 1,000 µm. Microparticles are commercially accessible in a wide range of materials, including ceramics, glass, polymers, and metals. Research, development, and sales of microparticles in a variety of applications are increasing at a rapid pace throughout the world and have piqued the interest of researchers owing to their large specific surface areas, high mobility, and facile recovery from dispersion.[2] Polymeric microparticles are typically either spherical, rod-shaped, or irregular-shaped particles formed by one or more polymer matrices.[3] The design and production of polymeric microparticles with customized morphologies (such as shape, size, size distributions, and porosity) and distinctive characteristics owing to the properties of components could bestow the particles with specific functionalities that are useful for a wide variety of advanced applications. Therefore, making unique structures out of functionalized components is a crucial method for generating cutting-edge functional polymeric microparticles. Use of polymeric microparticles involves both advantages and disadvantages. Among several advantages, tunable chemical and physical properties, use of non-toxic as well as biodegradable materials when desired, existence of stimuli-responsive properties, and easy functionalization when compared to other microparticles whereas disadvantages include the difficulty to scale-up, irreproducibility in case of natural polymers owing to varying molecular weights, insufficient toxicological assessment.

### 1.1.1. Methods of preparation of microparticles

Various methods and polymer matrices have been used to fabricate microparticles of various shapes and sizes. There are roughly two distinct microsphere synthesis processes. The spheres

may be created either from a pre-existing polymer or during the polymerization process using a monomer solution.[4] Generally, methods including spraying, dripping, emulsion, sacrificial template method, copolymer self-assembly, and extrusion can be employed to prepare microparticles.

*1.1.1.1.    Spraying*:  In this process, micron-sized droplets of a polymer solution or suspension are sprayed at a high velocity or under high air pressure. Spraying can be employed to prepare microparticles by two methods: i) spray drying, in which a solution or suspension is atomized and sprayed as a mist of fine droplets into a hot chamber. The carrier solvent vaporizes and solid microparticles are produced.[5] ii) In an alternate method, a polymer melt is sprayed in a cold chamber, where it hardens into free-flowing microparticles. The process is termed "spray   cooling".[6]   These   methods   are   continuous   and   effective   for preparing microparticles in large quantities.

*1.1.1.2.    Dripping*: When polymer solutions are ejected through a thin opening, depending on the velocity, either a constant stream or droplets are formed. The droplet size is larger compared to the spraying method. The size of these droplets is reduced by a few methods, such as electro-spraying, co-axial air flow, jet cutting, vibrating nozzle, rotating nozzle, and spinning disk atomization. With electrospraying, particles are formed from a polymer solution using a voltage-driven process guided by electrohydrodynamic processes.[7] Particles created by this method typically have a diameter ranging between 10 nm to 1 µm. This technique requires a syringe with a blunt needle, a source of high-voltage power, and a collector. The coaxial flow method works on the simple principle of blowing droplets from a needle tip before they fall to the ground due to gravity.[8] Using this method, one can get microparticles in the size range of 300-600 µm. The jet-cutting method involves forcing fluid via a nozzle in the form of a jet towards a spinning disc lined with fine wires. This disc splits liquid jets into cylinders that become spherical beads due to surface tension.[9] The nozzle diameter, number and diameter of

wires, rotation speed, and jet pressure can all influence the size of the beads. The vibrating nozzle process is based on the idea that a laminar jet can be broken up by giving it a certain amount of vibration.[10] Laminar jets split into short lengths due to vibration, followed by the formation of spherical droplets due to surface tension. In the rotating nozzle technique, polymer solutions can be ejected through a rotating nozzle to produce a large number of droplets in a short amount of time. Effective control of particle sizes is possible by varying the size of its outlet and rotating speed. In the spinning disk atomization method, a polymer solution is continuously spread onto a rotating disc, and as the disc rotates, centrifugal forces cause droplets to be ejected from the edge, forming tiny droplets. The created microdroplets are either physically dried or solidified via physico-chemical processes like coacervation[11] (polycation-polyanion interactions), gelation (crosslinking),[12] and co-extrusion.[13]

*1.1.1.3.* *Emulsion*: The preparation of an emulsion involves vigorously stirring the mixture of the two immiscible liquids or homogenizing it. Typically, the resulting emulsions are unstable and phase separate when left to rest, necessitating the use of a stabilizer. Emulsions consist of two phases: the dispersed phase and the continuous phase. The size of the droplet in the dispersed phase governs the size of the microparticle to be formed. The size of the emulsion droplet can be tuned by using various techniques and varying their parameters. Various methods are employed to prepare emulsions, such as turbine reactors, static mixtures, microfluidics, membrane extrusion, and stable micro-emulsion using a surfactant. Turbine reactors consist of pedals that move vigorously to agitate the mixture to prepare an emulsion, whereas a static mixer is a well-designed tool for continuously mixing liquids without any working components.[14] Microfluidics is an effective method for producing versatile droplets with narrow size distribution that can be utilized as templates for creating microparticles with tailored physical and chemical properties.[15] A membrane is used in the process of membrane emulsification to generate emulsion droplets with narrow size distribution.[16] Droplets form at

the membrane surface when the to-be dispersed phase is pushed through the pores and forms an emulsion. Also, using a surfactant may help to lower the interfacial tension and generate stable micro-emulsions. Emulsions formed using the above techniques are allowed to form microparticles by various methods, such as solvent evaporation, where the prepared polymer emulsion is heated to evaporate the carrier solvent. In a physico-chemical method, the dispersed phase solidifies due to phase separation upon a change in pH or the addition of salt.[17] Alternatively, microparticles can be formed by allowing the two monomers in different phases to react chemically at the interface of the micro-emulsion droplet, resulting in the formation of the solid polymeric wall at the interface.[18]

*1.1.1.4.* *Sacrificial template method*: Microparticles can take the form of the template by forming a polymeric shell around the surface of the sacrificial template using a variety of physical or physico-chemical methods. Finally, microparticles adapt the shape of the template, which is then removed, resulting in a hollow structure. Simply by manipulating the shapes of the templates, we can produce hollow structures of the desired form.[19] Simple steps make this technique superior to others for preparing hollow microparticles. Layer-by-layer deposition, solvent evaporation, microfluidics, etc., are a few methods used to prepare microparticles with this technique.

*1.1.1.5.* *Extrusion*: The extrusion technique is used to create highly dense microparticles. Hot-melt extrusion is a method of extruding polymer using a specific engineered device. The synthesis of solid polymer microparticles from a polymer involves passing it through a heated chamber with rotating screws, then cooling it or using a gelation bath in which the droplets fall and solidify.[20] Microparticles formed using this technique are bigger and denser than particles formed by other techniques. These pellets are further transformed into more spherical particles using the spheronisation method.[21] Hot-melt extrusion (HME) is a viable alternative that is gaining popularity since it does not require a

solvent, unlike emulsification and spray drying, and no pores or fractures are formed during the preparation due to solvent migration.

*1.1.1.6.* *Copolymer self-assembly*: One of the most adaptable theories in materials science for the bottom-up development of functional microparticles is block copolymer (BCP) self-assembly.[22] Block copolymers (BCPs) are composed of at least two polymer chains that are covalently bonded yet have distinct chemical compositions and inherit such opposing interactions. A covalent bond inhibits macrophase separation, while favorable interactions between blocks of the same chemistry led to the spontaneous formation of microstructures.[23] Both solid and porous microparticles can be formed using this method.
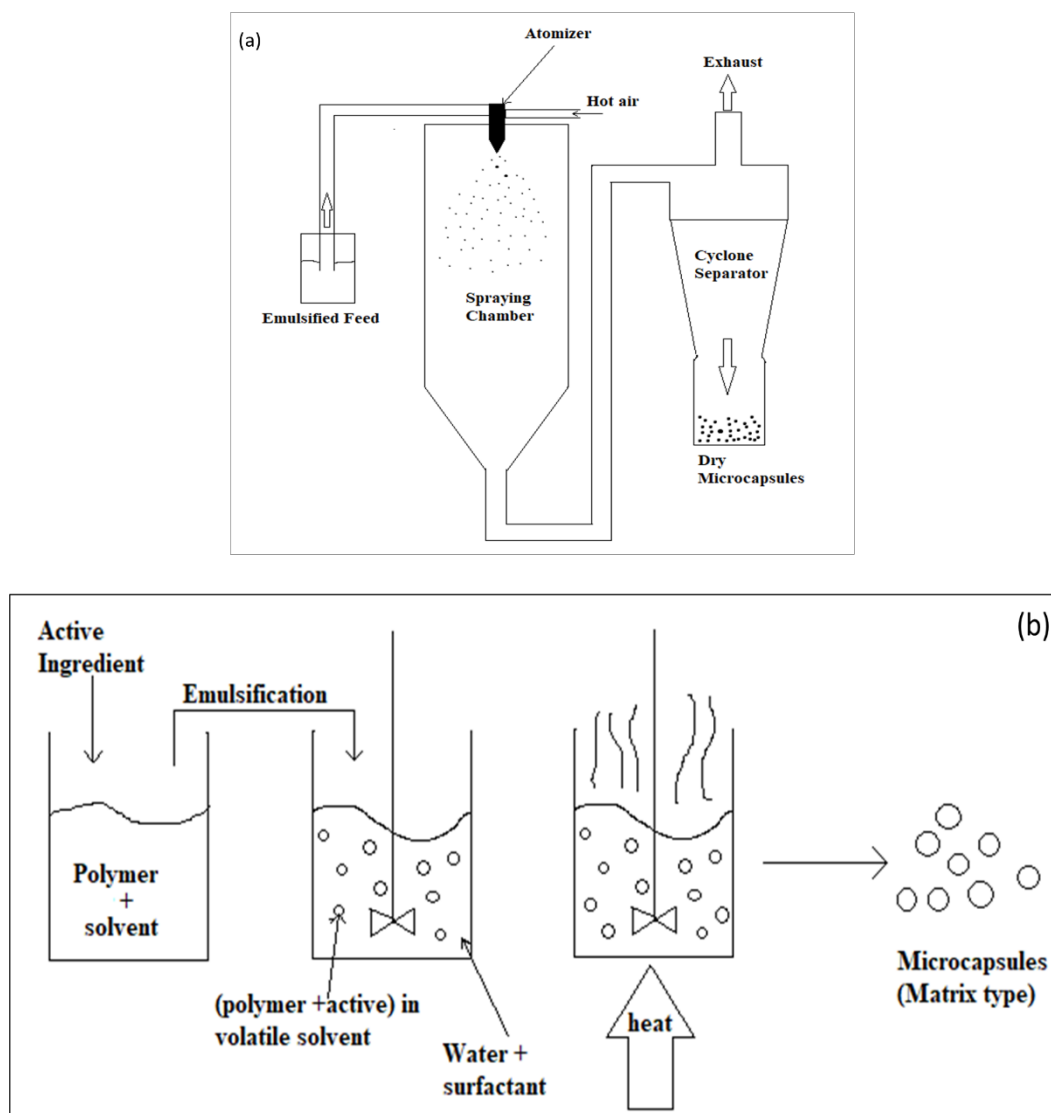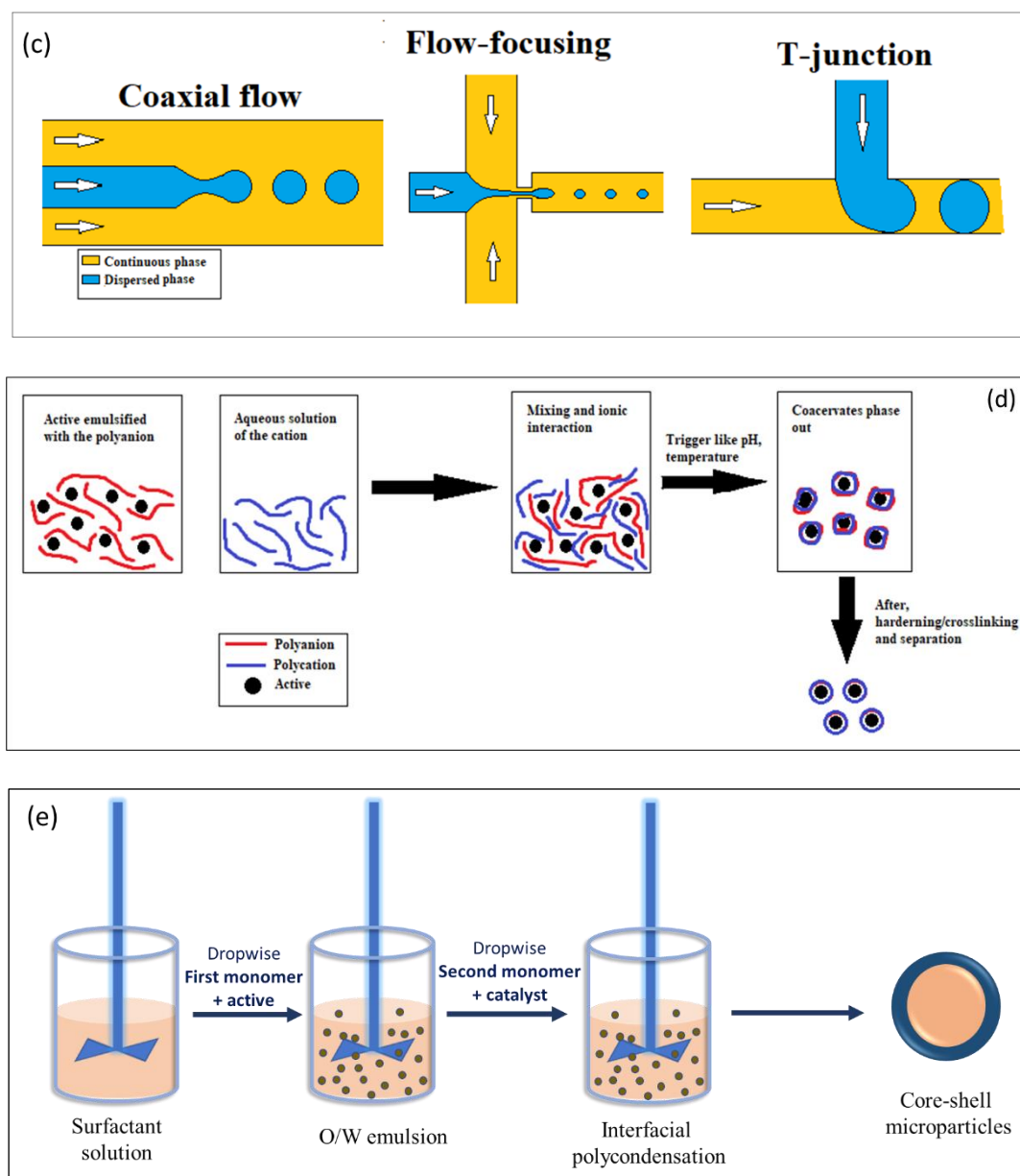
**Figure 1.1**. Illustration of common techniques used to prepare microparticles (a) spray drying, (b) solvent evaporation, (c) micro-fluidics, (d) coacervation (Reproduced with permission from reference 15, copyright Springer) and (e) interfacial polycondensation.

Uniformity in size and shape is critical to ensuring that each individual microparticle has a uniform and controllable performance because most of its physical and chemical properties are size and shape dependent.[24] However, each technique has drawbacks, such as restricted control over particle size and structure. Nonetheless, emulsification, microfluidics, and membrane filtration are a few methods that enable good control over the shape, size, and composition of the prepared microparticles.

### 1.2. Matrix material

Microparticles can be prepared using a variety of polymer or blend of polymers. These polymer matrices enable microparticles to be classified based on the origin i.e., synthetic or biobased, biodegradable or non-biodegradable, biocompatible or toxic, linear or branched or cross-linked. Polymer matrices that have been employed to prepare microparticles are polyurea,[25] polyurethanes,[26] polysaccharides,[27] polyesters,[28], copolymers,[29] polyolefins,[30] etc. Each polymer has different characteristics depending on the nature of the polymer. Based on the application, a desired polymer matrix or matrices can be chosen to attain desirable properties.

### 1.3. Evaluation of microparticles

The as prepared microparticles can be characterized using various analytical and physical methods to determine the particle size, its morphology, its thermal and chemical stability. Generally, particle size and size distribution can be determined using the particle size analyzer, optical microscope, and scanning electron microscope (SEM), whereas the morphology of the microparticles can be determined using SEM and optical microscopy. Thermal analysis can be done using differential scanning calorimetry (DSC) and thermogravimetric analysis (TGA). In addition, its chemical stability can be assessed by exposing the microparticles to solvent or UV radiation and determining if they are physically stable under specific conditions.

## 1.4. Application

Polymer microparticles with varying functionality, size, and shape can be used in myriads of applications such as biosensors, chromatography, water treatment, solid-phase synthesis support, protein/enzyme immobilization, microcapsules (controlled release), cell labeling and separation, magnetic resonance imaging, cosmetics, etc. Recent trends have shown an increase in the use of sustainable or biodegradable polymers to prepare microparticles with improved functionalities to replace conventional petroleum-based or formaldehyde-based microparticles.

### 1.4.1. Biosensor

The term "biosensor" refers to any device that utilizes a biological sensing element and measures signals resulting from biological interactions to determine the concentration of a target analyte.[31] Polymeric microparticles can serve as a template, whereas biological sensing elements like antibodies or enzymes grafted to the surface may sense the target analyte. Biosensors are used for disease screening, drug discovery, and detecting contaminants, microorganisms, and disease markers in physiological fluids such as blood, urine, saliva, and sweat.[32] There are several reports where enzyme-immobilized poly(vinyl imidazole)[33] and silica microparticles, ionic liquid polymeric microparticles,[34,35] phenylboronic acid grafted poly(acrylamide) microparticles, antibodies-grafted porous silicon microparticles[36] were used as a biosensor. Additionally, magnetic micro/nanoparticles can also be employed to make their separation easier.

### 1.4.2. Chromatography

Chromatography is described as the separation of the components of a mixture by gradual passing over or through a medium that absorbs the components differently. Microparticles with different functionality can serve the purpose by differently interacting with the components of the mixture. In size exclusion chromatography (SEC), it is undesirable for the stationary phase to interact specifically with the macromolecules. Hydrodynamic radii differences, which govern how long it takes a molecule to travel through the microparticles' pores, form the basis for selective separation. Silica microparticles have been extensively used in common organic labs to separate a mixture of compounds. Porous polystyrene microparticles are typically used in the SEC for macromolecule separation.[37] Porous cellulose microparticles have been used in SEC and gel filtering (desalting).[38] Commercially, JNC Corporation sells Cellufine™, 40–130

μm cellulose spherical beads used for purifying proteins, enzymes, and other macromolecules.[39,40]

### 1.4.3. *Water treatment*

The primary goal of wastewater treatment is to remove as many pollutants as possible before returning the leftover water, known as effluent, to the environment. Solid suspended contaminants are removed via filtration, whereas dissolved contaminants such as dyes and other chemicals from industry required special treatment. The soluble contaminants in the water are either catalytically degraded or absorbed by microparticles *via* physical and chemical interactions with specified functional groups and porosity. Industrial applications require adsorbents with a high adsorption capacity, thermal stability, and recyclability. Depending on their adsorption-desorption capacity, microparticles can be reused repeatedly. The presence of iron oxide in microparticles aids in separation from the water with the help of a magnet. Some synthetic polymers, such as vinylic polymers[41] and polydopamine (PDA)[42] and natural polymers, such as cellulose,[43] alginate,[44] and chitosan,[45] have been used to prepare microparticles for water treatment.

### 1.4.4. *Solid-phase synthesis support*

In chemistry, the term "solid-phase synthesis" refers to a technique in which molecules are covalently linked to a solid support material and then synthesized in a single reaction vessel using selective protecting group chemistry. In contrast to conventional liquid-state synthesis, the advantages include greater efficiency and throughput.[46] For example, in a report, nanostructured porous silicon microparticles were used as degradable support for the solid-phase synthesis of oligonucleotides.[47] Recently, chitosan microparticles were used as solid-phase support for the peptide synthesis for targeting tumor cells.[48] Partly crosslinked polystyrene microparticles have been used widely for reagent coupling, though their use is

limited owing to their insufficient swelling.[49] Functionalized cellulose microparticles were employed as biodegradable and biocompatible solid-phase support to generate polypeptides[50] and libraries of pyrazole and isoxazole derivatives.[51]

### 1.4.5. *Magnetic resonance imaging*

Superparamagnetic iron oxide nanoparticles (SIONPs) are extensively studied as contrast agents for magnetic resonance imaging due to their unique properties, which include high magnetization values, diameters ranging from 4 to 30 nm, and a narrow distribution of particle size. SIONPs cannot be used as it is due to their tendency to oxidize quickly. To boost the stability of magnetic iron oxide contrast agents in physiological conditions, appropriate surface coating procedures were devised. In addition, compared to SIONPs, the polymer-coated SIONPs have better biocompatibility.[52] Polymers such as alginate,[53] chitosan,[54] poly(lactic-co-glycolic acid) (PLGA),[55, 56] poly(lactic acid) (PLA),[57] poly (acrylic acid) (PAA)[58] can be used to coat SIONPs. Alternatively, gadolinium-containing poly(gadolinium methacrylate-co-methacrylic acid) copolymer microparticles were synthesized for use as an MRI contrast agent.[59]

### 1.4.6. *Cosmetics*

Essential oils (EO) play a major role in the cosmetic industry. They can be encapsulated in microcapsules to improve their stability and control their release. Synthetic and biopolymer-based microcapsules are employed in the microencapsulation of these EOs and in the majority of peeling solutions (exfoliators). Commercially available polyethylene microspheres from Cospheric have been used extensively in the cosmetics, personal care, and skin care industries. Increasing environmental concerns and government regulations are mandating industries to find benign alternatives for synthetic non-biodegradable polymer microparticles. Hence microparticles based on biopolymers such as cellulose and its derivatives,[60] alginate,[61] pectin,[62]

PLGA,[63] lignin,[64] PLA,[65] etc., which are biocompatible and non-toxic to the skin, have attracted tremendous interest.

### 1.4.7. Enzymes and Protein Immobilization

Enzyme immobilization on a solid support is often a prerequisite for their use on a commercial scale since it simplifies purification procedures and enables the re-use of the rather costly biocatalyst. Polymers that are biocompatible, sustainable, and easily functionalized can be used for enzyme and protein immobilization. Different reactive groups in functional cellulose beads have been thoroughly examined for the immobilization of numerous enzymes. Several of them are of rather industrial interest, like amylase (glucose production from starch), galactosidase (lactose-free dairy product production), and invertase (saccharose hydrolysis). With increased enzyme activity and reusability, alginate has been widely employed for immobilization in the form of xanthan-alginate beads, alginate-polyacrylamide gels, and calcium alginate beads. The stability of enzymes is increased by cross-linking alginate. Similarly, other natural polymers such as chitosan,[66] collagen,[67] carrageenan,[68] gelatin,[69] cellulose,[70] starch,[71] pectin and synthetic polymers such as Amberlite[72] and diethylaminoethyl cellulose,[73] polyurethane,[74] polyvinyl alcohol,[75] nylon-6,[76] polyvinyl chloride have been used to immobilize enzymes and have been used in various applications.

## 1.5. Classification of microparticles

In terms of their shape and construction, microparticles can be classified into three categories based on their morphology, i.e., 1) solid microparticles or microspheres, 2) hollow/porous microparticles, and 3) microcapsules. The microparticle's shape can be tuned in various ways to achieve either of these results.
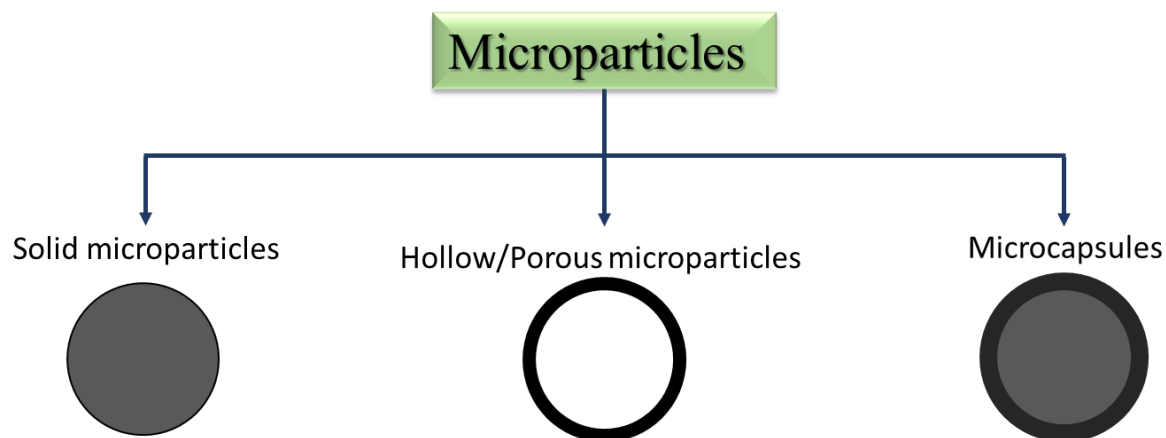
**Figure 1.2.** Classification of microparticles.

### 1.6. Solid microparticles (functional microparticles)

Solid microparticles are typically robust, non-porous particles made entirely of a polymer matrix or a polymer blend. They are denser compared to hollow or porous microparticles. Solid microparticles can be functionalized by covalent or physical coupling during or after synthesis utilizing various organic or inorganic dopants and are referred to as "functional microparticles".[77] The functionality of solid microparticles is determined by the matrix, the dopant, or both. The size, shape, and morphology of the solid microparticles govern the activity. The high sphericity of solid microparticles, as well as available functionalities such as colored fillers, fluorescence, and magnetic, are desirable for flow visualization or fluid flow analysis, microscopic techniques, and biological imaging. Based on the desired application and functionality, particular polymer and preparation techniques can be chosen. Monodisperse solid microparticles are particularly desirable for maximizing the efficiency and reproducibility of desired properties.[78] Various methods described earlier can be used to prepare solid microparticles with the required surface morphology, size, and size distribution. Microparticles can be evaluated to characterize their size, shape, and morphology using various techniques. The size and morphology of the microparticles can be elucidated using an optical microscope

or a scanning electron microscope (SEM). Size and size distribution can also be determined using a particle size analyzer.

Microparticles with charges are suitable to avoid agglomeration due to ionic charge repulsion. Microparticles with surface functionality that allows them to functionalize later with catalysts and enzymes are useful in heterogeneous catalysis as they provide a very high specific surface area. Solid microparticles can be used in applications such as chromatography, sensors, catalysis, solid-phase synthesis support, water treatment, protein and enzyme immobilization, adsorbents, etc. Furthermore, multi-stimuli responsive microparticles have an advantage over monofunctional microparticles, making them very desirable in a wide range of applications such as security, drug delivery, sensing, water purification, cytometry, and so on. In addition, microparticles immobilized with a catalyst or enzyme and magnetic nanoparticles can be utilized to catalyze the process, making separation simple and reusable.

## 1.7. Hollow or porous microparticles

Porous microparticles contain external pores as well as internal pores, which are usually interconnected. Fabrication of porous microparticles can produce permeable frameworks with a large surface area for load and release and for tissue engineering. The porous structure, large specific surface area, and low density are the defining features of such porous material. In comparison to conventional microparticles, porous microspheres have an exceptionally high capacity for absorption. Compared to the solid microparticles, they may possess improved properties owing to the enhanced surface area due to the porous structure. Pore size and other parameters are important to control for specific applications. The development of hollow or liquid cores in microparticles can result in compartmentalized structures with substantial interior volumes that are more advantageous for active encapsulation and confined micro-reactions. Various organic and inorganic polymer materials can be employed to prepare porous

microparticles, but the most commonly employed polymers are PLA, PCL, PLGA,[79] poly(methacrylic monomer-divinylbenzene),[80] chitosan, cellulose and its derivatives,[81] and other polymers or copolymers. There are a few organic and inorganic substances that can be used to create porous polymer structures, including calcium carbonate ($CaCO_3$), hydroxyapatite, and mesoporous silica. To make porous microspheres, porogens are typically added as inert agents to the polymer during preparation.[82] The formation of a porous structure results from the elimination of these organic/inorganic particles.

Methods such as the sacrificial template method, spray drying,[83] solvent evaporation,[84] polymer or co-polymer self-assembly,[85] double emulsion-solvent evaporation method, suspension polymerization,[86] phase-separated polymer precipitation[87] and microfluidics[88] can be used to prepare porous or hollow microparticles. Spray drying and sacrificial template methods are the most widely employed methods to prepare porous microparticles. The polydispersity in particle size can be considerably reduced using microfluidic methods. These methods are typically limited to specific materials and offer only modest control over particle size and pore size. More importantly, it is still challenging to use these approaches to controllably produce microparticles with intricate interior structures.

Prepared porous microparticles can be characterized to determine their size, morphology, and surface area before being used for any application because each of these parameters is highly crucial in the desired application. For example, in the case of tissue regeneration scaffolds, a highly interconnected porous structure is desired to achieve excellent cell seeding and facilitate the transport of nutrients and oxygen for cell proliferation. Optical microscopy, SEM, and particle size analyzers can all be used to determine the size. To further understand the morphology of the microparticles, SEM and x-ray micro-computed tomography (μ-CT) could be employed. Using these methods, particle size, pore size, and morphology can all be determined concurrently. Additionally, nitrogen adsorption-desorption studies and the

application of the Brunauer-Emmett-Teller (BET) absorption model can be used to quantify surface area and porosity. Hollow or porous microspheres are frequently employed in applications like high-speed protein chromatography,[89] protein/enzyme immobilization,[90] tissue regeneration scaffolds,[91] catalysis,[92] water treatment, etc. Porous microparticles have recently been used to create anodes for high-performance lithium-ion batteries.[93]

## 1.8. Microcapsules

The concept of microencapsulation is derived from cells, which contain biochemistry and provide immobilization and structure. Cell membranes offer protection and facilitate large-scale cellular inflow and outflow. In 1930, the development of gelatin microcapsules using the coacervation method marked the beginning of microencapsulation. The term "microcapsules" (MICs) refers to particles or droplets that are membrane-enclosed and scattered in a solid matrix. Microencapsulation is a technique in which relatively small particles or droplets of the active component(s) are enclosed in a coating or incorporated into a homogeneous or heterogeneous matrix, usually made of natural or synthetic polymeric materials, to produce small capsules with a variety of useful properties. MICs can be spherical or non-spherical (irregular) in shape, with sizes ranging from 10 microns to 1000 microns.

### *1.8.1.* Classification of Microcapsules

Microcapsules can be classified as core-shell, coated particles, multicore capsules, multiwall microcapsules, and matrix.[94]

*1.8.1.1.Core-Shell*: Core-shell microcapsules are a class of microcapsules that are created by two or more material layers. One of these serves as the structure's central core, while the others form the shell.[95] This kind of design gives the chance to fine-tune the composite material, which exhibits characteristics and properties that the core and shell's individual components cannot match. Depending on the design parameters and the intended use, the core might be

liquid, solid, or gaseous, and the shell could be built from organic or inorganic materials. Given their distinctive properties, core-shell beads are used in diverse areas, including food and cosmetics, biomedical research, medicine, and even materials science. Interfacial polymerization, spray coating, pan coating, layer-by-layer deposition are a few methods that form core-shell geometry MICs.[96] A coating serves as the wall, shell, or membrane around the core, which may be released via physical pressure, diffusion, wall dissolution, or degradation, depending on the features of the capsule wall.

*1.8.1.2.* *Irregular shaped microcapsules*: Irregular-shaped MICs are a class of MICs that are non-spherical in shape. They are generally formed by coating the active ingredient with a polymer to form a protective membrane that assumes the shape of the active ingredient which may not be spherical in shape. The protective coating serves the purpose of controlled release, but due to their irregular shape, it may be limited to certain applications only. For example, PLGA microcapsules were prepared using the emulsion-solvent evaporation technique to obtain elongated MICs with an aspect ratio of 50.[97] These irregularly shaped MICs were found to improve the self-healing properties of soy-protein-based resins compared to spherical MICs.

*1.8.1.3.* *Multi-core microcapsules:* A multi-core microcapsule is a type of microcapsule that contains more than one core.[98] The MICs' cores can be either liquid, solid, or both, miscible and non-miscible. Depending on whether the core is separated, mononuclear and polynuclear microcapsules can be identified.

*1.8.1.4.* *Multiwall microcapsules:* Multiwall microcapsules are a type of microcapsule in which a single nucleus is encased in many shells (in the form of shell layering). Methods such as layer-by-layer deposition, coacervation, double encapsulation, etc. are employed to prepare multiwall microcapsules.[99] Since the core travels through two walls instead of just one, the release of its contents may be made to last for much longer in multiwall MICs than in single-wall MICs.

*1.8.1.5.* *Matrix microcapsules:* Matrix microcapsules have the active ingredient distributed homogenously throughout the polymer matrix instead of forming a core. MICs formed using the spray drying technique are matrix-type MICs.[100]
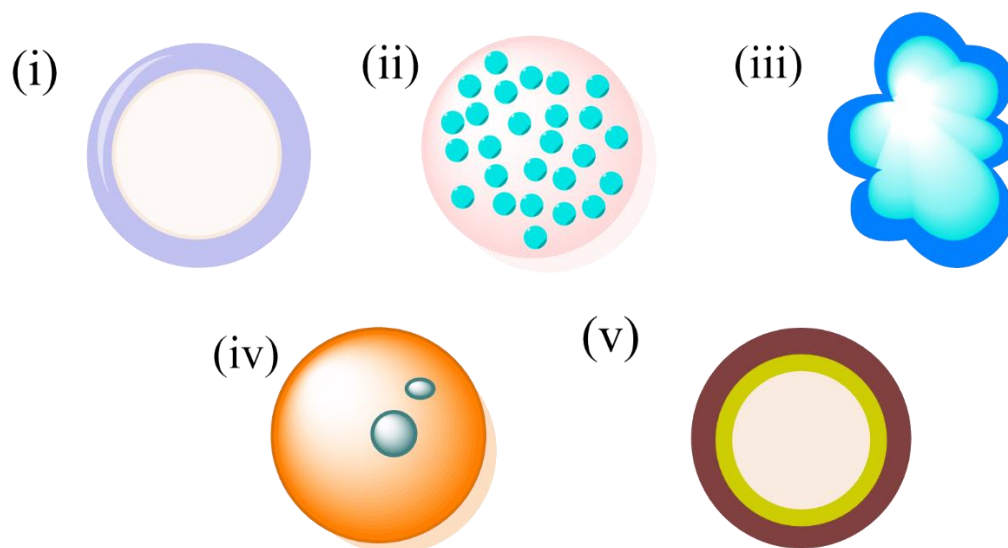
**Figure 1.3.** Different types of microcapsules: (i) core-shell microcapsule, (ii) matrix (microsphere), (iii) irregular microcapsule, (iv) multicore microcapsule, and (v) multiwall microcapsule.

Microcapsules can be either homogeneous (with a dissolved core) or heterogeneous (with a suspended core) in composition. Since most of their physical/chemical properties are size- and shape-dependent, uniformity in size and shape is vital for ensuring that each individual microcapsule has a uniform and controllable performance. Microcapsules, for instance, need to have consistent sizing and shape if they are to accomplish quantitative encapsulation and consistent release kinetics for sustained release.

Microencapsulation permits the transformation of liquids or sticky solids into solid, free-flowing powder and provides environmental protection against oxygen, moisture, etc.[101] Microencapsulation could also be utilized to isolate reactive substances from mixtures. The unpleasant flavour or odour of an active or chemical also can be concealed using microencapsulation.[102] Using various microencapsulation techniques, controlled release, or

delayed release of the active can be easily performed.[103] The active can be released at a targeted area by functionalizing the MIC's surface with specific receptors, especially in the case of drug delivery (pharmaceuticals). Microencapsulation may also be used to alter the properties of the active ingredient, such as altering the crystalline phase or changing the active from a crystalline into an amorphous state.[104] Most of these characteristics can be achieved using a variety of techniques, but microencapsulation stands out because of the small size of the covered microparticles and their subsequent use and adoption in a wide range of dosage samples and pharmaceutical formulations, which may not have been technically feasible previously.

The success of this technology is attributed to the proper selection of wall material, core release form, and encapsulation technique. The encapsulation of essential oils, colorants, flavors, sweeteners, and microbes, among others, is a common application of microencapsulation in industries such as the pharmaceutical, agricultural, medical, and food industries. The suitable technique is determined by the nature of the core, the use of the microcapsules, the required particle size, the physicochemical characteristics of the core and the wall, the required release mechanism, the cost, and scalability. Pharmaceuticals can now be delivered and improved using a variety of microencapsulation techniques. These methods have led to the widespread use of many coated particles in products. The exact quantity of particles needed to create a single dose can vary functionally in ultimate particle product size and be maintained in either the micrometer or nanometer range for micro and nanoparticulate drug delivery systems, respectively. The many microencapsulation techniques that have been explored are listed in **Table 1.1**. They can be divided into two primary groups: chemical processes and physical processes. The development of drug delivery systems using microencapsulation technology has significantly advanced pharmaceutics research, increasing therapeutic efficacy. As already stated, microencapsulation reduces dosage needs while boosting active stability.

### *1.8.2.* **Microencapsulation techniques**

Techniques commonly used to prepare microparticles have been discussed earlier, such as spraying, dripping, emulsion, the sacrificial template method, copolymer self-assembly, and extrusion. There are certain other methods that are used to prepare MICs, such as coating (spray coating, pan coating, and air suspension coating).

**Table 1.1**. Microencapsulation techniques.[105]

| Chemical Process | Physical Process | Physio-chemical process |
|---|---|---|
| Interfacial Polymerization | Spray drying | Polymer incompatibility |
| Polycondensation | Air-suspension coating | Ionotropic incompatibility |
| Polyelectrolyte complexation | Vibration nozzle | Sol-gel encapsulation |
| Solvent evaporation & extraction | Pan coating | Supercritical $CO_2$-assisted encapsulation |
| Phase separation (Coacervation) | Centrifugal extrusion | |
| Cryogenic solvent extraction | | |
| Interfacial poly. | | |
| Suspension/emulsion polymerization | | |
| Complex coacervation | | |
| Matrix polymerization | | |

### *1.8.3.* **Wall material**

Coatings can be chosen for their ability to facilitate segmental mobility, provide flexibility, reduce brittleness, and enhance coating film resistance. Selecting a suitable wall material is crucial, as it affects the microcapsule's encapsulation efficiency and stability. The ideal wall

material would be nonreactive with the core, capable of sealing and maintaining the core inside the capsule, capable of providing optimum protection to the core against adverse conditions, tasteless in the case of food application, and commercially viable. One polymer can seldom meet all the required properties; hence, a blend of two polymers is often used to meet the required properties. Polymers can be classified into various categories, such as biodegradable/non-biodegradable, or natural or synthetic polymers. The most commonly used natural polymers are polysaccharides such as cellulose, dextran, alginate, starch, chitosan, and pectin, whereas the most common synthetic polymers are polystyrene, polyesters, polyamides, polymethylacrylate, polyurethanes, and resins.

### *1.8.4.* Active ingredients

Active ingredients can be either solid, liquid, or both. Based on the nature of the actives, specific wall materials and techniques for higher encapsulation efficiency and sustained release can be chosen. Both the active and wall materials are chosen carefully to prevent any undesired chemical reactions. The core should have a consistent and regular shape. The polymer type, shape, and size of the core material must all be taken into consideration to achieve a homogeneous coating on spherical particles. Drugs with potentially dangerous side effects and high absorption rates can be administered in the desired amount and time with the help of microencapsulation. Long-term, precise dosing of pesticides and insecticides is now possible. Self-healing paints can be made by encapsulating the reactive species responsible for repairing the fissures. Encapsulation allows for the regulated release of actives like insect repellents, biocides, and fragrances over a longer period.

### *1.8.5.* Controlled core release

Encapsulation should protect the core from the external environment until it is desired.[106] As a result, the release at the optimum time and site is a crucial component of the encapsulation

process because it increases effectiveness, lowers the dosage of the active ingredient needed, and broadens the applications of the active ingredient. The solubility of the polymer in the solvent plays a role in encapsulation efficiency; the more soluble the polymer, the longer it will take to precipitate, which in turn reduces encapsulation efficiency as the active may diffuse. Additionally, in the case of an emulsification method, if the organic phase is partly soluble in the aqueous phase, active ingredient may diffuse in the continuous phase, leading to poor encapsulation efficiency. The effectiveness of encapsulation is also influenced by the concentration of the polymer. A high polymer concentration causes the material to solidify rapidly, which blocks the diffusion of actives in a continuous medium. In addition, a high polymer concentration leads to a higher viscosity, which slows the active's diffusion into the aqueous phase and improves encapsulation efficiency. To ensure the polymer solidifies during encapsulation, it is important that the solvent be immediately removed. High encapsulation efficiency requires prompt removal of the solvent to prevent the formation of the porous structure in the polymeric wall. The interactions between the wall material and the core are the key variables controlling the release rates.
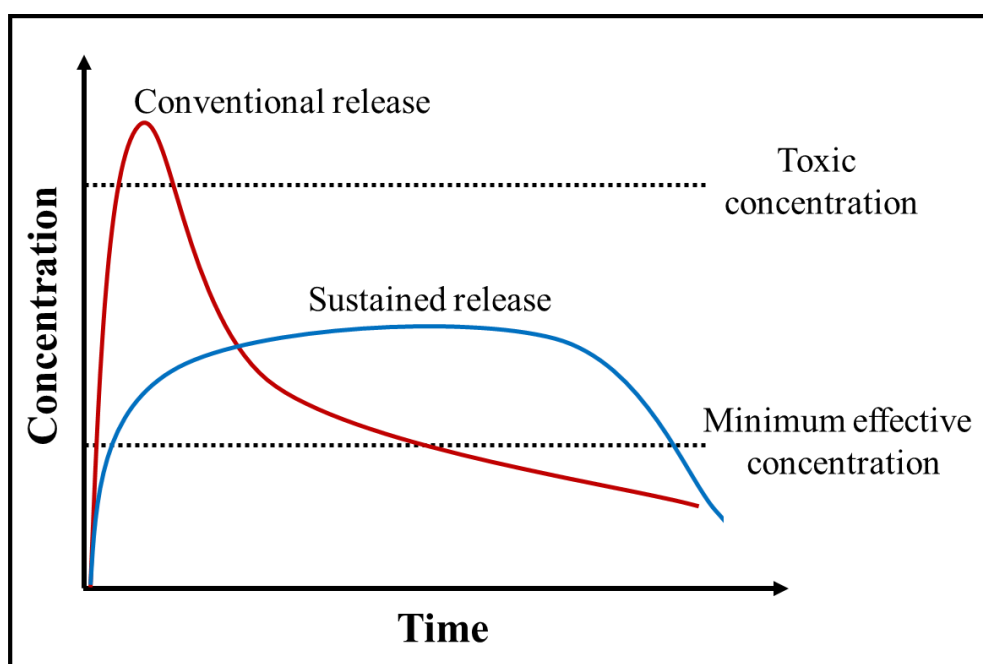


**Figure 1.4**. Comparison between the conventional and controlled release profile.

Additionally, other factors such as the core's volatility, the ratio of core to wall material, particle size, and grade of the wall material influence the release of active. The controlled core release has been characterized as a process in which active agents are released at the desired rate and time at the target site. The main goals of controlled release are to reduce target substance loss during processing and storage, as well as improve absorption and effectiveness. The active chemicals are delivered at controlled rates over a long period of time, which is one of the benefits of controlled release. Primarily, the release mechanisms involved in the core release are diffusion, polymer degradation or hydrolytic cleavage of drug-polymer linkers, use of solvents, and stimuli-responsive release such as with changes in temperature, pH, and pressure.[107] In general, the release of the core material is accomplished through a combination of mechanisms.[108] For separation and encapsulating applications, microcapsules with regulated stability and permeability are in high demand. When the microcapsule wall is still intact, diffusion can take place, and the rate of release is determined by the chemical properties of the core and wall materials, as well as a few physical properties of the wall. Degradation release occurs when a specific enzyme or molecule interacts with the polymer wall, resulting in the digestion of the polymer wall or digestion of the linker between the drug and polymer. With the use of solvent, the polymer wall either swells or dissolves, resulting in the release of actives from the core upon expanding, favoring the release. Changing the pH releases the core because it affects the solubility of the wall material. For instance, the bacteria used in probiotics can be encapsulated in a way that allows them to survive the stomach's acidic environment while remaining dormant until they reach the more alkaline environment of the intestine.[109] A change in temperature may stimulate the release of the core. There are two distinct ideas: fusion-activated release, which involves melting the wall material as a result of rising temperature, and temperature-sensitive release, which is involved in the case of materials that expand or collapse at a certain temperature. Pressure-induced release occurs with the

application of pressure on the capsule walls, triggering the release of the core, such as in the case of chewing gum, where flavor releases upon chewing.
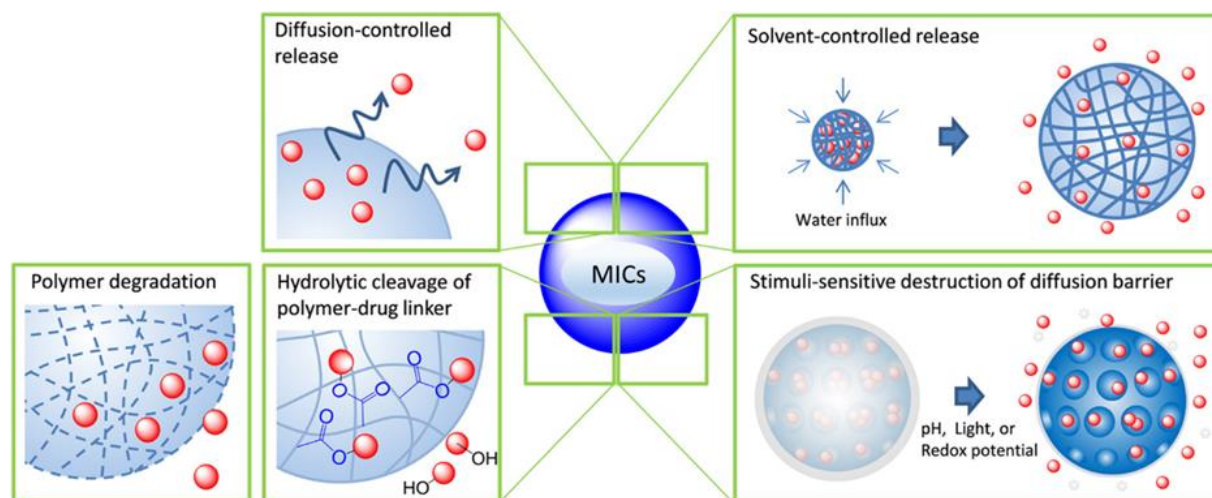


**Figure 1.5**. Drug release mechanisms (Reproduced with permission from reference 107, copyright Elsevier).

### *1.8.6.* Additives

Since most of the wall materials may fail to deliver all the required properties, certain additives can be incorporated into the wall during the preparation of MICs. Other than the protective coating colloids, a variety of additives such as solvents, plasticizers, fumed silica, or other anti-coagulants, stabilizers, and preservatives in the case of food are added to meet the requirements.

(a) Solvents: During microencapsulation, a suitable organic solvent can be used to coat the core with the polymer. To eliminate traces of solvents in MICs, volatile solvents such as methanol, ethanol, water, and chloroform can be used.

(b) Plasticizers: In the case of some polymers, plasticizers are used to reduce the fragility of the polymer. The amount of plasticizer must be optimized so as to avoid the deterioration of polymer wall properties. Plasticizers may also alter the drug's penetration through the polymer wall. A plasticizer is one of the most critical ingredients in the MICs'

formation.[110] Plasticizers are generally added to the polymer in air suspension coating and pan coating methods.

(c) Protective colloids: When charged polymers come into contact with surfactants or other polymers that have an opposite charge, they can be neutralized, resulting in the precipitation of polymers. Protective colloids stabilize the polymer wall membrane by concealing the charged polymers to prevent agglomeration. Protective colloids aid in wall stabilization, improving the efficiency of the wall material for encapsulation. Poly(vinyl alcohol) is one such protective colloid that is used to keep the polyurea wall membrane intact.[111]

(d) Anti-adherents: Agglomeration of MICs may alter the release of the active, and hence the addition of anti-coagulants or anti-adherents is necessary in some cases during the MICs' formation to avoid the agglomeration of the MICs. Fumed silica is commonly used to coat the MICs during preparation which prevents agglomeration of MICs.

(e) Stabilizers: Stabilizers are generally added to stabilize the emulsion when the emulsification technique is used to prepare MICs. The use of a stabilizer allows the emulsion to stabilize and helps in controlling the size of the tiny emulsion droplets, which is an important factor in the controlled release of active ingredients. In food applications, certain preservatives are used to protect the food ingredients from degradation, which increases the shelf life of the food ingredients.

### *1.8.7.* Factors that determine the properties of microcapsules

There are various factors that determine the properties of the microcapsules, such as mechanical stirring, viscosity of the polymer solution, osmotic gradient, volume of different phases, and stabilizers. Mechanical stirring influences the size of the MICs during emulsion formation and may alter the properties of MICs. The viscosity of the polymer solution may play an important role, as the more viscous polymer solution is difficult to break down into

tiny droplets either during stirring or spray drying and may result in the formation of large MICs. The use of solvents to prepare polymer solutions is essential for various polymers and may result in porous wall membranes when the solvent is evaporated. Hence, the amount of solvent used to prepare the solution is crucial to prepare a less porous to non-porous wall membrane. Also, the volume of the polymer solution may affect the solidification time and may result in the retention of some amount of solvent, which may leach out later, creating a porous channel to the core through the wall membrane.

### 1.8.8. Evaluation of microcapsules (physical and chemical)

Various analytical and physical techniques can be employed to characterize microcapsules and encapsulated actives. The size of the microcapsules can be determined using a particle size analyser (zeta potential), an optical microscope, and SEM. The morphology of the MICs can be determined using SEM and an optical microscope. Thermal analysis can be performed to check the thermal stability of the polymer wall using DSC and TGA, whereas TGA can also be used to check the encapsulation efficiency along with some solvent extraction methods and High-performance liquid chromatography (HPLC). Further, release studies can be done in different environments to verify the controlled release of actives. It can be done in various media, such as some solvents favorable for active and simulated body fluids. The physical stability of the MICs can be determined by exposing them to ultraviolet light, solvents, or simulated fluids, temperature, pressure, and moisture.

### 1.8.9. Mathematical evaluation

In recent years, many formulations have been developed to prepare MICs for controlled release, which may result in the formulation having varying physical properties that influence the release of actives from MICs. The release of actives from MICs can be divided into formulations that release active at a slow zero- or first order rate and formulations with an

initial burst release followed by a zero- or first order rate.[112] Therefore, mathematical modeling proves to be a useful tool to determine and predict the release kinetics before the release system is realized. It enables the measurement of certain physical parameters, like diffusion coefficients, by fitting models to experimental data. Hence, mathematical modeling plays an important role in the optimization of the microcapsule formulation process. There are various kinetic models established to describe the release of actives from MICs.

The release of the active from the core is determined by certain mechanisms discussed earlier. There are certain models that determine the type of release mechanism involved. The models can be selected from the literature by employing several sets of equations and determining the coefficients and fitting parameters. General models that are employed to determine release kinetics are first order, zero order, Higuchi square root time, Hixson-Crowell cube root, Baker-Lonsdale, Korsemeyer-Peppas, Hopfenberg, Nernst equation, and Weibull distribution models.

*1.8.9.1.Zero-order model*: To determine the rate of drug release from non-disaggregating, sustained-release dose forms, zero-order equation can be used:[113]

$$Q_o - Q_t = K_o t$$

where, $Q_o$ is the initial active concentration, $Q_t$ is the amount of active released at time $t$, and $K_o$ is the release constant for zero-order release. Zero-order kinetics is followed by formulations with constant active release, i.e., MICs release a fixed amount of active per minute until the maximum active is released.

*1.8.9.2.First-order model*: This model determines the adsorption and/or elimination of active from the MICs. It is represented by the equation:[114]

$$\log C = \log C_o - Kt/2.303$$

where $C_o$ is the initial amount of active, $t$ is the time, and $k$ is the rate constant for the first order. For a soluble active ingredient incorporated in a porous matrix, the amount

of drug released is proportional to the amount remaining in the matrix, which illustrates that the amount of active release tends to decrease over time.

*1.8.9.3.Higuchi Model*: This model describes the modeling of dissolved actives released from matrix-type MICs. This method is applicable to the actives that are less soluble than those that are highly soluble. It is represented by the simplified equation:[115]

$$Q = K_H \sqrt{t}$$

where, $K_H$ is Higuchi's release constant. Assumptions that should be considered while applying this model are: (a) the matrix contains an initial active concentration much higher than its solubility; (b) dissolution or swelling of the matrix is negligible; (c) active diffusion is constant; and (d) perfect sink conditions were observed during release.

*1.8.9.4.Hixon-Crowell model*: This model is based on the fact that the regular area of a particle is directly proportional to the cube root of its volume. Based on this, an equation was derived:[116]

$$W_o^{1/3} - W_t^{\frac{1}{3}} = kt$$

where $W_o$ is the initial drug concentration, $W_t$ is the remaining drug concentration at time $t$ and $k$ is the surface-volume relation constant. While using this model, it is presumed that the release of the active ingredient is controlled by dissolving velocity rather than diffusion through the polymer matrix.

*1.8.9.5.Ritger–Peppas–Korsmeyer model (Power law)*: This is a more comprehensive semi-empirical model to determine the drug release mechanism from polymer MICs. It is represented by an equation:[117]

$$\frac{M_i}{M_\infty} = K t^n$$

where $M_\infty$ is the amount of active at equilibrium, $M_i$ is the amount of drug release over time $t$, $K$ is the release velocity constant, and $n$ is the release exponent. This model is useful when the drug release mechanism is unknown or when multiple release mechanisms are involved. Release exponent ($n$) value may predict whether the release is Fickian (case I) or Non-Fickian (case II). In Case I i.e., the Fickian model, value of $n$ is 0.5, release is governed by diffusion, whereas in non-Fickian (Case II), $n=1$, release is governed by swelling or polymer relaxation and it follows zero order release kinetics. Moreover, when the value of $n$ lies between 0.5 and 1, it follows non-Fickian (anamolous) transport, and release is governed by both diffusion and swelling. In case II transport, where $n>1$, an extreme form of transport occurs where a breaking of polymer wall occurs. It is observed that the matrix has a high affinity for solvent.[118]

*1.8.9.6. Baker and Lonsdale model*: Baker and Lonsdale have developed this model for the release of actives based on the Higuchi model for spherical matrices. This model works well when the drug is uniformly dissolved in the matrices. It is represented by an equation:[119]

$$\frac{3}{2}[1 - (1 - \frac{M_t}{M_\infty})^{2/3}]\frac{M_t}{M_\infty} = kt$$

where $k$ is release constant. This equation can be employed for the linearization of release from MICs.

*1.8.9.7. Weibull model*: This model is useful for comparing the release profiles of matrix systems. It is represented by an equation:[120]

$$\frac{M_i}{M_\infty} = 1 - exp(-a.t^b)$$

where $a$ denotes the time dependency of the process, and $b$ characterizes the type of release curve. Intrinsic dissolution of the active was not considered in this equation. It applies to almost all kinds of release curves.

*1.8.9.8.Hopfenberg model*: Hopfenberg created a mathematical model to predict the drug release from polymers with eroding surfaces if the surface area is constant. At time *t*, the cumulative fraction of drug released is characterized as:[121]

$$\frac{M_t}{M_\infty} = 1 - [1 - k_0 t / C_L a]^n$$

where $k_0$ is the rate constant of zero-order describing polymer degradation, $C_L$ is the initial active amount, *a* is the radius of a sphere, and *n* is the exponent specific to geometries. This model illustrates the features of permeability, relaxation, and diffusion individually. Additionally, data from the composite profile, which basically showed site-specific biphasic release kinetics, is used to determine the mechanism of release from the optimized oilispheres.[122]

We have employed the Ritger–Peppas–Korsmeyer model and the Weibull model to establish the mechanism of the active released in this thesis, where the Ritger–Peppas–Korsmeyer model successfully predicts the release mechanism in two working chapters.

### *1.8.10.* **Application of microcapsules**

Microencapsulation can be used in various applications, such as agriculture to deliver pheromones,[123] pesticides,[124] insecticides,[125] etc. In food applications, they can be employed to mask the odour and release the aroma[126] and colour[127] at a specific time. Also, essential vitamins and minerals can be encapsulated to improve their bioavailability.[128] It can also increase the shelf life of the food product by protecting it from the environment.[129] One of the major areas where the microencapsulation technique can be used is in pharmaceuticals to deliver drugs in a controlled manner and for a longer time.[130] In certain cases, targeted drug delivery is possible to improve the efficiency of the drug along with its bioavailability.[131] In cosmetics, certain essential oils can be encapsulated and allowed to release in a sustained fashion.[132]
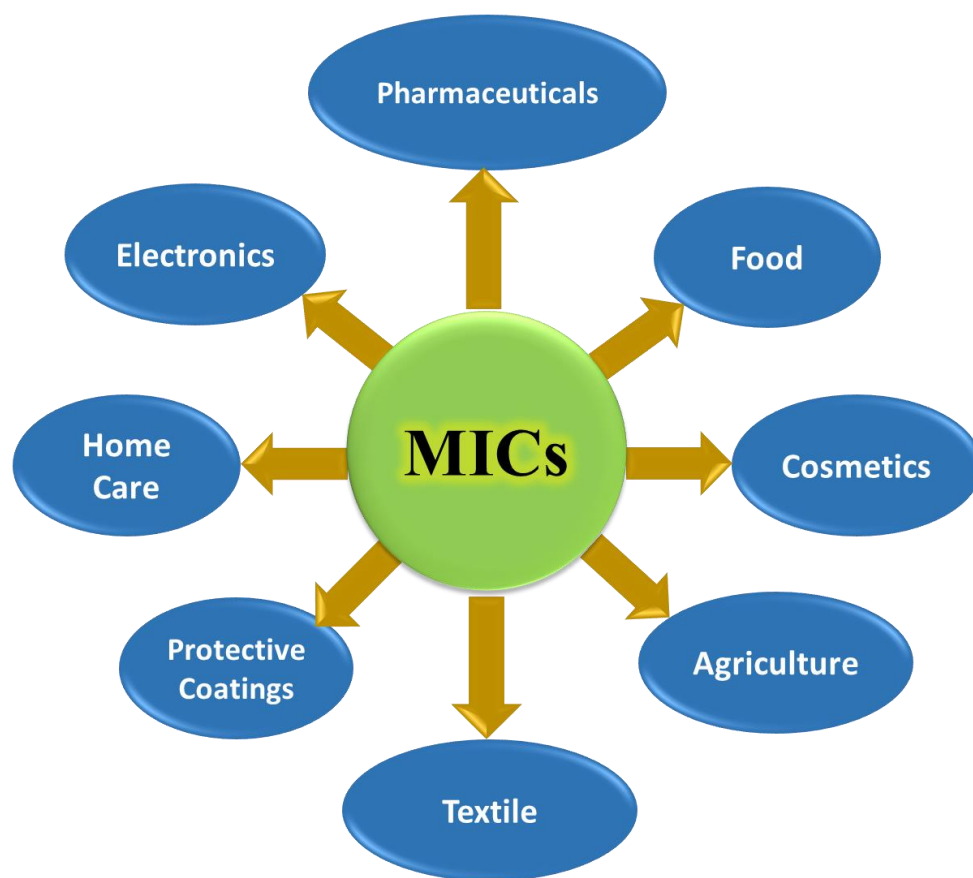
**Figure 1.6.** Applications of microcapsules.

## 1.9. Statement of the problems

In this thesis work, we have tried to address two problems related to dual responsive microparticles and sustained release microcapsules: (i) Cellulose is one of the most abundant biopolymers available to mankind. Structurally, cellulose is a linear polymer with β-glucopyranose repeating units linked by 1−4−glycosidic linkage. It forms strong intra- and intermolecular hydrogen bonding which makes cellulose reluctant to dissolve in common organic solvents limiting the processibility of cellulose. A greener solvent can be employed to dissolve and process cellulose to prepare microbeads and fibers. Also, materials that respond to multiple stimuli like UV−light and magnetic fields are appealing for security and medical

diagnostic applications. It is known that fluorescence emission can be quenched by the presence of magnetic nanoparticles (heavy metal quenching effect) and solid-state quenching owing to the aggregation of a fluorophore, which is one of the most serious concerns in preparation of dual-functional microspheres (MIS). To obtain cellulose microbeads with high solid-state fluorescence emission, the amount of iron oxide nanoparticles ($Fe_3O_4$ NPs) and fluorophore (1-pyrenebutyric acid, PBA) may be varied. (ii) The second part is focused on the preparation of sustained release poly(urethane) microcapsules. The barrier properties of polyurea-urethane (PUU) microcapsules (MIC) are dependent on polymer relaxation and hence may be limited by the use of soft aliphatic polyol components. Barrier properties can be improved by incorporating aromatic polyols dissolved in the aqueous phase that react interfacially with aromatic diisocyanates in the oil phase to yield more robust microcapsules. Although aromatic polyols have been used to synthesize polyurethanes, they have never been used in interfacial polymerization to prepare microcapsules due to their poor water solubility and reactivity. Further, the use of biodegradable components is desirable for preparing PUU MICs to reduce their harmful effects on the environment. For biodegradability, polyol components can be replaced by some biodegradable polyols which may include natural monomer or oligomer or polymer. These biodegradable components may be directly reacted or mixed with conventional polyols to yield MICs with biodegradable components. Finally, PLA, polycaprolactone (PCL), poly(glycolic acid) PGA, and PLGA are among the polyesters that have been utilised to make MICs employing the solvent evaporation approach. Linear polyesters are prone to hydrolysis and degrade in specific conditions. Solvent evaporation involves toxic solvents, a higher temperature for evaporation, and low encapsulation efficiency, making it a non-desirable approach for microencapsulation. As a result, PLA and PCL can be modified in such a way that they can be reacted interfacially with other monomer to prepare microspheres with improved encapsulation efficiency.

## 1.10. Outline of the Thesis

The outline of this thesis work is as follows:

**Chapter 1** provides an introduction to microparticles, their classification as solid microparticles, hollow or porous microparticles, and microcapsules, as well as their preparation, characterization, and applications.

**Chapter 2** focuses on the synthesis of functional microparticles with dual responsiveness, i.e., magnetic and fluorescence properties, with high solid-state fluorescence quantum yield. It highlights the preparation of dual responsive cellulose microbeads using an environmentally benign solvent, tetrabutylammonium hydroxide (TBAH), and investigate the effect of varying amount of $Fe_3O_4$ NPs and fluorophore (1-pyrenebutyric acid, PBA) on solid-state fluorescence quantum yield. The presence of $Fe_3O_4$ NPs was confirmed using TGA, X-ray photoelectron spectroscopy (XPS), and a vibrating sample magnetometer (VSM). The covalent linkage of PBA with cellulose microbeads was confirmed using Fourier transform infra-red spectroscopy FTIR and $^{13}C$ solid-state nuclear magnetic resonance (NMR).

**Chapter 3** outlines the synthesis of poly(urea-urethane) (PUU) microcapsules employing an aromatic diol as the polyol component to improve barrier properties for controlled release of model active ingredient dimethyl phthalate (DMP). These MICs prepared were systematically compared with the conventional PUU MICs prepared using ethylene glycol (EG) as polyol component. Extraction studies were performed to evaluate the encapsulation efficiency, and release studies were carried out to compare the barrier properties.

In **Chapter 4**, we examine how the conventional ethylene glycol can be replaced by up to 50 wt.% by the biodegradable hyperbranched polycarbonate polyol (PCPO) to prepare PUU MICs without impairing the barrier properties. Here, PCPO was dissolved in ethylene glycol and

reacted interfacially with a diisocyanate to prepare MICs. The as-prepared MICs were evaluated for their encapsulation efficiency using extraction studies and release characteristics.

**Chapter 5** demonstrates the preparation of microspheres using PLA/PCL diglycidyl ether (DGE) and reacting interfacially with diamine or polyamine using amine/epoxide chemistry. It describes the preparation of PCL and PLA diols using ring-opening polymerization followed by reacting with epichlorohydrin to prepare PCL-DGE and PLA-DGE respectively. The resulting DGEs were dissolved in the organic phase and reacted interfacially with the amines present in the continuous phase to result in the waxy microspheres.

**Chapter 6** provides a summary of the work described in the chapter 2 to chapter 5 and outlines the scope for future work.

## 1.10. References

1. Arshady, R. Preparation of polymer nano- and microspheres by vinyl polymerization techniques. *J. Microencapsulation*. **1988**, *5*, 104-114.

2. Kawaguchi, H. Functional polymer microspheres. *Prog. Polym. Sci*. **2000**, *25*, 8, 1171-1210.

3. Hejmady, P., van Breemen, L. C. A., Anderson, P. D. A processing route to spherical polymer particles via controlled droplet retraction. *Powder Technol*. **2021**, *388*, 401-411.

4. Saralidze, K., Koole, L. H., Knetsch, M. L. W. Polymeric microspheres for medical applications. *Materials* **2010**, *3*, 6, 3537-3564.

5. Aranaz, I., Panos, I., Peniche, C., Heras, A., Acosta, N. Chitosan spray-dried microparticles for controlled delivery of venlafaxine hydrochloride. *Molecules* **2017**, *22*, 11, 1980.

6. Dixit, M., Kini, A. G., Kulkarni, P. K. Preparation, and characterization of microparticles of piroxicam by spray drying and spray chilling methods. *Res. Pharm. Sci*. **2010**, 5, 2, 89–97.

7. Morais, A. I. S., Vieira, E. G., Afewerski, S., Sousa, R. B., Honorio, L. M. C., Cambrussi, A. N. C. O., Santos, J. A., Bezerra, R. D. S., Furtini, J. A. O., Silva-Filho, E. C., Webster, T. J., Lobo, A. O. Fabrication of polymeric microparticles by electrospray: the impact of experimental parameters. *J. Funct. Biomater*. **2020**, *11*, 1, 4-29.

8. Chang, M. -W., Stride, E., Edirisinghe, M. A new method for the preparation of monoporous hollow microspheres. *Langmuir* **2010**, *26*, 7, 5115–5121.

9. Lopez-Iglesias, C., Barros, J., Ardao, I., Gurikov, P., Monteiro, F. J., Smirnova, I., Avarez-Lorenzo, C., Garcia-Gonzalez, C. A. Jet cutting technique for the production of chitosan aerogel microparticles loaded with vancomycin. *Polymers* **2020**, *12*, 2, 273-285.

10. Freitas, S., Merkle, H. P., Gander, B. Microencapsulation by solvent extraction/evaporation: reviewing the state of the art of microsphere preparation process technology. *J. Control. Release*. **2005**, *102*, 313–332.

11. Napiorkowska, A., Kurek, M. Coacervation as a novel method of microencapsulation of essential oils-A review. *Molecules* **2022**, *27*, 5142-5159.

12. Manjanna, K. M., Shivakumar, B., Kumar, P. T. M. Microencapsulation: an acclaimed novel drug-delivery system for NSAIDs in arthritis. *Crit. Rev. Ther. Drug Carr. Syst*. **2010**, *27*, 6, 509-545.

13. Lucia, C., Marcela, F., Ainhoa, L. Encapsulation of almond essential oil by co-extrusion/gelling using chitosan as wall material. *J. Encapsulation Adsorpt. Sci*. **2017**, *7*, 1, 67-74.

14. Kiss, N., Brenn, G., Pucher, H., Wieser, J., Scheler, S., Jennewein, H., Suzzi, D., Khinast, J. Formation of O/W emulsions by static mixers for pharmaceutical applications. *Chem. Eng. Sci*. **2011**, 66*, 5084-5094.

15. Bhutkar, S., Shanmuganathan, K. Polymer Based Microcapsules for Encapsulation. In: Parameswaranpillai, J., V. Salim, N., Pulikkalparambil, H., Mavinkere Rangappa, S., Suchart Siengchin, I.h. (eds) Micro- and Nano-containers for Smart Applications. Composites Science and Technology. Springer, Singapore. **2022**.

16. Vladisavljevic, G. T. Structured microparticles with tailored properties produced by membrane emulsification. *Adv. Colloid. Interfac. Sci.* **2015**, *225*, 53-87.

17. Min, N. G., Kim, B., Lee, T. Y., Kim, D., Lee, D. C., Kim, S. -H. Anisotropic microparticles created by phase separation of polymer blends confined in monodisperse emulsion drops. *Langmuir* **2015**, *31*, 3, 937–943.

18. Arshady, R. Preparation of microspheres and microcapsules by interfacial polycondensation techniques. *J. Microencapsul*. **1989**, *6*, 1, 13-28.

19. Miao, J. -J., Jiang, L. -P., Liu, C., Zhu, J. -M., Zhu, J. -J. General sacrificial template method for the synthesis of cadmium chalcogenide hollow structures. *Inorg. Chem.* **2007**, *46*, 5673-5677.

20. Farinha, S., Moura, C., Afonso, M. D., Henriques, J. Production of lysozyme-plga-loaded microparticles for controlled release using hot-melt extrusion. *AAPS Pharm. Sci. Tech.* **2020**, *21*, 274-287.

21. Muley, S., Nandgude, T., Poddar, S. Extrusion–spheronization a promising pelletization technique: In-depth review. *Asian J. Pharm. Sci*. **2016**, *11*, 6, 684-699.

22. Wong, C. K., Qiang, X., Muller, A. H. E., Groschel, A. H. Self-Assembly of block copolymers into internally ordered microparticles. *Prog. Polym. Sci*. **2020**, *102*, 101211.

23. Farrell, R. A., Fitzgerald, T. G., Borah, D., Holmes, J. D., Morris, M. A. Chemical interactions and their role in the microphase separation of block copolymer thin films. *Int. J. Mol. Sci*. **2009**, *10*, 9, 3671-3712.

24. Gupta, A. S. Role of particle size, shape, and stiffness in design of intravascular drug delivery systems: insights from computations, experiments, and nature. *WIRES Nanomed. Nanobiotechnol*. **2015**, *8*, 2, 255-270.

25. Yu, B., Luo, Y., Cong, H., Gu, C., Wang, W., Tian, C., Zhai, J., Usman, M. Preparation of crosslinked porous polyurea microspheres in one-step precipitation polymerization and its application for water treatment. *RSC Adv*. **2016**, *113*, 6, 111806-111811.

26. Weems, A. C., Li, W., Maitland, D. J., Calle, L. M. Polyurethane microparticles for stimuli response and reduced oxidative degradation in highly porous shape memory polymers. *ACS Appl. Mater. Interfaces* **2018**, *10*, 39, 32998–33009.

27. Qiu, X., Leporatti, S., Donath, E., Mohwald, H. Studies on the drug release properties of polysaccharide multilayers encapsulated ibuprofen microparticles. *Langmuir* **2001**, *17*, 17, 5375–5380.

28. Molavi, F., Barzegar-Jalali, M., Hamishehkar, H. Polyester based polymeric nano and microparticles for pharmaceutical purposes: A review on formulation approaches. *J. Control. Release* **2020**, *320*, 265-282.

29. Yang, P., Ning, Y., Neal, T. J., Jones, E. R., Parker, B. R., Armes, S. P. Block copolymer microparticles comprising inverse bicontinuous phases prepared via polymerization-induced self-assembly. *Chem. Sci*. **2019**, *10*, 4200-4208.

30. Deshmukh, S. S., Sangwar, V. S. One-step synthesis of polyethylene microspheres using a modified chemical route for pulmonary drug delivery. *J. Taibah Univ. Sci*. **2016**, *10*, 4, 485-489.

31. Turner, A. P. F. Biosensors: sense and sensibility. *Chem. Soc. Rev.*, **2013**, *42*, 3184-3196.

32. Bhalla, N., Jolly, P., Formisano, N., Estrela, P. Introduction to biosensors. *Essays Biochem.* **2016**, *60*, 1, 1-8.

33. Lopez, M. S-P., Cabarcos, E. L., Ruiz, B. L. Biosensors based on poly(vinylimidazole) microparticles. *Electrocatalysis*, **2009**, *21*, 512-520.

34. Lopez, M. S-P., Mecerreyes, D., Cabarcos, E. L., Ruiz, B. L. Ampherometric glucose biosensor based on polymeric ionic liquid microparticles. *Biosens. Bioelectron.* **2006**, *21*, 2320-2328.

35. Lopez, M. S-P., Ruiz, B. L. Electrochemical biosensor based on ionic liquid polymeric microparticles. An analytical platform for catechol. *Microchem. J.* **2018**, *138*, 173-179.

36. Guan, B., Magenau, A., Kilian, K. A., Ciampi, S., Gaus, K., Reecec, P. J., Gooding, J. J. Porous silicon photonic crystal microparticles: towards single-cell optical biosensors. *Faraday Discuss.* **2011**, *149*, 301-317.

37. Tobias, C., Climent, E., Gawlitza, K., Rurack, K. Polystyrene Microparticles with Convergently Grown Mesoporous Silica Shells as a Promising Tool for Multiplexed Bioanalytical Assays. *ACS Appl. Mater. Interfaces* **2021**, *13*, 1, 207–218.

38. Oliveira, W. D., Glasser, W. G. Hydrogels from polysaccharides. I. Cellulose beads for chromatographic support. *J. Appl. Polym. Sci*. **1996**, *60*, 1, 63-73.

39. Yao, T., Song, J., Gan, Y., Qiao, L., Du, K. Preparation of cellulose-based chromatographic medium for biological separation: A review. *J. Chromatography A*, **2022**, *1677*, 463297.

40. Luo, X., Zhang, L. Creation of regenerated cellulose microspheres with diameter ranging from micron to millimeter for chromatography applications. *J. Chromatography A* **2010**, *1217*, 38, 5922-5929.

41. Deng, J., Chen, Q., Hu, B., Li, W., Jia, M., Shi, Y., Xiong, S., Bai, J., Yin, H. Synergic effect of adsorption and biodegradation by microsphere immobilizing bacillus velezensis for enhanced removal organics in slaughter wastewater. *Processes* **2021**, *9*, 7, 1145-1157.

42. Feng, M., Yu, S., Wu, P., Wang, Z., Liu, S., Fu, J. Rapid, high-efficient and selective removal of cationic dyes from wastewater using hollow polydopamine microcapsules: Isotherm, kinetics, thermodynamics and mechanism. *Appl. Surf. Sci*. **2021**, *542*, 148633.

43. Yu, Y., Liu, S., Pei, Y., Luo, X. Growing Pd NPs on cellulose microspheres via in-situ reduction for catalytic decolorization of methylene blue. *Int. J. Biol. Macromol*. **2021**, *166*, 1419-1428.

44. Zhang, J., Deng, R., Ren, B., Yaseen, M., Hursthouse, A. Enhancing the removal of sb (iii) from water: a fe3o4@hco composite adsorbent caged in sodium alginate microbeads. *Processes* **2020**, *8*, 1, 44-57.

45. Jiang, F., Zhang, D., Ouyang, X., Yang, Li. -Y. Fabrication of porous polyethyleneimine-functionalized chitosan/Span 80 microspheres for adsorption of diclofenac sodium from aqueous solutions. *Sustain. Chem. Pharm*. **2021**, *21*, 100418.

46. Palomo, J. M. Solid-phase peptide synthesis: an overview focused on the preparation of biologically relevant peptides. *RSC Adv*. **2014**, *4*, 32658-32672.

47. McInnes, S. J. P., Voelcker, N. H. Porous silicon-based nanostructured microparticles as degradable supports for solid-phase synthesis and release of oligonucleotides. *Nanoscale Res Lett*. **2012**, *7*, 385-394.

48. Meerovich, I., Smith, D. D., Dash, A. K. Direct solid-phase peptide synthesis on chitosan microparticles for targeting tumor cells. *J. Drug Deliv. Sci*. **2019**, *54*, 101288.

49. Guillier, F., Orain, D., Bradley, M. Linkers and Cleavage Strategies in Solid-Phase Organic Synthesis and Combinatorial Chemistry. *Chem. Rev.* **2000**, *100*, 6, 2091–2158.

50. Englebretsen, D.R. and Harding, D.R., Solid phase peptide synthesis on hydrophilic supports. *Int. J. Pept. Prot. Res.* **1992**, *40*, 487-496.

51. Luca, L. D., Giacomelli, G., Porcheddu, A., Salaris, M., Taddei, M. Cellulose beads: a new versatile solid support for microwave- assisted synthesis. preparation of pyrazole and isoxazole libraries. *J. Comb. Chem.* **2003**, *5*, 4, 465–471.

52. Salehipour, M., Rezaei, S., Mosafer, J. et al. Recent advances in polymer-coated iron oxide nanoparticles as magnetic resonance imaging contrast agents. *J. Nanopart. Res*. **2021**, *23*, 48-82.

53. Bar-Shir, A., Avram, L., Yariv-Shoushan, S., Anaby, D., Cohen, S., Segev-Amzaleg, N., Frenkel, D., Sadan, O., Offen, D. and Cohen, Y. Alginate-coated magnetic nanoparticles for noninvasive MRI of extracellular calcium. *NMR Biomed.* **2014**, *27*, 774-783.

54. Kim, E. H., Ahn, Y., Lee, H. S. Biomedical applications of superparamagnetic iron oxide nanoparticles encapsulated within chitosan. *J. Alloys Compd.* **2007**, *434*, 633-636

55. Zhou, D., Sun, Y., Zheng, Y., Ran, H., Li, P., Wang, Z., Wang, Z. Superparamagnetic PLGA–iron oxide microspheres as contrast agents for dual-imaging and the enhancement of the effects of high-intensity focused ultrasound ablation on liver tissue. *RSC Adv*. **2015**, *5*, 35693-35703.

56. Xu, S., Yang, F., Zhou, X., Zhuang, Y., Liu, B., Mu, Y., Wang, X., Shen, H., Zhi, G., Wu, D. Uniform PEGylated PLGA Microcapsules with Embedded Fe3O4 Nanoparticles for US/MR Dual-Modality Imaging. *ACS Appl. Mater. Interfaces* **2015**, *7*, 36, 20460–20468.

57. Awada, H., Sene, S., Laurencin, D., Lemaire, L., Franconi, F., Bernex, F., Bethry, A., Garric, X., Gauri, Y., Nottelet, B. Long-term in vivo performances of polylactide/iron oxide nanoparticles core–shell fibrous nanocomposites as MRI-visible magneto-scaffolds. *Biomater. Sci.* **2021**, *9*, 6203-6213.

58. Qin, X.-Y., Liu, X. -X., Li, Z. -Y., Guo, L. -Y., Zheng, Z. -Z., Guan, H. -T., Song, L., Zou, Y. -H., Fan, T. -Y. MRI detectable polymer microspheres embedded with magnetic ferrite nanoclusters for embolization: in vitro and in vivo evaluation. *Int. J. Nanomed.* **2019**, *14*, 8989–9006.

59. Dong, X., Tahir, M. A., Zhang, L., Schafer, C. G. Gadolinium-containing polymer microspheres: a dual-functional theranostic agent for magnetic resonance imaging and cancer therapy. *New J. Chem.* **2019**, *43*, 5987-5995.

60. Kozlowska, J., Stachowiak, N., Sionkowska, A. Collagen/Gelatin/Hydroxyethyl cellulose composites containing microspheres based on collagen and gelatin: design and evaluation. *Polymers* **2018**, *10*, 4, 456-471.

61. Łętocha, A.; Miastkowska, M.; Sikora, E. Preparation and Characteristics of Alginate Microparticles for Food, Pharmaceutical and Cosmetic Applications. *Polymers* **2022**, *14*, 3834.

62. Dhat, S., Naik, S. R., Agharkar, A., Parimal, K. Vitamin E loaded pectin alginate microspheres for cosmetic application. *J. Pharm. Res.* **2009**, *2*, 6, 1098-1102.

63. Haddadi, A., Aboofazeli, R., Erfan, M., Farboud, E. S. Topical delivery of urea encapsulated in biodegradable PLGA microparticles: O/W and W/O creams. *J. Microencapsulation*, **2008**, *25*, 379 —386.

64. Qian, Y., Zhong, X., Li, Y., Qiu, X. Fabrication of uniform lignin colloidal spheres for developing natural broad-spectrum sunscreens with high sun protection factor. *Ind. Crops Prod.* **2017**, *101*, 54 —60

65. Abu Hajleh, MN, AL-Samydai, A, Al-Dujaili, EAS. Nano, micro particulate and cosmetic delivery systems of polylactic acid: A mini review. *J. Cosmet. Dermatol.* **2020**, *19*, 2805– 2811.

66. Gomez, L., Ramirez, H. L., Carrillo, N. C., Villalonga, R. Polyelectrolyte complex formation mediated immobilization of chitosan-invertase neoglycoconjugate on pectin-coated chitin. *Bioprocess. Biosyst. Eng*. **2006**, *28*, 387–395.

67. Katwa, L. C., Ramakrishna, M., Rao M. R. R. Spectrophotometric assay of immobilized tannase. *J. Biosci.*, **1981**, *3*, 135-142.

68. Tumturk, H., Karaca, N., Demiral, G., Sahin, F. Preparation and application of poly(N,N-dimethylacrylamide-co-acrylamide) and poly(N-isopropylacrylamide-co-acrylamide)/-Carrageenan hydrogels for immobilization of lipase. *Int. J. Biolog*. *Macromol*. **2007**, *40*, 281–285.

69. Emregul, E., Sungur, S., Akbulut, U. Polyacrylamide–gelatine carrier system used for invertase immobilization. *Food Chem*. **2006**, *97*, 591–597.

70. Roy, I., Gupta, M. N.  Lactose hydrolysis by LactozymTM immobilized on cellulose beads in batch and fluidized bed modes. *Process Biochem*. **2003**, *39*, 325-332.

71. Matto, M., Husain, Q. Calcium alginate–starch hybrid support for both surface immobilization and entrapment of bitter gourd (Momordica charantia) peroxidase. *J. Mol. Catal.* **2009**, *57*, 164-170.

72. Kumari, A., Kayastha, A. M. Immobilization of soybean (Glycine max) α-amylase onto Chitosan and Amberlite MB-150 beads: Optimization and characterization. *J. Mol. Catal. B*, **2011**, 69, 8–14.

73. Chen, L.F., Gong, C.S. and Tsao, G.T. Immobilized glucose isomerase on deae cellulose beads. *Starch*, **1981**, *33*, 58-63.

74. Romaskevic, T., Viskantiene, E., Budriene, S., Ramanaviciene, A., Dienys, G. Immobilization of maltogenase onto polyurethane microparticles from poly(vinyl alcohol) and hexamethylene diisocyanate. *J. Mol. Catal*. **2010**, *64*, 172–176.

75. Bai, X., Gu, H., Chen, W. Shi, H., Yang, B., Huang, X., Zhang, Q. Immobilized laccase on activated poly(vinyl alcohol) microspheres for enzyme thermistor application. *Appl. Biochem. Biotechnol*. **2014**, *173*, 1097–1107.

76. Pahujani, S., Kanwar, S. S., Chauhan, G., Gupta, R. Glutaraldehyde activation of polymer Nylon-6 for lipase immobilization: enzyme characteristics and stability. *Bioresour Technol*. **2008**, 99*, 2566-2570.

77. Gericke, M., Trygg, J., Fardim, P. Functional cellulose beads: preparation, characterization, and applications. *Chem. Rev*. **2013**, *113*, 4812−4836.

78. Lagreca, E., Onesto, V., Natale, C. D., Manna, S. L., Netti, P. A., Vecchione, R. Recent advances in the formulation of PLGA microparticles for controlled drug delivery. *Prog. Biomater.* **2020**, *9*, 153-174.

79. Wu, J., Ding, J., Xiao, B. Chen, D., Huang, D., Ma, P., Xiong, Z. A facile strategy for controlling porous PLGA microspheres via o/w emulsion method. *J. Polym. Res*. **2022**, *29*, 508.

80. Guo, F., Ding, Y., Wang, Y., Gao, X., Chen, Z. Functional monodisperse microspheres fabricated by solvothermal precipitation co-polymerization. *Chin. J. Chem. Eng*. **2021**, *34*, 323-331.

81. Sun, P., Yang, S., Sung, X., Wang, Y., Pan, L., Wang, H., Wang, X., Guo, J., Nie, C. Functional porous carboxymethyl cellulose/cellulose acetate composite microspheres: Preparation, characterization, and application in the effective removal of HCN from cigarette smoke. *Polymers* **2019**, *11*, 181-191.

82. Ou, J. N., Wu, M. H., Chen, H. Swelling of oligomeric polystyrene seed particles to prepare porous microspheres using n-hexane as porogen. *J. Mater. Sci. Lett*. **2001**, *20*, 24, 2221–2223.

83. Straub, J. A., Chickering, D. E., Church, C.C., Shah, B., Hanlon, T., Bernstein, H. Porous PLGA microparticles: AI-700, an intravenously administered ultrasound contrast agent for use in echocardiography. *J. Control. Release*. **2005**, *108*, 1, 21–32.

84. Takai, C., Hotta, T., Shiozaki, S., Matsumoto, S., Fukui, T. Key techniques to control porous microsphere morphology in S/O/W emulsion system. *Colloids Surf. A Physicochem. Eng. Asp*. **2011**, *373*, 1–3, 152–157.

85. Cheng, X., Hunag, Z., Li, J., Liu, Y., Chen, C., Chi, R., Hu, Y. Self-assembled growth and pore size control of the bubble-template porous carbonated hydroxyapatite microsphere. *Cryst. Growth Des*. **2010**, *10*, 3, 1180–1188.

86. Jayakrishnan, J., Thanoo, B. C. Suspension polymerization of 2-hydroxyethyl methacrylate in the presence of polymeric diluents: A novel route to spherical highly porous beads for biomedical applications. *J. Biomed. Mater. Res*. **1990**, *24*, 7, 913–927.

87. Li, W. H., Stöver, H. D. H. Porous monodisperse poly(divinylbenzene) microspheres by precipitation polymerization. *J. Polym. Sci. A Polym. Chem*. **1998**, *36*, 10, 1543–1551.

88. Duncanson, W. J., Zieringer, M., Wagner, O., Wilking, J. N., Abbaspourrad, A., Haag, R., Weitz, D. A. Microfluidic synthesis of monodispersed porous microspheres with size-tunable pores. *Soft Matter*. **2012**, *8*, 10636–10640.

89. Sun, H. H., Li, X. N., Ma, G. H., Su, Z. G. Polystyrene-type uniform porous microsphere enables high resolution and low-pressure chromatography of natural products – a case study with Icariin purification. *Chromatographia*. **2005**, *61*, 1–2, 9–15.

90. Li, Y., Gao, F., Wei, W., Qu, J. B., Ma, G. H., Zu, W. Q. Pore size of microporous polystyrene microspheres affects lipase immobilization. *J. Mol. Catal. B Enzym*. **2010**, *66*, 1–2, 182–189.

91. Kim, T. K., Yoon, J. J., Lee, D. S., Park, T. G. Gas foamed open porous biodegradable polymeric microspheres. *Biomaterials*. **2006**, *27*, 2, 152–159.

92. Lee, P. F., Zhang, X. W., Sun, D. D., Du, J., Leckie, J. O. Synthesis of bimodal porous structured TiO2 microsphere with high photocatalytic activity for water treatment. *Colloids Surf. A Physicochem. Eng. Asp*. **2008**, *324*, 1–3, 202–207.

93. Wang, H., Wu, Y., Bai, Y., Zhou, W., An, Y., Li, J., Guo, L. The self-assembly of porous microspheres of tin dioxide octahedral nanoparticles for high performance lithium ion battery anode materials. *J. Mater. Chem*. **2011**, *21*, 10189–10194.

94. Zambrano, V., Bustos, R., Mahn, A. Insights about stabilization of sulforaphane through microencapsulation. *Heliyon*, **2019**, *5*, 11, e02951.

95. He, D., Wang, S., Lei, L., Hou, Z., Shang, P., He, X., Nie, H. Core-shell particles for controllable release of drug. *Chem. Eng. Sci*. **2015**, *125*, 108-120.

96. Blatt, Y., Pinto, R., Safronchik, O., Sedlov, T., Zelkha, M. Stable coated microcapsules. US7097868B2, **2001**.

97. Shi, S., Netravali, A. N. Bacterial cellulose integrated irregularly shaped microcapsules enhance self-healing efficiency and mechanical properties of green soy protein resins. *J. Mater. Sci*. **2021**, 56, 12030–12047.

98. Jadhav, R. S., Mane, V., Bagle, A. V., Hundiwale, D. G., Mahulikar, P. P., Waghoo, G. Synthesis of multicore phenol formaldehyde microcapsules and their application in polyurethane paint formulation for self-healing anticorrosive coating. *Int. J. Ind. Chem*. **2013**, *4*, 31-39.

99. Cui, J., Liu, Y., Hao, J. Multiwalled carbon-nanotube-embedded microcapsules and their electrochemical behavior. *J. Phys. Chem. C* **2009**, *113*, 10, 3967–3972.

100. Drusch, S., Diekmann, S. Microencapsulation by spray drying; Handbook of encapsulation and controlled release, CRC Press, **2015**.

101. Singh, M. N., Hemant, K. S. Y., Ram, M. Shivakumar, H. G. Microencapsulation: A promising technique for controlled drug delivery. *Res. Pharma. Sci*. **2010**, *5*, 2, 65-77.

102. Amaral, P. H. R. d., Andrade, P. L., de Conto, L. C. Microencapsulation and its uses in food science and technology: A review. In: Salaün, F., editor. Microencapsulation - processes, technologies and industrial applications. London, Intech Open, **2019**.

103. Trojer, M. A., Nordstierna, L., Bergek, J., Blanck, H., Holmberg, K., Nyden, M. Use of microcapsules as controlled release device for coatings. *Adv. Colloid Interface Sci*. **2015**, *222*, 18-43.

104. Hassan, A., Laghari, M. S., Rashid, Y. Microencapsulated phase change materials: A review of encapsulation, safety and thermal characteristics. *Sustainability* **2016**, *8*, 10, 1046-1077.

105. Hassani, A., Hussain, S. A., Abdullah, N., Kmaruddin, S. Review on micro-encapsulation with Chitosan for pharmaceuticals applications. *MOJ Curr. Res. & Rev*. **2018**, *1*, 2, 77-84.

106. Gouin, S. Microencapsulation: industrial appraisal of existing technologies and trends. *Trends Food Sci. Technol.* **2004**, *15*, 330-347.

107. Lee, J. H., Yeo, Y. Controlled drug release from pharmaceutical nanocarriers. *Chem. Eng. Sci.* **2015**, 125, 75-84.

108. Desai, K. G. H., Park, H. J. Recent developments in microencapsulation of food ingredients. *Drying Tech.* **2005**, *23*, 1361-1394.

109. Toldra, F., Reig, M. Innovations for healthier processed meats. *Trends Food Sci. Technol.* **2011**, 22, 9, 517-522.

110. Csóka, G., Gelencsér, A., Kiss, D., Pásztor, E., Klebovich, I., Zelkó, R. Comparison of the fragility index of different eudragit polymers determined by activation enthalpies. *J. Therm. Anal. Calorim.* **2007**, *87*, 469-473.

111. Lee, E., Kim, H., Park, S. Effects of protective colloids on the formation of polyurea microcapsules. *Text. Color. and Finish.* **2007**, *19*, 5, 30-36.

112. Dash, G., Murthy, P. N., Nath, L., Chowdhury, P. Kinetic modeling on drug release from controlled drug delivery systems. *Acta Pol. Pharm.* **2010**, *67*, 3, 217-223.

113. Yang, L., Fassihi, R. Zero-order release kinetics from a self-correcting floatable asymmetric configuration drug delivery system. *J. Pharm. Sci.* **1996**, *85*, 170-173.

114. Bourne D.W.: Pharmacokinetics. in: Modern pharmaceutics. 4th ed. Banker GS, Rhodes CT, Eds., Marcel Dekker Inc, New York, **2002**.

115. Higuchi, T. Mechanism of sustained-action medication. Theoretical analysis of rate of release of solid drugs dispersed in solid matrices. *J. Pharm. Sci.* **1963**, *52*, 1145-1149.

116. Hixson, A. W., Crowell, J. H. Dependence of reaction velocity upon surface and agitation. *Ind. Eng. Chem.* **1931**, *23*, 8, 923–931.

117. Korsmeyer, R. W., Gurny, R., Doelker, E., Buri, P., Peppas, N. A. Mechanisms of solute release from porous hydrophilic polymers. *Int. J. Pharm.* **1983**, *15*, 25-35.

118. Riger, P. L., Peppas, N. A. A simple equation for description of solute release II. Fickian and anomalous release from swellable devices. *J. Control. Rel.* **1987**, *5*, 37-42.

119. Baker, R. W., Lonsdale, H. S., in Controlled release of biologically active agents, Tanquary A.C., Lacey R.E. Eds., Plenum Press, New York **1974**.

120. Thawatchai, P., Tamotsu, K., Garnpimol, C. R. Chitosan citrate as film former: compatibility with water-soluble anionic dyes and drug dissolution from coated tablet. *Int. J. Pharm.* **2000**, *198*, 97-111.

121. Hopfenberg, H. B.: in Controlled Release Polymeric Formulations, Paul D.R, Haris F.W. Eds., (ACS Symposium Series No. 33), American Chemical Society, Washington **1976**.

122. Sibanda, W., Pillay, V., Danckwerts, M. P., Viljoen, A. M., van Vuuren, S., Khan, R. A. Experimental design for the formulation and optimization of novel crosslinked oilispheres developed for in vitro site-specific release of mentha piperita oil. *AAPS Pharm. Sci. Tech*. **2004**, *5*, 1, 128-141.

123. Desauziers, V., Sicre, E., Vignau-Laulhère, J., Bourrigaud, S., Plaisance, H. Suspension of pheromone microcapsules on vine leaves acting as passive dispensers against pests. *Environ. Sci. Pollut. Res. Int*. **2022**, *29*, 10, 14975-14986.

124. Tsuji, K. Microencapsulation of pesticides and their improved handling safety. *J. Microencapsulation* **2008**, *18*, 2, 137-147.

125. Wang, R., Liu, S., Sun, F., Yu, X., Liu, X., Li, B., Mu, W., Zhang, D., Liu, F. Balance the rapid release of insecticide microcapsules using double-layer shielding effect when the foliar application. *Chem. Eng. J*. **2023**, *455*, 2, 140899.

126. Sue, I. T., Wang, P. Odor-masking coating for a pharmaceutical preparation. WO2001049270A2, 2001.

127. Thepwatee, S., Adam, P., Boonpongha, P., Suktham, K., Ketchart, O., Jangkena, S., & Iemsam-Arng, J. Color masking of betel nut extract using encapsulation technology for nutricosmeceutical applications. *Key Eng. Mater*. **2019**, *824*, 245–253.

128. Jeyakumari, A., Zynudheen, A. A., Parbathy, U. Microencapsulation of bioactive food ingredients and controlled release-a review. *MOJ Food Process Technol*. **2016**, *2*, 6, 214-224.

129. Hosseini, H., Jafari, S. M.  Introducing nano/microencapsulated bioactive ingredients for extending the shelf-life of food products. *Adv Colloid Interface Sci*. **2020,** *282*, 102210.

130. Adepu, S., Ramakrishna, S. Controlled drug delivery systems: Current status and future directions. *Molecules* **2021,** *26*, 19, 5905.

131. Wang, Y., Li, P., Tran, T. T. -D., Zhang, J., Kong, L. Manufacturing techniques and surface engineering of polymer-based nanoparticles for targeted drug delivery to cancer. Nanomaterials **2016**, *6*, 26-43.

132. Carvalho, I. T., Estevinho, B. N., Santos, L. Application of microencapsulated essential oils in cosmetic and personal healthcare products – a review. *Int. J. Cosmet. Sci.* **2015**, *38*, 2, 109-119.

# Chapter 2

# Dual Responsive Cellulose Microspheres with High Solid-State Fluorescence Emission

Contents of this chapter is published in, "*Colloids Surf., A Physicochem Eng. Asp.* **2020**, *591*, 124510−124519" and reproduced with permission from Elsevier.

## 2.1. Introduction

Functional microspheres or microbeads have attracted significant interest due to their broad applications in the fields of chromatography,[1] water treatment,[2] protein/enzyme immobilization,[3,4] solid-phase synthesis support,[5] drug loading, drug release,[6] magnetic resonance imaging,[7] cell labeling and separation,[8] biosensors,[9] etc. Various polymer matrices have been used to form these beads including poly(styrene),[10] poly(ethylene),[11] poly(propylene),[12] chitosan,[13] poly(ethylene glycol dimethacrylate-n-vinyl imidazole),[14] cellulose and its derivatives. These beads have been doped with various organic as well as inorganic dopants such as iron oxide nanoparticles,[15,16] quantum dots,[17,18] tungsten carbide,[19] nickel powder,[20] titanium oxide ($TiO_2$),[21] etc. Due to the added functionality brought by dopant they are termed as "functional beads".[22]

Among various polymers used for the preparation of microspheres, polysaccharides offer excellent chemical and mechanical properties along with properties such as non-toxicity, low cost, renewability, biodegradability, and natural abundance. Cellulose is preferred over other synthetic non-biodegradable polymers such as poly(ethylene), poly(styrene), poly(propylene), etc. Further, the presence of multiple hydroxyl groups makes cellulose amenable to functionalization. Almost all reports on cellulose-based microbeads involve dissolving a cellulose derivative such as cellulose acetate,[23] cellulose stearate,[24] cellulose xanthate (via viscose method),[25] 2,3-dialdehyde cellulose,[26] etc. The difficulty in dissolving and processing native cellulose arises from its strong intra- as well as inter-molecular hydrogen bonding.[27] Various specific solvents have been used for cellulose dissolution such as Dimethylacetamide/Lithium chloride (DMAc/LiCl),[28] N-Methylmorpholine N-oxide (NMMO),[29] acetone/dimethyl sulfoxide (DMSO),[30] Cuprammonium hydroxide (cuoxam),[31] sodium hydroxide/urea (NaOH/Urea),[32] NaOH/$CS_2$ (Cellulose xanthate).[25] These solvents either involve high temperature (as high as 100 °C) or cryogenic conditions (as low as -20 °C)

making the processes energy intensive. Recently, Abe *et al.*[33] have reported dissolution of cellulose at room temperature using 40% tetrabutylammonium hydroxide (TBAH) and tetrabutylphosphonium hydroxide (TBPH). The fact that cellulose can be dissolved at ambient conditions and TBAH can be recovered and reused. This makes TBAH a greener solvent for cellulose processing. Herein, we made an attempt to prepare cellulose microspheres having dual functionality, viz. magnetic and fluorescent property using 40% aqueous TBAH solution. Independently, either the magnetic nanoparticles or the fluorophore could be loaded/incorporated into the cellulose material to a larger extent. Larger incorporation of the magnetic material could in principle impart larger magnetic properties to the modified cellulose. As far as the fluorophore is concerned, there could be a higher limit of incorporation beyond which the emission would start to decrease due to solid-state quenching effects due to the proximity of the fluorophore. In presence of a metal nanoparticle, this upper limit would be reached much earlier due to the added quenching effect introduced by the presence of the heavy metal. Despite such constraints, through our systematic investigations, the current work demonstrates a workable loading of magnetic nanoparticles along with covalent incorporation of the fluorophore pyrene which has imparted the highest reported solid-state fluorescence quantum yields. Dual functional microsphere are more preferred as security features such as authenticate documents for example passports, degree certificates, currency notes, financial documents etc. as it increase the counterfeit resistance compared to monofunctional microspheres. In earlier reports, the fluorescent molecules such as rhodamine B dye[24] or quantum dots[34] have been physically blended in the magnetic microspheres to prepare dual functional cellulose nanospheres or nanoparticles making them susceptible to leaching. In other reports, cellulose is either physically added or covalently linked to prepare monofunctional cellulose microbeads but the solid-state quantum yield is not reported and only solution based quantum yield is reported. In this work, fluorescent molecule pyrene has been covalently linked

to the microspheres making them more stable. Pyrene is a well-studied fluorophore with long fluorescence lifetimes, large quantum yield and formation of excimers.[35-40] In **Table 2.1**, current work is compared with the previously reported work and distinguishes the novelty of the work. To the best of our knowledge, this is the first report demonstrating a facile approach to prepare dual functional i.e., fluorescent magnetic cellulose microspheres with high solid-state fluorescence emission and significant magnetization.

**Table 2.1** Comparison of reports on functionalized cellulose from literature.

| System | Process | Magnetic property | Fluorescence property | Solid-state Quantum Yield ($\Phi$) | Leaching resistance | Ref. |
|---|---|---|---|---|---|---|
| Cellulose nanofibers (CNF) | Spray drying | No | Yes (water-soluble CdTe quantum dots (QDs) | Not reported | No (physical blends) | 18 |
| Cellulose stearate | Nanoprecipitation | Yes ($Fe_3O_4$) | Yes (Stearoylaminoethyl rhodamine B) | Not reported | No (physical blends) | 24 |
| Surface adsorbed quantum dots ethyl cellulose nanospheres | Spray drying | Yes (oleic acid capped $Fe_3O_4$) | Yes (Cysteamine-capped CdTe QDs) | Not reported | No (physical blends) | 34 |
| Pyrene labelled hydroxypropyl cellulose | Microbeads were not prepared | No | Yes (Covalently linked pyrene butyric acid) | Not reported Methanol: 0.6 $H_2O$: 0.5 | Yes | 41 |
| Allyl cellulose derivative | Microbeads were not prepared | No | Yes | Not reported. DMSO: 0.38 | Yes (Covalently linked) | 42 |
| **Microcrystalline cellulose** | **Precipitation and ball milling** | **Yes ($Fe_3O_4$ NPs)** | **Yes (PBA)** | **Yes. $\Phi_{max}$ 0.57** | **Yes** | **This Work** |

## 2.2.  Materials and Methods

Sigmacell cellulose Type 50 (50 μm) micro crystalline cellulose (MCC), Iron (II, III) oxide nanoparticles (50-100 nm particle size), 40 wt.% tetrabutylammonium hydroxide (TBAH), 1-

pyrenebutyric acid (PBA), 4-dimethylaminopyridine (DMAP), N, N'-Dicyclohexylcarbodiimide (DCC) were all purchased from Sigma-Aldrich Chemicals Co. LLC and used without further purification. Sodium Chloride (LR Grade) and methanol (AR Grade) were acquired from Leonid Chemicals Pvt. Ltd. and used without further purification. Dimethylformamide (DMF) was purchased from Leonid Chemicals Pvt. Ltd. and was dried using standard procedure and kept over molecular sieves (4 Å×1.5 mm).

### 2.2.1. *Preparation of Magnetic Cellulose Beads (MB)*
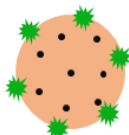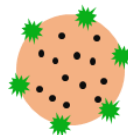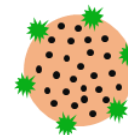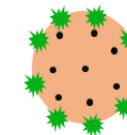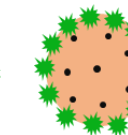
In a vial, 4, 8 and 12 wt.% $Fe_3O_4$ NPs (with respect to the weight of cellulose) were uniformly dispersed in 40 % aqueous TBAH using vortex mixer and sonication for 10 min. To the above dispersion, MCC was dissolved to obtain a pale-yellow solution with a final concentration of 7 wt.%. This solution was degassed and ejected dropwise using a 5 mL syringe with an 18-gauge (0.838 mm inner diameter) needle placed at a height of 8-10 cm from a 250 mL beaker containing 20% saline as coagulation bath. As the droplets contacted the anti-solvent coagulation bath, they precipitated into spherical beads. Beads were washed with deionized water three times and were lyophilized using Labconco make Freeze Dryer.

### 2.2.2. *Preparation of Fluorescent Magnetic Cellulose Micro-beads (FMB)*

The as-prepared MB was reacted with PBA using a previously reported procedure with slight modifications.[43] In brief, in a two-neck round-bottomed flask containing MB (1 g, 6.17 mmol glucopyranose units), 50 mL dry DMF was added under nitrogen atmosphere. In separate two-neck round-bottomed flasks varying equivalents of PBA (1.76 g, 6.17 mmol; 3.55 g, 12.34 mmol; 7.1 g, 24.68 mmol), and DMAP (0.75 g, 6.17 mmol; 1.5 g, 12.34 mmol; 3.0 g, 24.68 mmol) were added to DMF. Each of these mixtures was combined separately with separate flasks containing MB using a glass syringe. The reaction mixture was stirred for another 10 min and cooled to 0 °C. Finally, DCC (1.27 g, 12.34 mmol; 2.54 g, 24.68 mmol; 5.08 g, 49.36 mmol) was added as per the amount of PBA and the mixture stirred for another 30 min at 0 °C.

The reaction mixture was stirred for another 24 h at ~25 °C. After 24 h, these fluorescence magnetic cellulose beads (FMB) were recovered by centrifugation, washed with deionized water three times and air dried at ambient conditions. After complete drying, these beads were crushed using a ball mill (Retsch Mixer Mill MM 400) for 45 min at a frequency of 25 s$^{-1}$ to obtain a free-flowing powder and was further characterized using various techniques. The samples were coded as shown in **Table 2.2**. For example, in FMB411, FMB denotes fluorescent magnetic beads, the last two digits signifies the ratio of no. of equivalents of glucopyranose units in beads to pyrene butyric acid and preceding number indicates iron oxide NPs content in the beads in wt.% w.r.t cellulose, i.e., FMB411 implies 4 wt.% iron nanoparticles, and glucopyranose units to pyrene butyric acid ratio is 1:1.

**Table 2.2** Sample coding with different stoichiometry.



| | FMB011 | FMB411 | FMB811 | FMB1211 | FMB412 | FMB414 |
|---|---|---|---|---|---|---|
| % Iron oxide NPs | 0 | 4 | 8 | 12 | 4 | 4 |
| Molar ratio of glucopyranose units to PBA | 1 | 1 | 1 | 1 | 2 | 4 |



**Scheme 2.1** Reaction of cellulose beads with pyrene butyric acid (PBA).
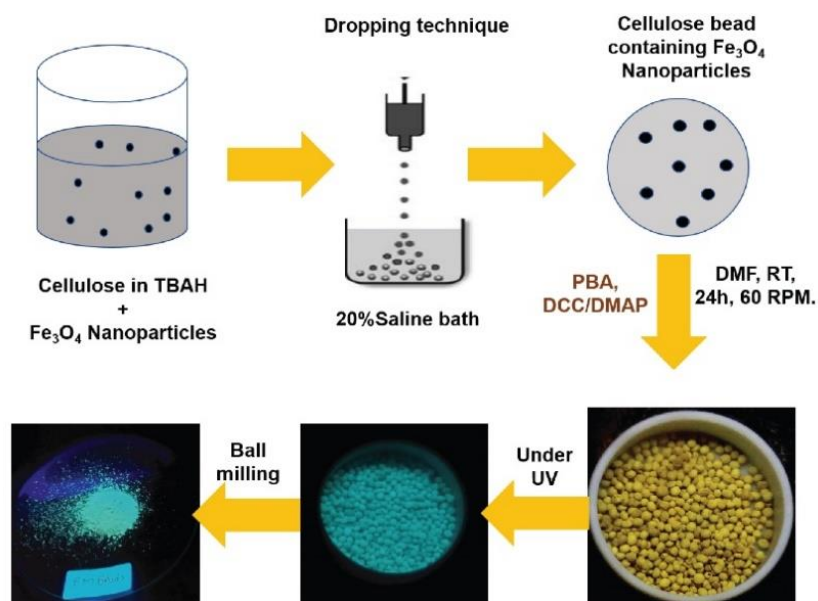
**Scheme 2.2** Preparation of fluorescent magnetic beads (FMB).

*2.2.3. Characterization*

FTIR was used to confirm the reaction between pyrene butyric acid and magnetic cellulose beads. KBr pellets were prepared using the standard procedure, and FTIR spectrum was acquired using Perkin Elmer Q5000 GX IR instrument with 32 scans and resolution of 4 cm$^{-1}$. The reaction of magnetic beads with pyrenebutyric acid was also confirmed using solid-state $^{13}$C Cross Polarization/Magic Angle Spinning (CP/MAS) NMR. For this purpose, beads were prepared without iron oxide NPs, and this powder (FMB011) was analyzed using Bruker Spectrometer (200 MHz) broad band 4 mm CP/MAS probe. Scanning electron microscope (SEM) with tungsten filament as electron source (FEI, QUANTA 200 3D) was used at 15 kV to obtain images of magnetic beads. FMB411 was dispersed in acetone at a concentration of 1 mg/mL and was drop casted on silicon wafers. The solvent was allowed to evaporate at room temperature (~25 °C) in air for 12 h. The samples were sputter-coated with gold to dissipate charge. Energy dispersive X-ray spectroscopy (EDX) was used along with SEM for the elemental mapping. XPS analysis was performed using ThermoScientific K-Alpha (+).

FMB411 sample was used for this analysis. The free-flowing powder was compressed to form a pellet of diameter 10 mm and data was recorded using this pellet. Magnetic measurements were made on an EG&G PAR 4500 vibrating sample magnetometer (VSM). Magnetization (M) as a function of magnetic field (H) was measured in the field range ±15 kOe. Thermogravimetric analysis was performed to quantify the amount of $Fe_3O_4$ NPs in the cellulose beads using Perkin Elmer thermal analyzer STA 6000 by heating the samples from 40 °C to 800 °C at a heating rate of 10 °C/min under nitrogen. Solid-state UV-VIS spectra were recorded using Agilent Cary 5000 series UV-VIS spectrophotometer, and the measurements were performed using a solid sample holder. Solid-state quantum yield ($\Phi_{Solid-state}$) was determined using integrating sphere Quanta Horiba Jobin Yvon Fluorolog 3 spectrophotometer attachment using Tris-(8-hydroxyquinolinato) aluminium as a standard sample. Quantum yield ($\Phi$) is defined by the number of photons emitted divided by the number of photons absorbed. It is the emission efficiency of the fluorophore. The sample was inserted into the chamber and was excited at $\lambda_{max}$ = 355 nm, and the emission spectrum was obtained in the range $\lambda_{excitation}$= 365-700 nm. Steady-state fluorescence studies were performed using Horiba Jobin Yvon Fluorolog 3 having a Xenon lamp of 450 W. The emission and excitation slit was maintained at 1 nm throughout the experiments, and the data was obtained in "S1" mode and both emission and excitation spectrums were recorded. Fluorescence microscopic images were acquired using Carl Zeiss Fluorescence microscope using filter Alexa Fluor 350. A well-dispersed solution of FMB obtained by sonication was drop casted on a glass slide and then covered with a coverslip. The slide was examined using 10X objective with a 346 nm excitation light and 442 nm emission light under Carl Zeiss Axio Observer Z1 microscope.

## 2.3. Results and Discussion

Fluorescent magnetic beads (FMB) were synthesized as per **Scheme 2.1** by optimizing the process variables. Since the reaction occurs at the accessible hydroxyl groups at the surface

and not in bulk, only partial modification of primary hydroxyl groups occurs. In the scheme, partial modification is shown by showing modification at one primary hydroxyl group only. We found that 7 wt.% MCC in aqueous TBAH provides the required viscosity to form beads consistently. Above this concentration, higher viscosity leads to the formation of a continuous stream of fluid when ejected through a syringe pump. In the regeneration process, saline disrupts the strong ionic interaction between cellulose and TBAH and allows the formation of stronger intra- and intermolecular hydrogen bonding between the cellulose chains resulting in precipitated beads.[44]

In order to impart fluorescence responsiveness, the magnetic cellulose beads were reacted with PBA. This esterification reaction was confirmed by FTIR and solid-state NMR. The stretching band appearing at 1687 cm$^{-1}$ [45,46] (**Fig. 2.1a**) corresponding to (C=O) stretching of PBA was shifted to 1704 cm$^{-1}$ due to esterification of the carboxyl group of PBA with cellulose hydroxyl group. The reaction was also confirmed by $^{13}$C CP/MAS solid-state NMR (**Fig. 2.1c**) where the peaks appearing at 126.6 ppm and 191.19 ppm correspond to aromatic and carbonyl carbons of PBA respectively. Also, peaks appearing at 105.2, 89.02, 84.3, 75.0, 72.0 and 65.5 ppm correspond to the cellulose backbone peaks (**Fig. 2.1b**) and peaks appearing in **Fig. 2.1c** at 33.7 ppm and 26.1 ppm correspond to the methylene groups of pyrenebutyric acid.

**(b)**

Peaks labeled: 105.28, 89.10, 84.33, 75.17, 72.79, 65.21

Chemical Shift (ppm)



**(c)**

Carbonyl Peak — 191.19

Aromatic Peaks — 126.64

Cellulose Backbone Peaks — 105.23, 89.02, 84.32, 74.95, 71.99, 65.48

Aliphatic Peaks — 33.69, 26.12

Chemical Shift (ppm)
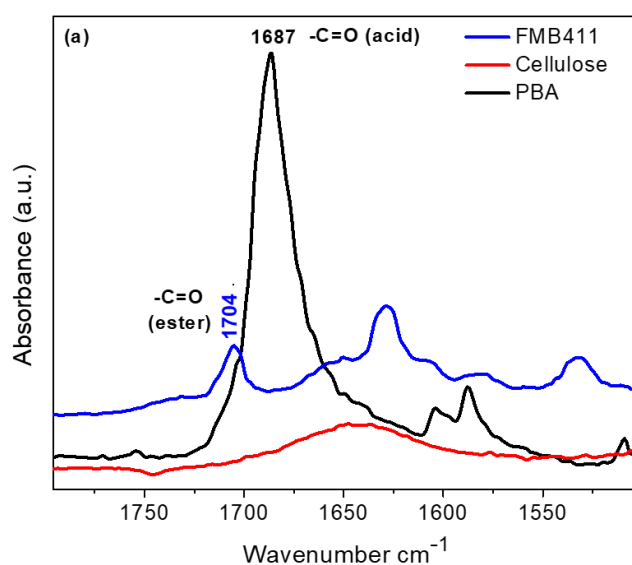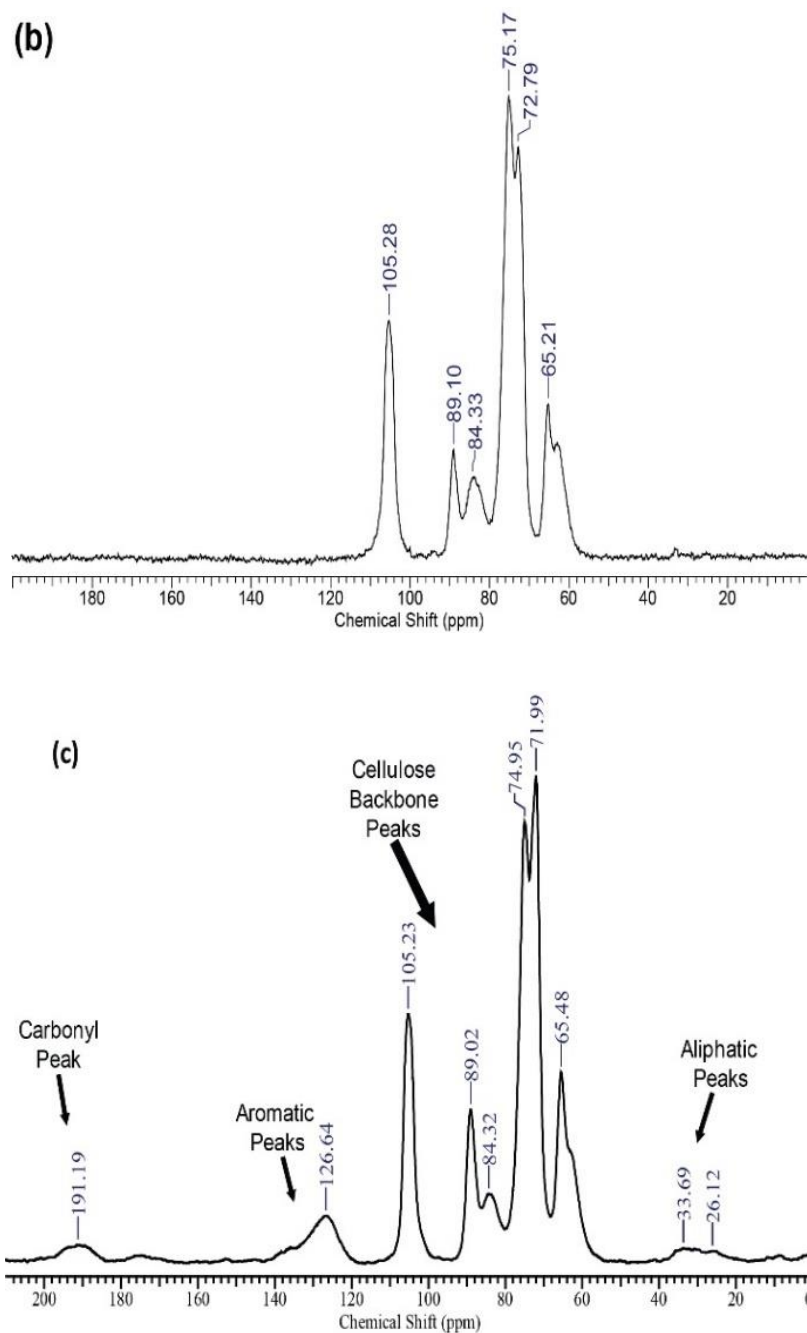
**Figure 2.1** (a) FTIR spectrum of FMB411; ^{13}C CPMAS solid-state NMR of (b) cellulose and (c) FMB011.

Presence of $Fe_3O_4$ NPs in the beads was confirmed by elemental mapping using EDX as shown in **Fig. 2.2**, where it is observed that the iron oxide NPs, shown in red color, were homogeneously dispersed throughout the matrix in fluorescent magnetic microspheres.[47]
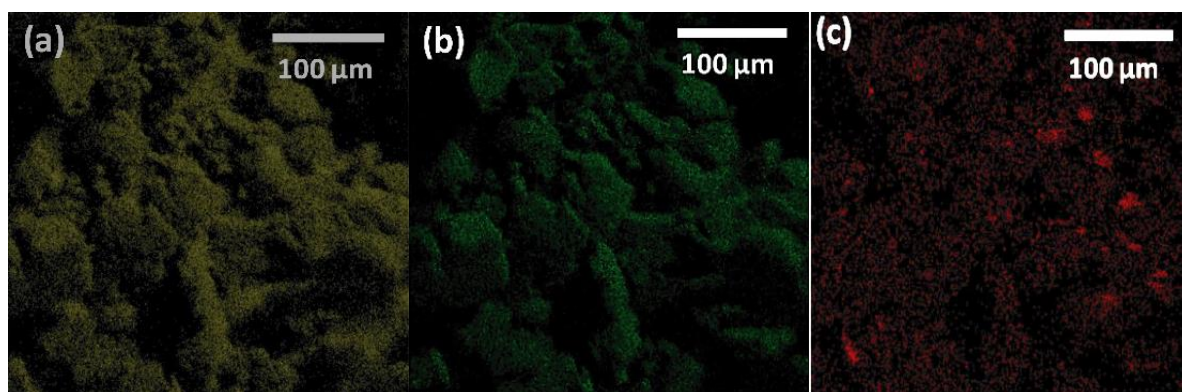
**Figure 2.2** Elemental mapping of FMB411 (a) for carbon (yellow) (b) for oxygen (green) and (c) for $Fe_3O_4$ NPs (red).
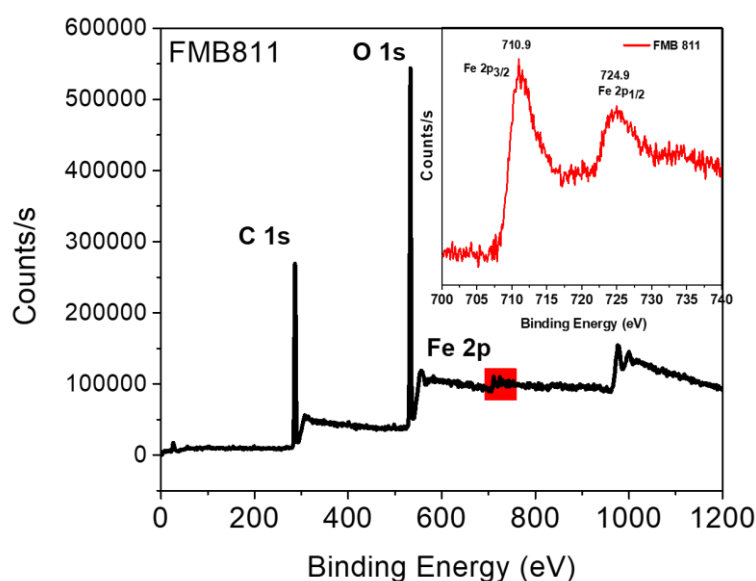


**Figure 2.3** XPS data of FMB811 and zoomed plot for Fe 2P (inset red color).

XPS analysis was used to probe the surface of FMB811. In the spectra (**Fig. 2.3**), in addition

to C 1s and O 1s signals (located at about 284.8 and 532 eV, respectively) two peaks appearing

at binding energies of 710.9 and 724.19 eV (**Fig. 2.3 (inset)**) could be attributed to Fe 2p3/2

and Fe 2p1/2 respectively[48,49] due to the presence of $Fe_3O_4$ NPs.

Thermogravimetric analysis was performed to quantify the amount of $Fe_3O_4$ NPs in the

fluorescent magnetic beads. The inorganic $Fe_3O_4$ NPs remained as a residue after heating the

sample to 800 °C whereas no residue was obtained in case of cellulose beads without $Fe_3O_4$

NPs. Samples FMB011 (contains no $Fe_3O_4$ NPs), FMB411, FMB811 and FMB1211 yielded a

residue approximately 0%, 4.42%, 8.24%, and 11.82% respectively as shown in **Fig. 2.4**. This serves to confirm the successful incorporation of $Fe_3O_4$ in the cellulose matrix without much loss during the precipitation. The beads were also subjected to multiple washing cycles with deionized water to check the stability of $Fe_3O_4$ NPs. The amount of $Fe_3O_4$ NPs in the beads remained same even after washing.
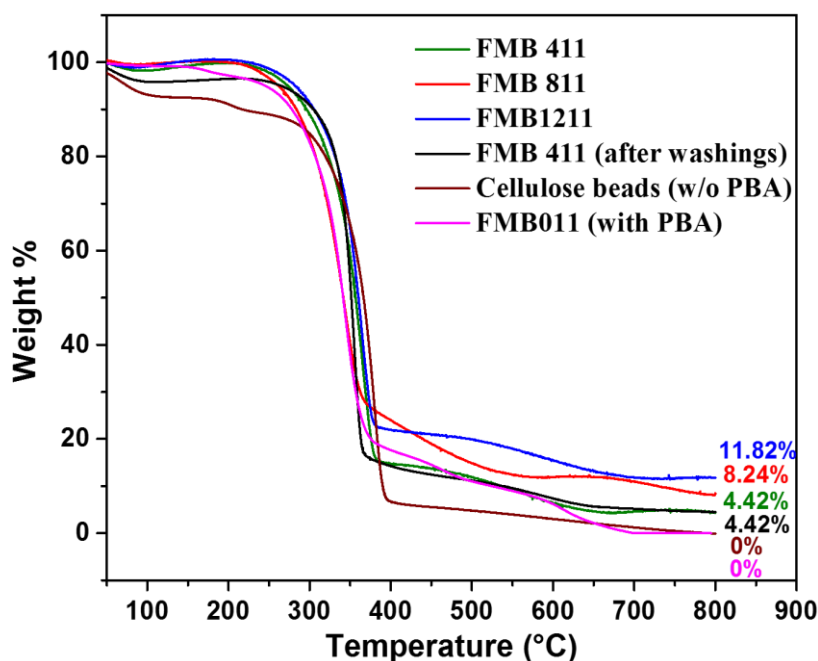


**Figure 2.4** Thermogravimetric analysis data for FMB411, FMB811, FMB1211, FMB411 (after washing), cellulose beads without PBA and FMB011 (with PBA).

Scanning electron microscopy (SEM) of FMB (**Fig. 2.5a**) revealed beads of spherical shape of around 1000 µm or more in size, which after ball milling yielded irregular shaped particles with size ranging between 1-10 µm (**Fig. 2.5c**). The magnetic beads were porous with interconnected pores which could be due to the lyophilization process, where the water present in the beads crystallizes and sublimates leaving behind pores ranging from 0.5 µm to 2 µm (**Fig. 2.5b**).
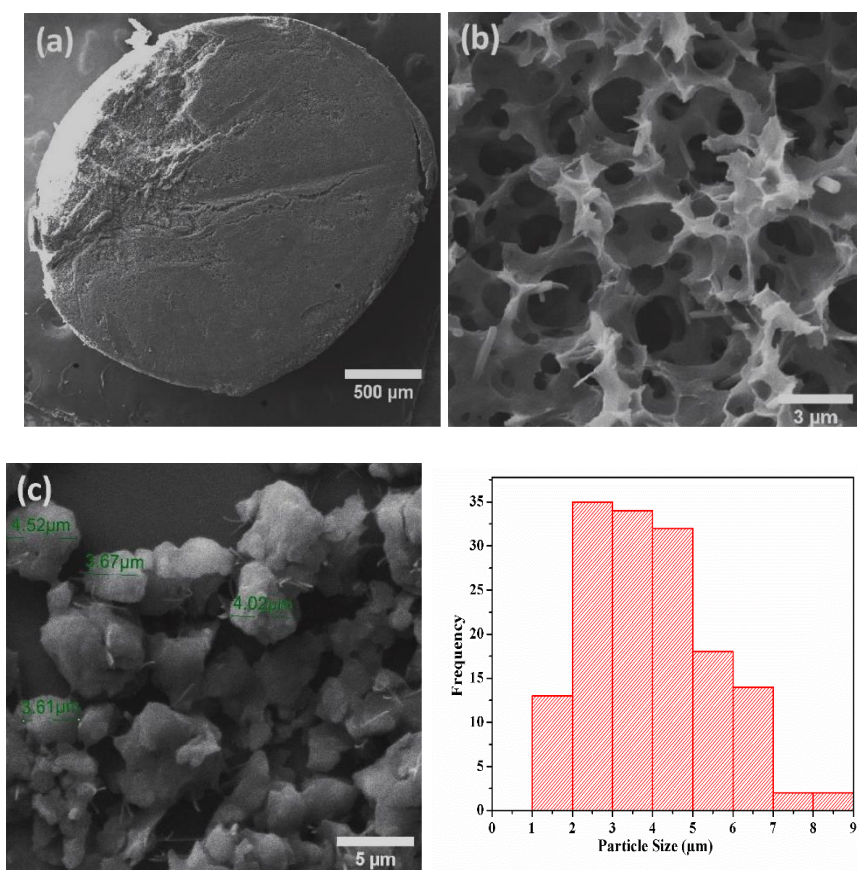
**Figure 2.5** SEM images of (a) magnetic bead, (b) magnified image of the magnetic bead, (c) FMB411, and (d) histogram plot of the particle size distribution of the ball milled FMB411.
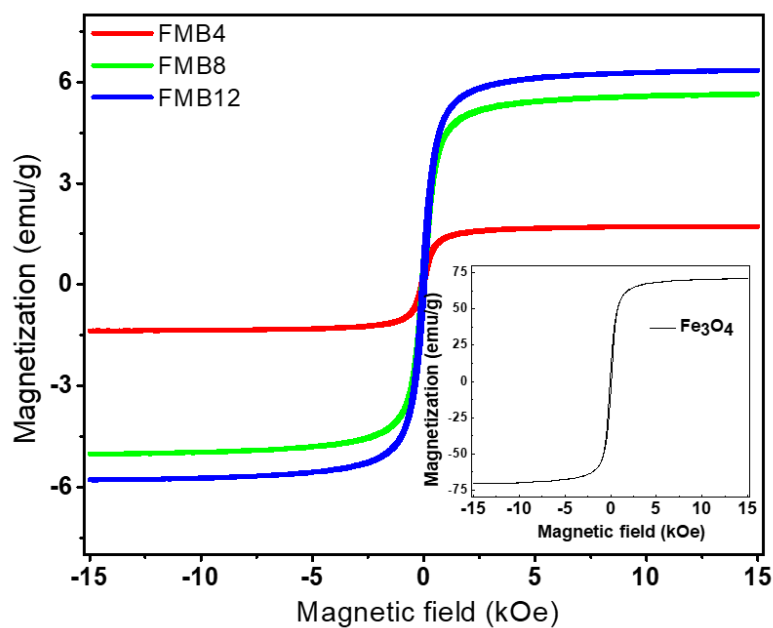


**Figure 2.6** VSM MH Hysteresis of FMB411, FMB811, FMB1211 and $Fe_3O_4$ NPs (inset) and an image showing magnetic responsiveness of the beads (inset).

Magnetization versus field curves of the $Fe_3O_4$ NPs, FMB411, FMB811, and FMB1211 were measured at room temperature, using a VSM, up to a maximum field strength of 15 kOe (**Fig. 2.6**). A small magnetic hysteresis loop is observed for $Fe_3O_4$ with a coercivity of ~70 Oe (inset in **Fig. 2.6**), suggesting that the $Fe_3O_4$ nanoparticles are not superparamagnetic. The iron oxide nanoparticles show a magnetization of ~71 emu/g at high fields which is less than the saturation magnetization for bulk $Fe_3O_4$ (~80 emu/g). The reduced magnetization is due to the smaller size of the nanoparticles. The magnetizations of FMB411, FMB811, and FMB1211 at 15 kOe are obtained as 1.54 emu/g, 5.37 emu/g, and 6.08 emu/g, respectively. The large reduction in the magnetization of the microspheres with respect to that of the $Fe_3O_4$ NPs is due to the incorporation of the particles in the non-magnetic cellulose matrix. The experimental magnetizations are comparable to the expected values of 2.85, 5.70, and 8.54 emu/g for 4, 8, and 12 wt.% of $Fe_3O_4$ in FMB411, FMB811, and FMB1211, respectively. Such lower saturation magnetization of magnetic beads as compared to that of bare magnetic nanoparticles has been reported in the literature, where incorporation of magnetic particles in cellulose or other non-magnetic matrix results in reduced magnetization due to the low concentration of the magnetic nanoparticles such as $MnFe_2O_4$ or $Fe_3O_4$ in the final matrix.[50-52] Although the FMB samples have low magnetization, they exhibit sensitive magnetic responsiveness and therefore, the magnetization is still sufficient enough for security and diagnostic applications as can be compared with the previous report by Xie *et al.*[34] where the saturation magnetization of fluorescent magnetic nanospheres exhibit 0.025 emu/g of saturation magnetization for the applications in security and anti-counterfeiting. In another report by Wu *et al.*,[53] they have synthesized magnetic cellulose composites for applications in packaging, security paper, and information storage by using citric acid modified $Fe_3O_4$ nanoparticles exhibiting 8.00 to 9.60 emu/g of saturation magnetization where the loading of iron oxide nanoparticles is 7.5 wt.% and 13.2 wt.%. In another report by Luo *et al.* (2009),[15] where they synthesized $Fe_3O_4$/cellulose

microspheres for magnetic induced protein delivery. These microspheres exhibit 5.16 to 8.36 emu/g of saturation magnetization upon loading 10.2 to 19.6 wt.% $Fe_3O_4$ nanoparticles.

In **Fig. 2.7**, the solid-state UV-VIS absorption spectra of two of the fluorescent magnetic beads –FMB011 (no iron content, only pyrene incorporation) and FMB411 (both pyrene and iron incorporated) is compared. The sharp peak observed for FMB011 at 355 nm wavelength corresponds to the absorbance of PBA covalently linked to cellulose beads. The samples were irradiated at 355 nm, and their emission spectra were recorded between 365-700 nm.
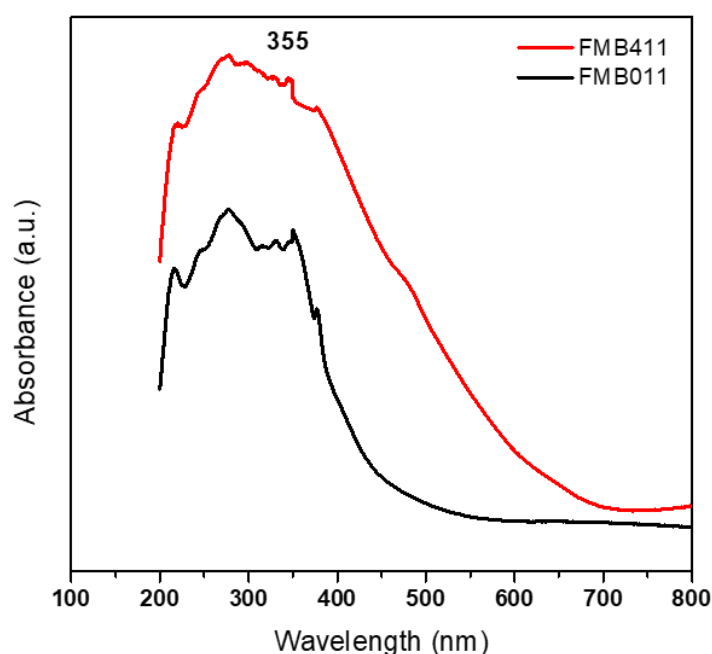


**Figure 2.7** Solid-state UV-VIS spectrum of FMB411 and FMB011.

Fluorescence quantum efficiency is not exactly equal to fluorescence intensity but related to the fluorescence intensity; greater the intensity greater is the emission quantum yield. The absolute quantum yield is defined as the ratio of the number of photons absorbed, to the number of photons emitted by a material. The fluorescence intensity (F) is proportional to the amount of light absorbed and $F = \Phi(I_0 - I)$, where $\Phi$ is the emission quantum yield, $I_0$ and $I$ are intensity of incident and transmitted light respectively. As per Beer-Lambert law, $I/I_0 = 10^{-\varepsilon lc}$ where $\varepsilon$ is molar extinction coefficient, $l$ is the optical path length, and $c$ is the concentration. Combining

these two, we get $F=\Phi I_0(1-10^{-\varepsilon lc})$. Thus the fluorescent intensity is linear with concentration and quantum yield at low concentration of the fluorophore. The absolute emission quantum yield measurements in the solid-state are carried out by preparing the sample as a fine powder and similar quantities are used as far as possible for every sample and measured under identical experimental conditions. The calculation of the absolute emission quantum yield takes into account the excitation profile of the sample (absorption), which automatically accounts for the actual amount of fluorescent dye present in the sample.[54]

**Fig. 2.8a** shows the normalized emission spectra of fluorescent magnetic microbeads containing both pyrene and iron with the iron content kept constant at 4 wt.% and pyrene incorporation varied from 1 to 4 equivalents. The fluorescent magnetic microbeads exhibited broad emission characteristic of pyrene excimer emission. Generally, pyrene solutions at low concentrations ($< 10^{-5}$ M) are characterized by emission with vibronic fine structures in the 370 - 390 nm range. As concentration increases above $10^{-5}$ M, the monomeric emission decreases and a broad, featureless emission appears beyond 390 nm, known as the pyrene excimer emission, which is due to the aromatic $\pi$-$\pi$ interaction of the pyrene moieties. In the present work, even at the lowest pyrene incorporation i.e., FMB011 the emission spectra were characterized by noticeable excimeric characteristics. For all samples, the pyrene monomeric emission which is usually observed at 377 nm and 398 nm was almost negligible with only a small shoulder peak observed at 377 nm for FMB411 and FMB412. It could be speculated that the covalent binding of the pyrene on to the cellulose surface enables the $\pi-\pi$ interaction among the pyrene units leading to the excimeric emission. It is quite interesting to note that the excimeric emission was observed with peak maxima at 440 nm and not at 480 nm, which usually recognized as the typical pyrene excimeric emission. Pyrene as a fluorophore is greatly influenced by its environment, and the excimeric emission observed around 440 nm is usually associated with the pyrene in a constrained surrounding such as embedded in films, adsorbed

on surfaces or in solids where they are not oriented favorably with respect to one another.[55]

With increase in pyrene content, we could observe the emergence of the characteristic pyrene

excimer emission band at 480 nm as a shoulder peak in FMB412 and FMB414. **Fig. 2.8b** shows

the excitation spectra collected at 450 nm for the three samples. The excitation spectra of
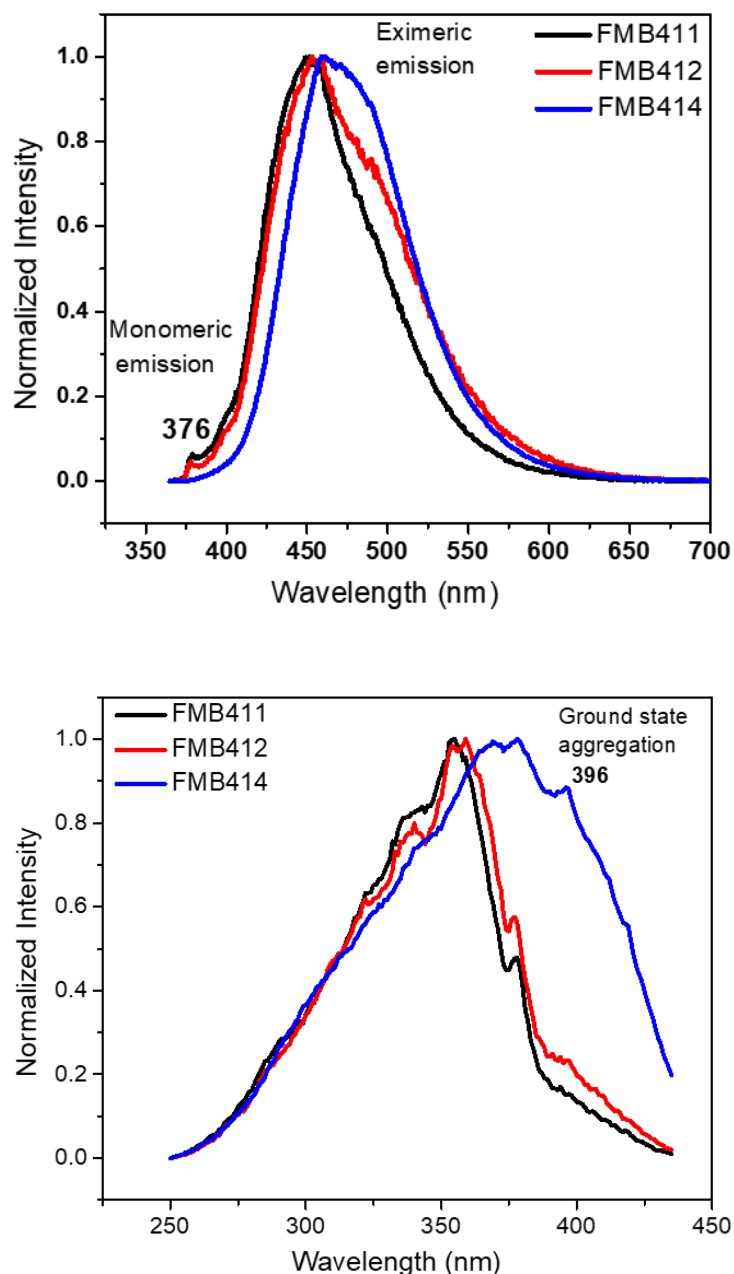
**Figure 2.8** Steady-state fluorescence spectrum (a) emission spectrum and (b) excitation spectrum.

FMB411 and FMB412 were very similar with vibronic fine structures as well as a prominent $S_1 \leftarrow S_0$ absorption band at 375 nm. The excitation spectrum of FMB414, on the other hand, was distinct with a prominent shoulder peak at 396 nm, which is usually associated with static excimer.[56] The static excimer has its origin in pre-arranged pyrene moieties in the ground state. FMB414, with the highest pyrene incorporation has pre-arranged pyrene moieties in close proximity in the ground state. The emission quantum yield in the solid-state was also measured using the integrated sphere set up, and the results are shown in **Fig. 2.9a**. As expected, a steady increase in the emission quantum yield was observed with increasing pyrene incorporation in samples FMB411, FMB412, and FMB414 (**Fig. 2.9a**). On the other hand, a clear reduction in emission quantum yield was observed in samples FMB411, FMB811 and FMB1211 having similar pyrene incorporation but with increasing iron oxide content (**Fig. 2.9b**) as $Fe^{3+}$ is an effective quencher of pyrene emission.[57,58,59] Highest solid-state fluorescence of 0.57 is achieved with an FMB414 sample containing both pyrene and iron oxide. FMB414 has 4 wt.% $Fe_3O_4$ incorporation and has been surface modified by reacting with 4 equivalents of pyrene to the glucopyranose units. It is a known fact that the environment of a dye can affects its optical properties. Unlike in solution, the dyes in a microsphere (whether encapsulated or covalently bound) are screened from oxygen or other impurities that can quench its emission. The covalent incorporation not only prevents dye leakage, but it also restricts the mobility of the dye thereby limiting aggregation induced emission quenching. This could form the theoretical basis for the high emission quantum yield in the solid-state. The solid-state fluorescence quantum yield that has been reported for polymeric polystyrene beads containing fluorescent active oligo(p-phenylenevinylene)-based cross-linker (OPV) is as high as 0.72.[60] In another report, pyrene labeled hydroxypropyl cellulose has shown solution state fluorescence quantum yield of 0.6 in water-methanol mixture.[41] The above two reports reveal high quantum yield with mono-functionalization only i.e., it does not contain any other functionality other than fluorescence.

In this report, we have shown dual functionality with high quantum yield which is a significant advancement over existing materials.

The microspheres were observed under epifluorescence microscope (**Fig. 2.10**). All the compositions exhibited green fluorescence under microscope. One can tune the amount of fluorophore and magnetic particle and the dual responsive microspheres can be used in inks for
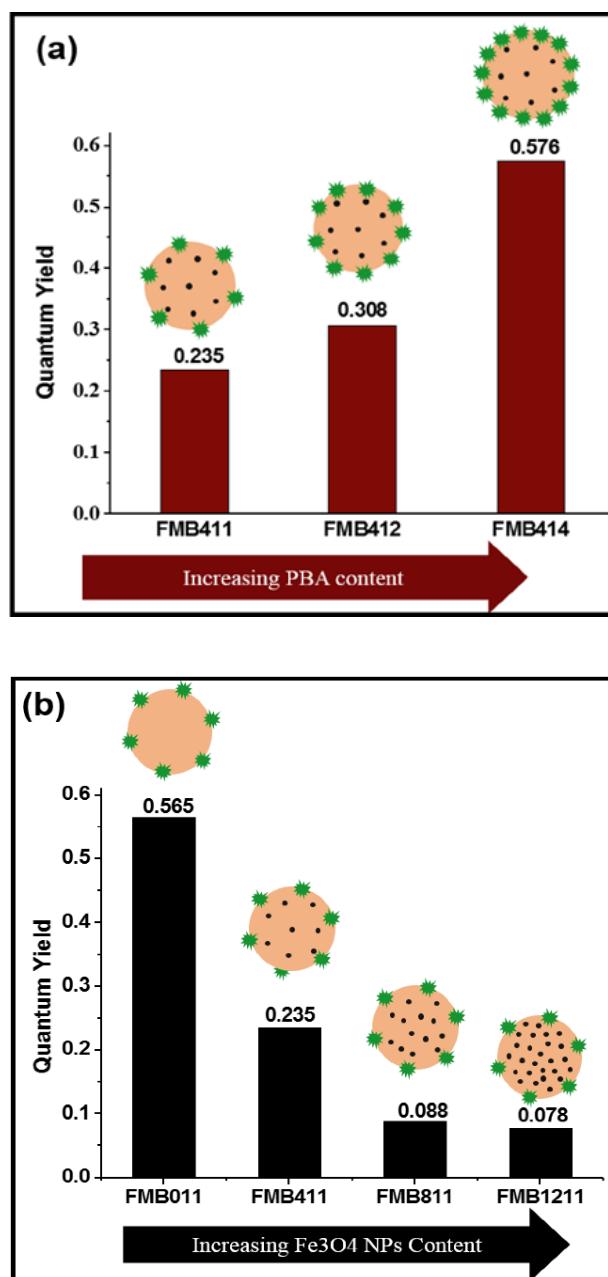


**Figure 2.9** Solid-state quantum yield with (a) varying PBA equivalents and (b) varying Iron oxide NPs.

creating special tags or features in security documents such as passports, degree certificates, currency notes, financial documents etc. according to the desired application. These can be used as overt security features (detectable with UV light source) for authenticating security documents. Having both magnetic and fluorescent characteristics would enhance counterfeit resistance of these security documents. Therapeutic protein molecules can be adsorbed on the magnetic microbeads, wherein the magnetic property can be used for targeted drug delivery, and the fluorescence property can aid in bioimaging.[61,62]
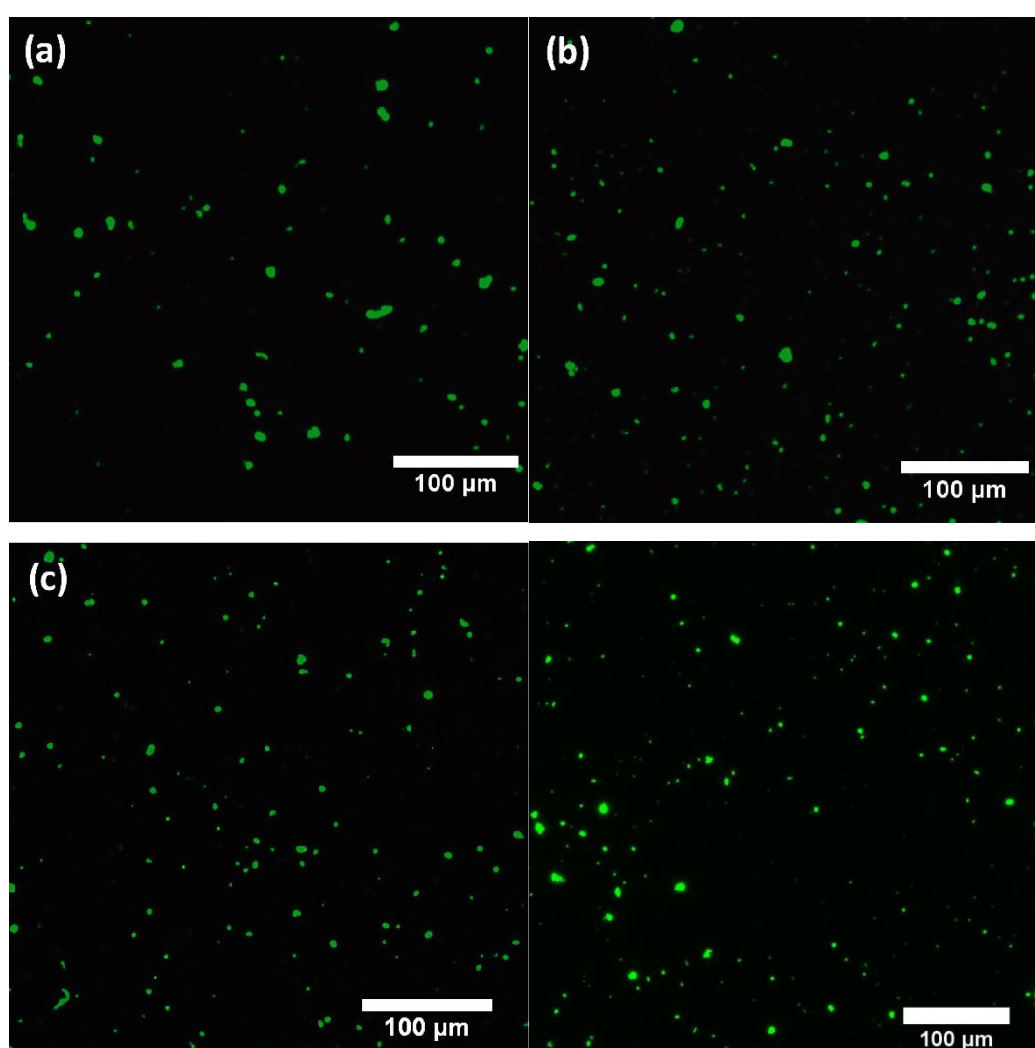


**Figure 2.10** Fluorescent microscope images of (a) FMB011 (b) FMB411 (c) FMB1211 and (d) FMB414 using a green filter.

## 2.4.    Conclusions

A simple and facile process has been developed to prepare dual responsive cellulose microbeads. A greener solvent, i.e., 40% aqueous TBAH, was used to dissolve and process native cellulose into functional microspheres. Microspheres exhibit a saturation magnetization of 2.85 to 8.54 emu/g, which has sufficient responsiveness. The fluorophore 1-pyrenebutyric acid has been covalently linked to the cellulose beads to provide durable fluorescence effect even after subjecting to multiple washing cycles. The quenching effect of $Fe_3O_4$ nanoparticles on fluorophore and solid-state quenching due to aggregation of PBA was studied systematically using solid-state quantum yield experiments and quantum yield as high as 0.57 has been achieved. Such a high quantum yield has not been reported before for dual responsive fluorescent microspheres.

## 2.5.    References

1.  Oliveira, W. D., Glasser, W. G. Hydrogels from polysaccharides. I. Cellulose beads for chromatographic support. *J. Appl. Polym. Sci*. **1996**, *60*, 63-73.

2.  Peška, J., Štamberg, J., Hradil, J. Chemical transformations of polymers. XIX. Ion exchange derivatives of bead cellulose. *Angew. Macromol. Chem*. 1976, *53*, 73-80.

3.  Chen, H., Kaminski, M., Liu, X., Torno, M. A novel human detoxification system based on nanoscale bioengineering and magnetic separation techniques. *Med. Hypotheses* **2007**, *68*, 1071-1079.

4.  Sheldon, R. A. Enzyme immobilization: The quest for optimum performance. *Adv. Syn. & Cat.* **2007**, *349*, 1289.

5.  Luca, L. D., Giacomelli, G., Porcheddu, A., Salaris, M., Taddei, M. Cellulose beads: a new versatile solid support for microwave-assisted synthesis. Preparation of pyrazole and isoxazole libraries. *J. Comb. Chem*. **2003**, *5*, 465-471.

6.  Trygg, J., Yildir, E., Kolalovic, R. Anionic cellulose beads for drug encapsulation and release. *Cellulose* **2014**, *21*, 1945-1955.

7.  Iscan, T., Dokur, Z., Olmez, T. Tumor detection by using Zernike moments on segmented magnetic resonance brain images. *Expert Syst. Appl.* **2010**, *37*, 3, 2540-2549.

8.  Piotr, W., Jesus, R.-C., Dorota, A. K., Assaf, A. G., Sopo, L., Bradley, B., Lu, Q., Hyam, L., Jeff, W. M. B. Magnetoelectroporation: improved labeling of neural stem cells and leukocytes for cellular magnetic resonance imaging using a single FDA-approved agent. Nanomedicine: Nanotechnology. *Biol. Med.* **2006**, *2*, 89-94.

9.  Cui, M., Shao, Z., Li, Z., Lu, D. A kind of composite fluorescence biosensor, its preparation method and application. China Patent 107632002 A, **2018**.

10. Sonawane, S. L., Asha, S. K. Fluorescent polystyrene microbeads as invisible security ink and optical vapor sensor for 4-nitrotoluene. *ACS Appl. Mater. Interfaces* **2016**, *8*, 10590-10599.

11. Kim, J. W., Choi, H. S. Surface crosslinking of high-density polyethylene beads in a modified plasma reactor. *J. Appl. Polym. Sci*. **2002**, *83*, 2921–2929.

12. Sipheira, R., Chawla, A. S., Chang, T. M. S. Enhanced albumin binding to polypropylene beads *via* anhydrous ammonia gaseous plasma. *Biomaterials* **1986**, *7*, 471-473.

13. Iglesias, R. B., Coronilla, R., Concheiro, A. Alvarez-Lorenzo, C. Preparation of chitosan beads by simultaneous cross-linking/insolubilisation in basic pH: Rheological optimization and drug loading/release behavior. *Eur. J. Pharm. Sci.* **2005**, *24*, 77-84.

14. Kara, A., Uzun, L., Besirli, N., Denizli, A. Poly(ethylene glycol dimethacrylate-*n*-vinyl imidazole) beads for heavy metal removal. *J. Hazard. Mater.* **2004**, *106*, 93-99.

15. Luo, X., Zhang, L. High effective adsorption of organic dyes on magnetic cellulose beads entrapping activated carbon. *J. Hazard. Mater*. **2009**, *171*, 340-347.

16. Luo, X., Zhang, L. Immobilization of penicillin g acylase in epoxy-activated magnetic cellulose microspheres for improvement of biocatalytic stability and activities. *Biomacromolecules* **2010**, *11*, 2896-2903.

17. Sathe, T. R., Agrawal, A., Nie, S. Mesoporous silica beads embedded with semiconductor quantum dots and iron oxide nanocrystals: dual-function microcarriers for optical encoding and magnetic separation. *Anal. Chem*. 2006, *78*, 5627-5632.

18. Guan, Q., Song, R., Wu, W., Zhang, L., Jing, Y., Dai, H., Fang, G. Fluorescent CdTe-QD-encoded nanocellulose microspheres by green spraying method. *Cellulose* **2018**, *25*, 7017–7029.

19. Phottraithip, W., Lin, D. -Q., Shi, F., Yao, S. -J. A novel method for the preparation of spherical cellulose-tungsten carbide composite matrix with NMMO as non-derivatizing solvent. *J. Appl. Polym. Sci*. **2011**, *121*, 2985-2992.

20. Xia, H.-F., Lin, D.-Q., Yao, S.-J. Spherical cellulose–nickel powder composite matrix customized for expanded bed application. *J. Appl. Polym. Sci*. **2007**, *104* , 740-747.

21. Lei, Y. -L., Lin, D. -Q., Yao, S. -J., Zhu, Z.-Q. Preparation and characterization of titanium oxide-densified cellulose beads for expanded bed adsorption. *J. Appl. Polym. Sci*. **2003**, *90*, 2848–2854.

22. Gericke, M., Trygg, J., Fardim, P. Functional cellulose beads: preparation, characterization and applications. *Chem. Rev*. **2013**, *113*, 4812-2836.

23. Takeda, Y., Ohba, M., Ueno, M., Saniabadi, A. R., Wakabayashi, I. Cellulose acetate beads activate the complement system but inactivate the anaphylatoxins generated. *Artif. Organs*. **2010**, *34*, 1144–1149.

24. Geissler, A., Scheid, D., Li, W., Gallei, M., Zhang, K. Facile formation of stimuli-responsive, fluorescent and magnetic nanoparticles based on cellulose stearoyl ester via nanoprecipitation. *Cellulose* **2014**, *21*, 4181-4194.

25. Heinze, T., Liebert, T. Unconventional methods in cellulose functionalization. *Prog. Polym. Sci*. **2001**, *26*, 1689–1762.

26. Lindh, J., Carlsson, D. O., Stromme, M., Mihranyan, A. Convenient one-pot formation of 2,3-dialdehyde cellulose beads via periodate oxidation of cellulose in water. *Biomacromolecules* **2014**, *15*, 1928−1932.

27. Holbrey, J. D., Chen, J., Tumer, M. B., Swatloski, R. P., Spear, S. K., Rogers, R. D. Applying ionic liquids for controlled processing of polymer materials. In: Brazel CS, Rogers RD, eds. Ionic Liquids in Polymer Systems: Solvents, Additives, and Novel Applications.  ACS Symposium Series 913, American Chemical Society, Washington DC, **2005**, 71–87.

28. Dupont, A. L. Cellulose in lithium chloride/N, N-dimethylacetamide, optimization of a dissolution method using paper substrates and stability of the solutions. *Polymer* **2003,** *44*, 4117-4126.

29. Fink, H. -P., Weigel, P., Purz, H. J., Ganster, J. Structure formation of regenerated cellulose materials from NMMO-solutions. *Prog. Polym. Sci*. **2001**, *26*, 1473-1524.

30. Courtney, E. J. Method of making a cuprammonium cellulose solution. US Patent 2651582, **1952**.

31. Cai, J., Zhang, L., Zhou, J., Li, H., Chen, H., Jin, H. Novel fibers prepared from cellulose in NaOH/urea aqueous solution. *Macromol. Rapid Commun*. **2004**, *25*, 1558−1562.

32. Sihtola, H., Nizovsky, B. Process for manufacturing cellulose xanthate and viscose prepared from said cellulose xanthate. US Patent 3728330 A, **1971**.

33. Abe, M., Fukaya, Y., Ohno, H. Fast and facile dissolution of cellulose with tetrabutylphosphonium hydroxide containing 40 wt% water. *Chem. Commun.* **2012**, *48*, 1808-1810.

34. Xie, Y., Wu, Y., Chub, M., Yub, X., Wu, Q. A highly efficient route for preparing porous magnetic nanospheres with surface-adsorbed quantum dots. *J. Exp. Nanosci.* **2013**, *8*, 752-761.

35. Birks, J. B. Photophysics of Aromatic Molecules; Wiley/ Interscience: New York, **1970**.

36. Lakowicz, J. R. Principles of Fluorescence Spectroscopy, 3rd ed.; Kluwer Academics/Plenum: New York, **2006**.

37. Berlman, I. B. Handbook of fluorescence spectra of aromatic molecules; Academic Press: New York, **1971**.

38. Winnik, F. M. Photophysics of preassociated pyrenes in aqueous polymer solutions and in other organized media. *Chem. Rev.* **1993**, *93*, 587−614.

39. Conlon, P., Yang, C. J., Wu, Y., Chen, Y., Martinez, K., Kim, Y., Stevens, N., Marti, A. A., Jockusch, S., Turro, N. J., Tan, W. Pyrene excimer signaling molecular beacons for probing nucleic acids. *J. Am. Chem. Soc.* 2008, 130, 336−342.

40. Birks, J. B., Dyson, D. J., Munro, I. H. The relations between the fluorescence and absorption properties of organic molecules. *Proc. R. Soc. London, Ser. A* **1963**, *275*, 135−148.

41. Winnick, F. M., Winnick, M. A., Tazuke, S. Synthesis and characterization of pyrene-labeled (hydroxypropyl)cellulose and its fluorescence in solution. *Macromolecules* **1987**, 20, 38-44.

42. Hu, H., Wang, F., Yu, L., Sugimura, K., Zhou, J., Nishio, Y. Synthesis of novel fluorescent cellulose derivatives and their applications in detection of nitroaromatic compounds. *ACS Sustainable Chem Eng.* **2018**, *6*, 1436−1445.

43. Neises, B., Steglich, W. Simple method for the esterification of carboxylic acids. *Angew. Chem. Int. Ed.* **1978**, *17*, 522-524.

44. Alves, L., Medronho, B., Antunes, F. E., Mignuel, M. G., Lindman, B., Romano, A. On the role of hydrophobic interactions in cellulose dissolution and regeneration: colloidal and molecular solutions. *Colloids Surf., A Physicochem Eng. Asp.* **2015**, *483*, 257-263.

45. Majeed, S., Filiz, V., Shishatskiy, S., Wind, J., Abetz, C., Abetz, V. Pyrene-POSS nanohybrid as a dispersant for carbon nanotubes in solvents of various polarities: its synthesis and application in the preparation of a composite membrane. *Nanoscale Res. Lett.* **2012**, *7*, 296-306.

46. Yang, S., Wu, X., Wang, X., Samuelson, L. A., Cholli, A. L., Kumar, J. Synthesis and characterization of fluorescent cellulose. *J. Macromol. Sci. A* **2003**, *40*, 1275-1282.

47. Shah, S. T., Yehye, W. A., Saad, O., Simrani, K., Chowdhury, Z. Z., Alhadi, A. A., Al-Ani, L. A. Surface functionalization of iron oxide nanoparticles with gallic acid as potential antioxidant and antimicrobial agents. *Nanomaterials* **2017**, 7, 306-322.

48. Lu, W., Ling, M., Jia, M., Huang, P., Li, C., Yan, B. Facile synthesis and characterization of polyethyleneimine-coated $Fe_3O_4$ superparamagnetic nanoparticles for cancer cell separation. *Mol. Med. Rep*. **2014,** *9*, 1080-84.

49. Yu, X., Kansg, D., Hu, Y.,Tong, S., Ge, M., Cao, C., Song, W. One-pot synthesis of porous magnetic cellulose beads for the removal of metal ions. *RSC Adv*. **2014,** *4*, 31362-31369.

50. Fragouli, D., Bayer, L. S., Corato, R. D., Brescia, R., Bertoni, G., Innocenti, C., Gatteschi, D., Pellegrino, T., Cingolani, R., Athanassiou, A. Superparamagnetic cellulose fiber networks via nanocomposite Functionalization. *J. Mater. Chem*. **2012**, *22*, 1662.

51. Huang, H., Wang, X., Ge, H., Xu, M. Multifunctional magnetic cellulose surface-imprinted microspheres for highly selective adsorption of artesunate. *ACS Sustainable Chem. Eng*. **2016**, *4*, 3334−3343.

52. Sun, N., Swatloski, R. P., Maxim, M. L., Rahman, M., Harland, A. G., Haque, A., Spear, S. K., Daly, D. T., Rogers, R. D. Magnetite-embedded cellulose fibers prepared from ionic liquid. *J. Mater. Chem.* **2008,** *18*, 283–290.

53. Wu, W. -B., Jing, Y., Gong, M. -R., Zhou, X. -F., Dai, H. -Q. Preparation and properties of magnetic cellulose fiber composites. *Bio. Resources* **2011**, *6*, 3396-3409.

54. Palsson, L. -O., Monkman, A. P. Measurements of solid-state photoluminescence quantum yields of films using a fluorimeter. *Adv. Mater.* **2012,** *14*, 757-758.

55. Jang, H. -S., Wang, Y., Lei, Y., Nieh, M. -P. Controllable formation of pyrene ($C_{16}H_{10}$) excimers in polystyrene/ tetrabutylammonium hexafluorophosphate films through solvent vapor and temperature annealing. *J. Phys. Chem. C* **2013**, *117*, 1428−1435.

56. Winnik, F. M. Photophysics of preassociated pyrenes in aqueous polymer solutions and in other organized media. *Chem. Rev.* **1993**, *93*, 587-614.

57. Mandal, S. K., Lequeux, N., Rotenberg, B., Tramier, M., Fattaccioli, J., Bibette, J., Dubertret, B. Encapsulation of magnetic and fluorescent nanoparticles in emulsion droplets. *Langmuir* **2005**, *21*, 4175-4179.

58. Li, X- G., Liu, Y- W., Huang, M- R., Peng, S., Gong, L- Z., Moloney, M. G. Simple efficient synthesis of strongly luminescent polypyrene with intrinsic conductivity and high carbon yield by chemical oxidative polymerization of pyrene. *Chem. Eur. J.* **2010**, *16*, 4803-4813.

59. Li, X- G., Liao, Y., Huang, M- R., Kaner, R. B. Interfacial chemical oxidative synthesis of multifunctional polyfluoranthene. *Chem. Sci.* **2015**, *6*, 2087-2101.

60. Sonawane, S. L., Asha, S. K. Blue, green, and orange-red emission from polystyrene microbeads for solid-state white-light and multicolor emission. *J. Phys. Chem. B* **2014**, 118 (2014), 9467−9475.

61. Luo, X., Liu, S., Zhou, J., Zhang, L. In situ of $Fe_3O_4$/Cellulose microspheres with magnetic-induced protein delivery. *J. Mater. Chem.* **2009**, *19*, 3538-3545.

62. Dong, S., Roman, M. Fluorescently labelled cellulose nanocrystal for bioimaging applications. *J. Am. Chem. Soc*. **2007**, 129, 13810-13811.

# Chapter 3

# Sustained Release Polyurethane Microcapsules by Interfacial Polycondensation using Aromatic Polyols

## 3.1. Introduction

Microencapsulation is a widely used technology for a variety of applications, including food,[1] pharmaceutical,[2] paints and surface coatings,[3] textiles,[4] and corrosion resistance.[5] Microencapsulation techniques enable the encapsulation of active ingredients in various phases, such as solid, liquid or gas, to yield capsules in the micrometer to millimeter range. They serve to protect the encapsulated material from degradation or evaporation and/or controlled release of the active components in the environment.[6] Controlled release encompasses several aspects, including immediate release,[7] targeted delivery,[8] and sustained release.[9,10] Different physical processes, such as spray drying,[11] solvent evaporation,[12] layer-by-layer (L-B-L) assembly,[13] and chemical approaches, including sol-gel encapsulation,[14] in-situ/interfacial polymerization,[6] etc., can be used to produce microcapsules. Various polymers such as urea-formaldehyde (U-F),[15] melamine-formaldehyde (M-F),[16] polystyrene (PS),[17] polyurea-urethane (PUU),[18] polyurea,[19] have been used as polymer shell in the microencapsulation process.

Among many microencapsulation techniques, interfacial has a range of advantages, including the ability to control the mean size and membrane thickness of capsules, high loading efficiency, and scalability.[20] The procedure involves dispersing one phase containing a reactive monomer into a second immiscible phase, and then adding a second monomer to the continuous phase of the emulsion. At the droplet interface, both monomers react to form a polymeric membrane. The dispersed phase contains active, which gets encapsulated upon polymeric film formation. Interfacial polymerization techniques can be used to prepare polyurea-urethane microcapsules from diisocyanates, which are oil-soluble, and diols, which must be water-soluble, when they are used as monomers. The advantages of using PUU include its wide range of chemical and mechanical characteristics, smooth surface, and absence of formaldehyde, a

chemical posing serious concerns to the environment and human health. In recent years, PUU core-shell structured MICs made with aliphatic polyols (monomeric diol) have been extensively explored employing water-in-oil (W/O),[21] oil-in-water (O/W),[22] and oil-in-oil (O/O)[23] emulsion methods to enable sustained release of the active. A variety of studies have been undertaken to evaluate and improve the performance of PUU MICs by influencing the reaction parameters as well as monomers (diols and diisocyanates). Lukaszczyk et al. (1997)[24] evaluated the efficiency of aromatic and aliphatic diisocyanates, concluding that aromatic diisocyanates are more effective than aliphatic diols in terms of controlled release of the active.

There are several reports where polyurea-urethane is prepared using aromatic diisocyanates such as methylene diphenyl diisocyanate (MDI) and tolylene-2,4-diisocyanate (TDI) and aliphatic diisocyanates like isophorone diisocyanate (IPDI) and hexamethylene diisocyanate (HMDI). Diols such as ethylene glycol (EG), diethylene glycol (DEG), propylene glycol (PG), butane-1,4-diol (BDO), polyethylene glycol (PEG), hexane-1,6-diol (HDO), cyclohexyl-1,4-dimethanol, etc.[25, 26] are used as the other monomer. Although a number of aromatic and aliphatic diols and polyols have been used to produce PU foams and films, use of aromatic diols to synthesize PUU MICs via interfacial polymerization is an unexplored domain due to the restricted solubility of aromatic diols in water.[27] However, we can expect the polymeric shell to be mechanically robust and have enhanced barrier properties if PUU MICs are prepared from fully aromatic monomers.

We report here our attempt to prepare PUU MICs using benzene-1,4-dimethanol (BDM), an aromatic diol, to encapsulate water-insoluble and water-sensitive active DMP, which is a safer yet effective insect repellent for mosquitos and flies. Due to the restricted solubility of aromatic diols in water, it is challenging to prepare PUU MICs by the typical interfacial polycondensation procedures reported earlier. By modifying our earlier reported procedure, we were able to successfully prepare PUU MICs based on both aromatic monomers, BDM and

TDI. As compared to phenols and their derivatives such as hydroquinone and bisphenol A, the presence of a primary alcohol group on the benzene ring of BDM serves to increase the reactivity with isocyanates and results in a highly rigid polymer due to the restricted mobility. The use of BDM also led to a rigid polymeric shell that is stiff and thermally stable as compared to aliphatic diols, resulting in sustained active release of active molecules.

## 3.2. Materials and methods

Benzene-1,4-dimethanol (BDM) and ethylene glycol (EG) were procured from TCI chemicals Pvt. Ltd. Toluene-2,4-diisocyanate (technical grade 80%) (TDI), 1,4-diazabicyclo[2.2.2]octane DABCO), polyvinyl alcohol (PVA) (Mw 13000 to 23000 Daltons) and fumed silica powder (mean size 0.007 µm) were procured from Sigma Aldrich, USA. Polyvinylpyrrolidone (PVP-K90) was procured from S D fine chem Pvt. Ltd. Dimethyl phthalate (DMP) was procured from Thomas Bakers. All the chemicals were used as procured. Distilled water was used to prepare surfactant solution and washings.

### 3.2.1. Preparation of EG-TDI microcapsules (MIC_EG_TDI).

PUU microcapsules were prepared using interfacial polycondensation process in an aqueous media.[23] In brief, a surfactant solution was prepared by dissolving PVP-K90 (5 wt.%) in water, which was used as the continuous phase. To this phase, a mixture of DMP (7.83 g, 50% loading) and TDI (6.33 g, 36.3 mmol, 1.5 equiv.) was added dropwise at 1000 rpm and 30 °C resulting in an oil-in-water emulsion. The emulsion was stabilized by mechanical stirring at 1000 rpm for 15 minutes. Separately prepared mixture of EG (1.5 g, 24.2 mmol, 1 equiv.), DABCO (catalyst) (0.156 mg), and PVP-K90 surfactant (5 mL) was added dropwise to the stabilized emulsion over a period of 12-15 min. After the complete addition of the EG, the reaction mixture was stirred for 4 h at 30 °C, followed by stirring for another hour at 50 °C. After 5 h, 2 wt.% fumed silica with respect to the polymer weight was added, and the reaction

mixture was cooled down to 27 °C and stirred at 500 rpm for an additional 15 h. Finally, the milky reaction suspension was centrifuged, washed three times, and filtered through a Buckner funnel with Whatman filter paper no. 1 to extract MICs. MICs were further dried in an incubator at 37 °C and stored in a closed container at ambient conditions for further use.

### 3.2.2. *Preparation of BDM_TDI microcapsules (MICs).*

The above method was used with minor modifications to prepare the MICs utilizing BDM as an aromatic diol. In brief, a solution of TDI (2.84 g, 16.3 mmol, 1.5 equiv.) and DMP (4.34 g, 50% loading) was added dropwise to a continuous aqueous phase i.e., 40 mL 5% PVP-K90 surfactant solution at 1000 rpm and 30 °C to form an emulsion. The reaction temperature was raised to 40 °C and stirred for another 15 min at 1000 rpm to stabilize the emulsion. To the stabilized emulsion, a solution of BDM (1.5 g, 10.87 mmol, 1 equiv.) with concentration of 100 mg/mL, DABCO (0.087 g, 2 wt.% of polymer weight), and aqueous surfactant (10 mL) was added dropwise over a time period of 15 min and continued stirring for 4 h at 40 °C and then for an hour at 50 °C. After 5 h, 2 wt.% fumed silica to the polymer weight was added and the reaction mixture was cooled to 27 °C and stirred at 500 rpm for an additional 15 h to result in core-shell structured microcapsules[28]. Finally, the milky reaction suspension was centrifuged, washed three times, and filtered through a Buckner funnel with Whatman filter paper no. 1 to extract MICs. MICs were further dried in an incubator at 37 °C and stored in a closed container at ambient conditions for further use.
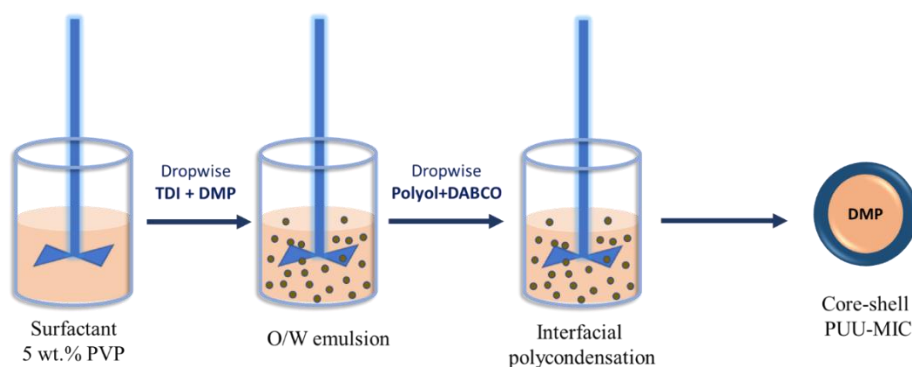


**Scheme 3.1** Preparation of microcapsules using interfacial polycondensation.
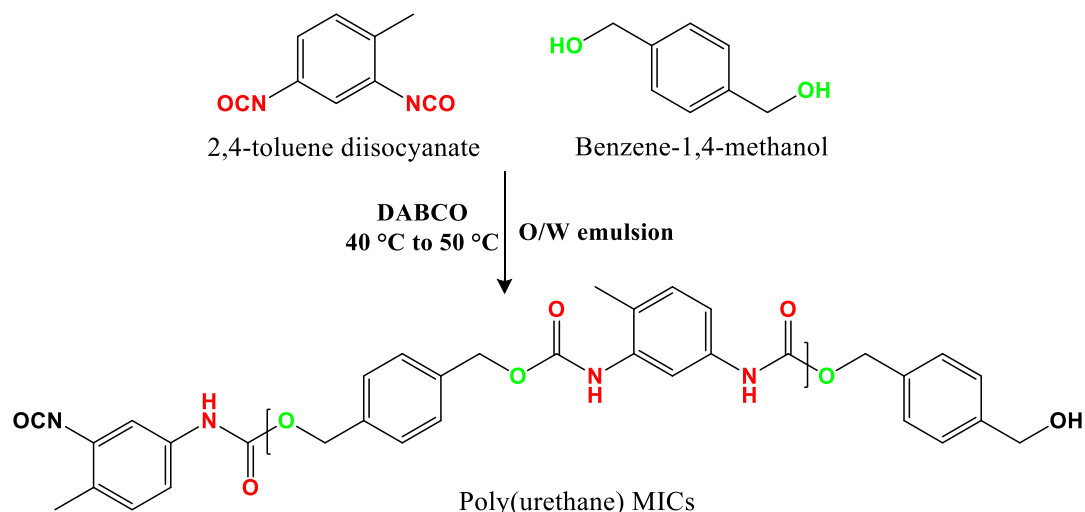
**Scheme 3.2** Structural representation of the polymer wall.

### 3.2.3. *Preparation of EG_TDI and BDM_TDI microspheres.*

Microspheres of EG and BDM were prepared using the same methods as for respective MICs with the same stoichiometry but without the use of DMP (active).

### 3.2.4. *Characterization*

The MIS and MIC formation was monitored using an Olympus BX-60, USA optical microscope equipped with an Olympus SC30 digital camera. The morphology of the capsules was examined using field emission scanning electron microscopy (FE-SEM) (Hitachi S-4200). MIS and MICs were dispersed in water, drop casted on conducting carbon tape, dried in an incubator and sputter-coated with gold before SEM imaging to prevent charging. Thermogravimetric analysis (TGA) was used to determine the thermal stability of the microcapsules and to quantify the active content using the TGA-550 (TA instruments) under a nitrogen atmosphere at a heating rate of 20 °C/min. The $T_g$ of the polymer shell of the microcapsules was determined using the differential scanning calorimetry (DSC) technique using DSC Q250 (TA instruments) with a nitrogen purge stream of 50 mL/min. The samples were heated at a rate of 10 °C/min from 20 to 250 °C, with the results from the first heating cycle taken into consideration. FTIR spectrum was acquired using the Perkin Elmer Q5000 GX

IR instrument with 32 scans and a resolution of $4\,cm^{-1}$. Release study was carried out using dissolution test apparatus (LAB INDIA- DS8000). For release and extraction studies, Hitachi 220 UV-VIS spectrophotometer was used to record the absorbance.

*3.2.5.   Extraction studies*

Extraction studies were done using the previously reported protocol with slight modification.[29] In brief, 100 mg of MICs containing DMP as an active was weighed and transferred to a 100 mL round bottom flask. The flask was filled with 50 mL of 50% (v/v) aqueous methanol and refluxed for 6 h. After 6 h, the mixture was cooled down to ambient temperature and filtered using Grade-3 sintered glass crucible and washed using aqueous methanol. The filtrate obtained was transferred to a 100 mL volumetric flask and was diluted with aqueous methanol up to the mark. Further 1 mL of this stock solution was measured and transferred to a 10 mL volumetric flask in triplicates and diluted with aqueous methanol up to the mark to bring the concentration within the calibration range. Finally, the absorbance was measured using a UV-Vis spectrophotometer (Hitachi 220 UV-VIS spectrophotometer) at 276 nm ($\lambda_{max}$ of DMP) and the DMP content was measured using the following formula:

$$Active\ ingredient\ (\%) = \frac{Dilution\ factor\ \text{x}\ Absorbance}{Calibration\ slope\ \text{x}\ amount\ of\ sample\ (mg)}\text{x}\ 100$$

*3.2.6.   Release measurements*

Release study of MICs was carried out in dissolution test apparatus in perfect sink conditions i.e., well within the saturation limit of the active in the water using previously reported methods.[30,31,32] Perfect sink conditions prevent dissolving rates from dropping significantly over time and causing errors in release tests because of the solubility issues. 100 mg MICs (50% loading) were dispersed in 1000 mL of distilled water and stirred at 100 rpm and 30 °C for 48 h. To maintain the concentration gradient, aliquots (10 mL) were taken at regular intervals and replaced with the same amount of distilled water. The absorbance of the collected

aliquots was measured using a UV-Vis spectrophotometer $\lambda_{max}=276$ nm to calculate the percentage release of the DMP from the MICs.

## 3.3. Results and discussion
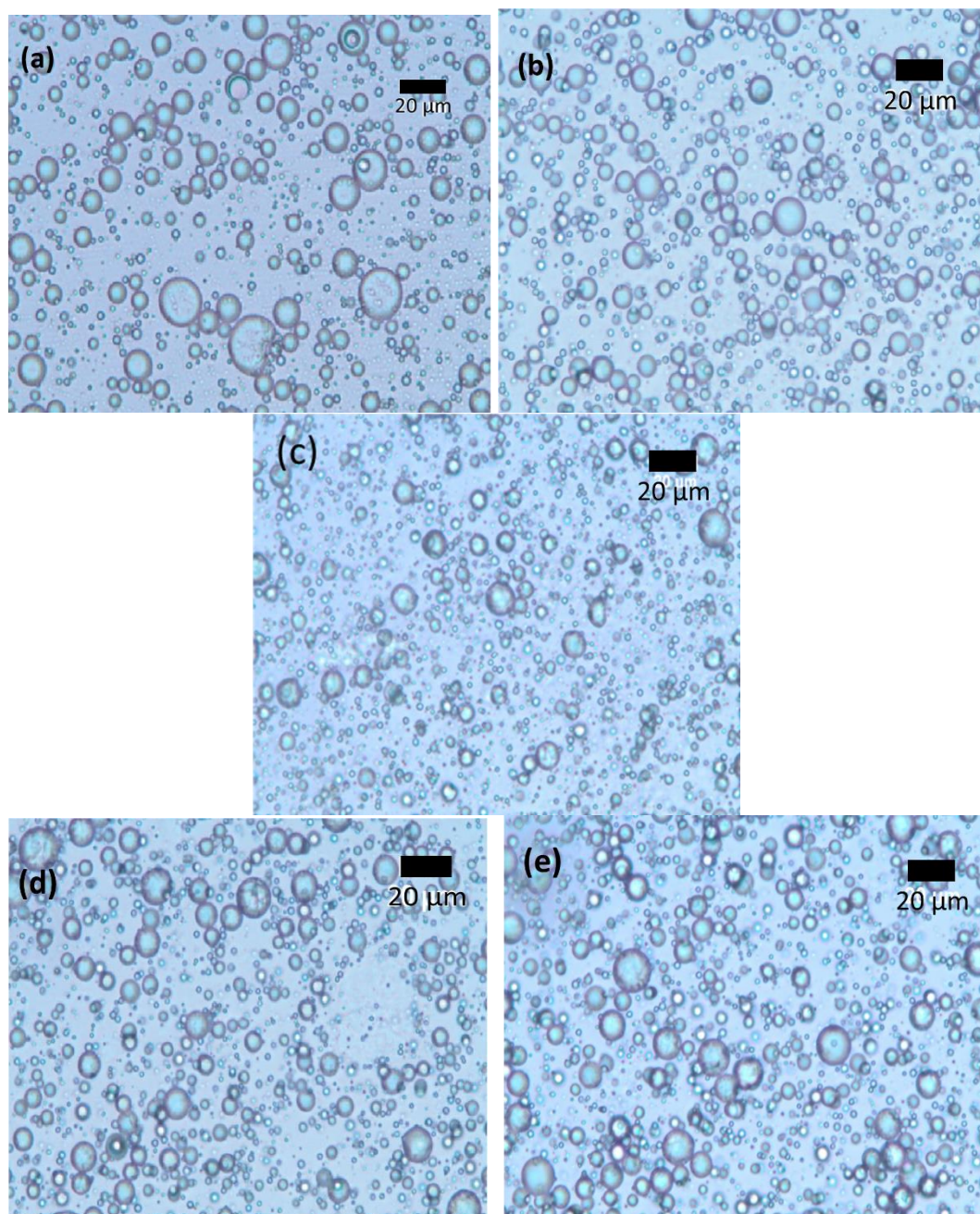


**Figure 3.1** Optical images of emulsion of (a) MIC_EG_TDI, (b) MIC_BDM_TDI, (c) after addition of BDM to prepare MIC_BDM_TDI and redispersed microcapsules of (d) MIC_EG_TDI, (e) MIC_BDM_TDI.

**Fig**. **3.1(b)** illustrates the formation of a uniform stable emulsion. Since BDM has low solubility in water or aqueous surfactant solution compared to aliphatic diols like EG, BDO, and PEG, it was dissolved at a high temperature of 40 °C with the catalyst (DABCO) in surfactant solution resulting in a clear solution of the second monomer. The temperature of the emulsion was raised to 40 °C before the addition of a second monomer (diol) solution to assist the solubility of BDM in a continuous phase. Optical images shown in **Fig. 3.1 (c)** confirmed that the BDM remains soluble in continuous phase post addition. The primary polymerization reaction between TDI (oil phase) and BDM (aqueous phase) occurs at the oil/water interface when BDM solution is added dropwise to the emulsion, forming a thin solid polymeric shell around the DMP (active). Over the course of five hours, the unreacted diol diffuses through the thin polymeric shell to react with the diisocyanate and thicken the shell. The size of the
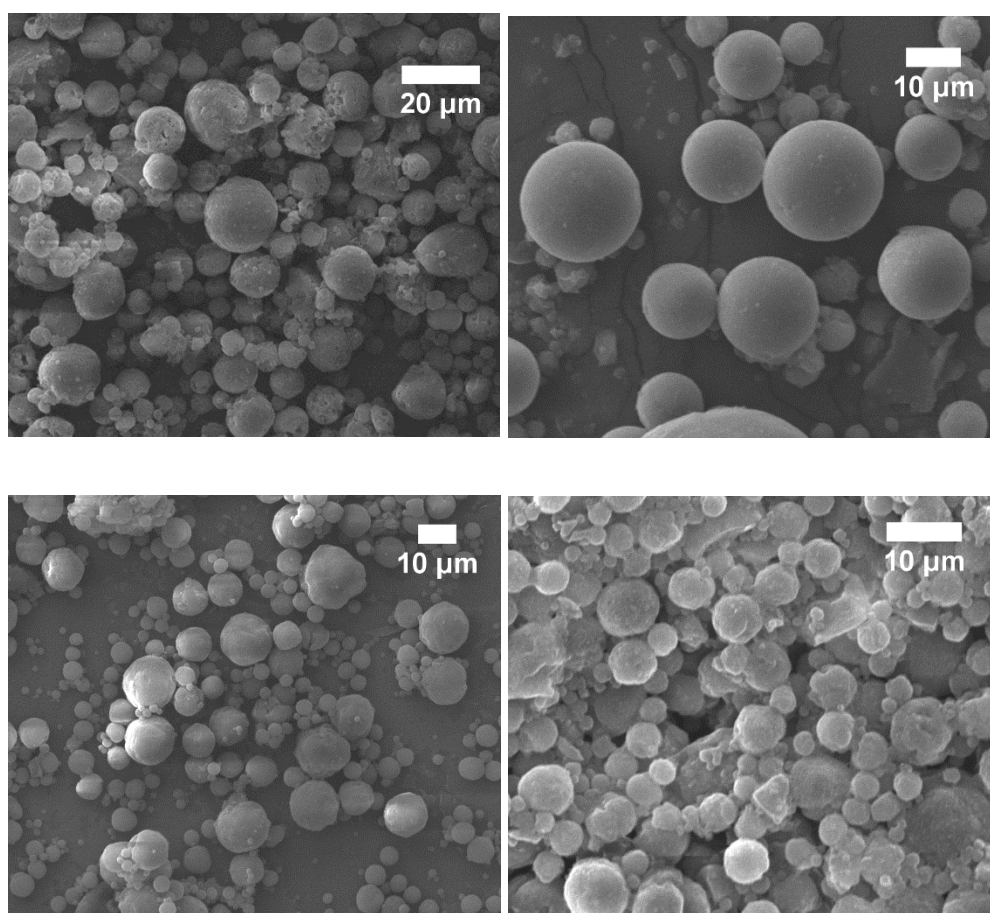


**Figure 3.2** FE-SEM images of (a) MIS_EG_TDI, (b) MIS_BDM_TDI, (c) MIC_EG_TDI and (d) MIC_BDM_TDI.

emulsion droplet in the O/W emulsion determines the size of microcapsules. **Fig. 3.1(d)** and **3.1(e)** illustrate optical microscopic images of the aqueous redispersion of solid microcapsules of EG and BDM respectively, confirming the formation of robust MICs with diameter in the range of 1-20 µm for both MIC_EG_TDI and MIC_BDM_TDI.

The surface morphology of the MIS and MICs was examined using FE-SEM. SEM images illustrate that the MIS and MICs are spherical with a smooth surface, as shown in **Fig. 3.2**. The size of the microcapsules obtained from SEM images correlates with the optical microscopic images, which are in the range of 1-20 µm. This also confirms that the solid polymer shell formed around the oil phase via interfacial polymerization remains intact during the microencapsulation process.

PUU polymer shell formation was characterized using FTIR. In the FTIR spectrum shown in **Fig. 3.3,** characteristic symmetric stretching bands appearing at 1720 cm$^{-1}$ and 1640 cm$^{-1}$ corresponding to carbonyl (C=O) of urethane and urea bond, respectively, along with the appearance of -NH bending vibration at 1594 cm$^{-1}$ for urethane confirms the PUU shell
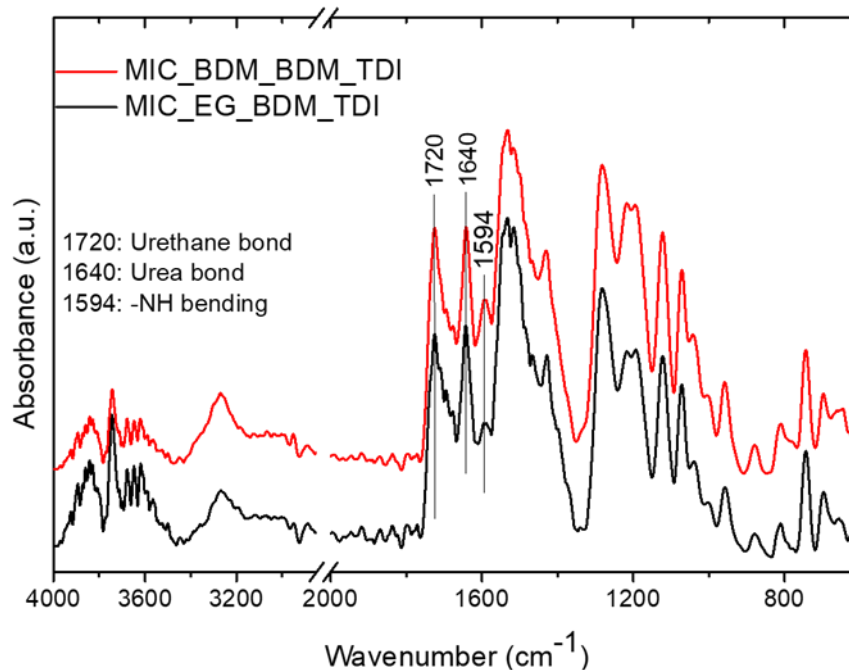


**Figure 3.3** FTIR spectra of polyurea-urethane (PUU) microcapsules.

formation encapsulating the active using both EG and BDM to form MIC_EG_TDI and MIC_BDM_TDI.[33]

Extraction studies were performed to determine the encapsulation efficiency of DMP in MIC_EG_TDI and MIC_BDM_TDI using aqueous methanol as a solvent. The DMP content in the MICs was 47 % for MIC_EG_TDI and 48 % for MIC_BDM_TDI, which is close to the theoretical loading (50 % with respect to the polymer weight), as shown in **Table 3.1**. Overall encapsulation efficiency achieved was 94-96%, consistent with the previous reports[15]. Higher encapsulation efficiency with BDM implies that the PUU shell with BDM is as good as MICS with ethylene glycol (MIC_EG_TDI).

TGA was used to investigate the thermal stability of MICs and quantify the encapsulation efficiency of the active.[34] The resulting thermogram (**Fig. 3.4**) revealed a two-step degradation curve for the MICs due to the degradation of DMP and polymer shell at different temperatures

**Table 3.1**. Encapsulation efficiency of the active using extraction method and TGA.

| Sample | Theoretical Loading (%) | Obtained Loading (Extraction method) (%) | Encapsulation efficiency (%) | Obtained Loading (TGA) (%) | Encapsulation efficiency (%) |
|---|---|---|---|---|---|
| MIC_EG_TDI | 50 | 47 | 94 | 46 | 92 |
| MIC_BDM_TDI | 50 | 48 | 96 | 46 | 92 |

and a single-step degradation curve for microspheres (MIS) and DMP. In the thermogram for DMP, the on-set temperature was 120 °C, whereas the on-set degradation temperatures for microspheres, MIS_EG_TDI and MIS_BDM_TDI were 225 °C and 260 °C respectively. The increase in the thermal stability of MIS_BDM_TDI was due to the introduction of rigid

aromatic diol compared to the aliphatic flexible diols.[35] In the case of MICs, the first degradation step may be attributed to the loss of DMP from the capsules at 130 °C, while the second degradation step at 260 °C corresponds to the on-set degradation temperature of the PUU shell. DMP content was determined from the first weight loss step of the MICs which was around 46%, which is in agreement with the extraction studies shown in **Table 3.1**.
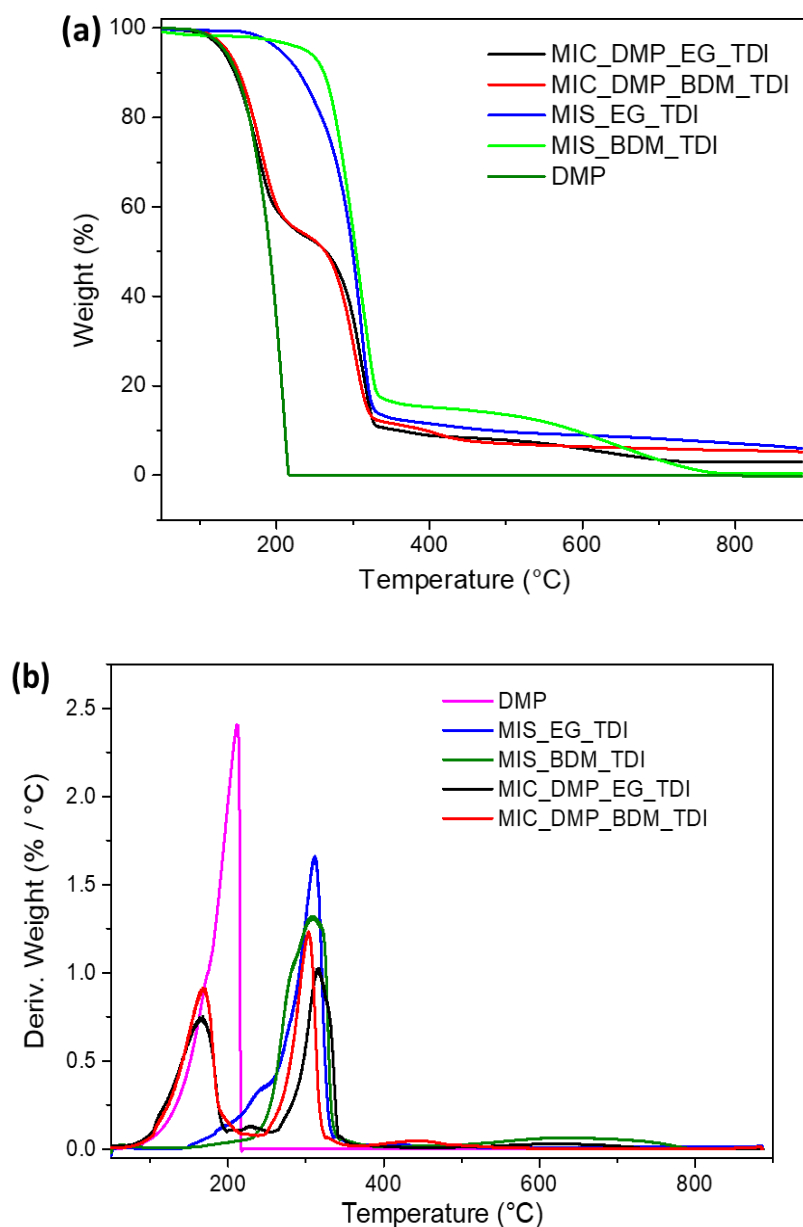


**Figure 3.4** (a) TGA and (b) differential thermogravimetry curves of DMP, microspheres and microcapsules.

Use of aromatic diol and diisocyanates for microencapsulation has led to significant shift in the glass transition temperature of the microcapsules. Differential scanning calorimetry (DSC) thermograms obtained from the first heating cycle at a heating rate of 10 °C/min (**Fig. 3.5**) revealed a glass transition temperature ($T_g$) of 108.5 °C for the MIC_EG shell, whereas the $T_g$ for the MIC_BDM shell was 143 °C. This enhancement is attributed to the addition of aromatic diols to the polymeric shell, which makes it more rigid as compared to MICs with aliphatic diols.
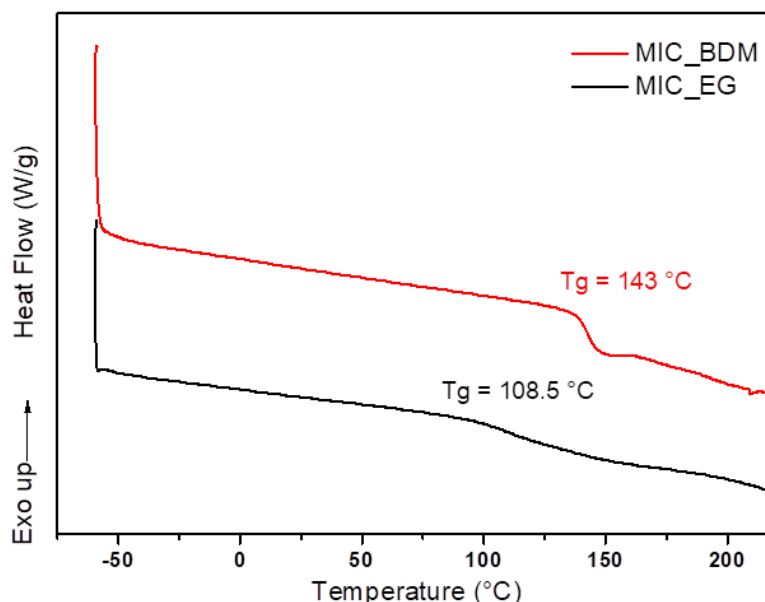


**Figure 3.5** DSC thermogram of MIC_EG (shell) and MIC_BDM (shell).

The higher $T_g$ achieved using aromatic diols as monomers in PUU MICs in place of aliphatic diols can influence the release profile of encapsulated active compounds. The release curves shown in **Fig. 3.6** were plotted using average values of two samples performed in duplicates (i.e., each data point is an average of 4 samples). After 48 h, cumulative release of the MIC_EG_TDI was around 65%, while only 54% release of DMP was found with MIC_BDM_TDI. Both the burst release, as well as the overall release were significantly reduced by using BDM and TDI as monomers for PUU MICs. This is due to the introduction

of an aromatic diol with aromatic diisocyanate, which enhances the polymer rigidity. Increased rigidity of capsule shell wall facilitates the sustained release of active from the core by increasing the barrier to small molecule permeation.
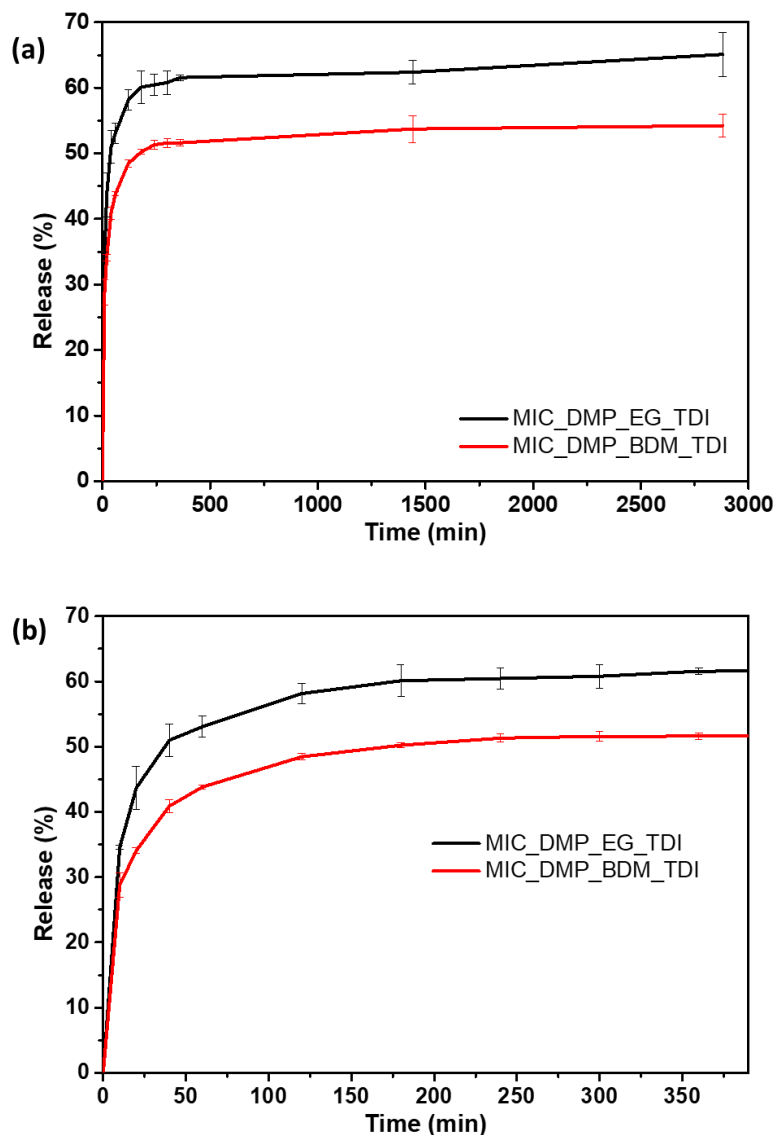
**Figure 3.6** (a) Release profile of DMP from MICs in distilled water at room temperature (b) zoomed initial release profile.

In order to better understand the process of controlling active ingredient release from microcapsules, we aimed to examine the release results using existing mathematical models.[36] The hydrophilicity and hydrophobicity of the active core govern their release behavior. The release of hydrophilic actives is frequently controlled by diffusion, whereas the release of

hydrophobic actives is controlled by swelling or matrix erosion.[37] We propose that diffusion controls the release of DMP, which has a high solubility in water (4200 parts per million; ppm) and PUU shell, which is relatively hydrophobic. As a result, we applied a semi-empirical equation given by Korsmeyer, Ritger, and Peppas, which may provide a comprehensive explanation for the release of the active component from polymeric systems.[38,39]

$$\frac{M_i}{M_\infty} = K.t^n$$

$M_i/M_\infty$ is the fractional release of the active at time $t$ in the above expression whereas $K$ is the release rate constant, and the time exponent $n$ represents the mechanism of release. **Table 3.2** displays the values of $K$, $n$ and $R^2$. The $K$ value decreased from 0.36 in the case of MIC_EG to 0.26 in the case of MIC_BDM suggesting that the introduction of aromatic monomer influence the barrier properties of the polymeric shell which result in the slow release of the active from the core as can be correlated with the release profile in **Fig. 3.6**. The exponent $n$ is less than 0.43, indicating that the diffusion range is not Fickian. Ritger and Peppas, on the other hand, obtained values as low as 0.3 for polydisperse Fickian materials, where the range cannot be determined for samples with particle size distribution.[40]

We also explored the Weibull model, which was established in 1972 and applies to drug release systems.[41] The mechanism of the controlled release curves was determined using the equation below.[42]

$$\frac{M_i}{M_\infty} = 1 - \exp\left(-a.t^b\right)$$

$a$ and $b$ are constants in the equation above. Exponent $b$ has a critical value of 0.75, which indicates the Fickian diffusion limit, beyond which other variables begin to influence the release. The values of $a$, $b$, and $R^2$ fitted to both systems are shown in **Table 3.2**. The Weibull model fits both the systems in this study very well and the values for $b$ i.e., 0.14 and 0.15 for

MIC_EG and MIC_BDM respectively are all below 0.75 which concludes that the release is primarily controlled by diffusion. The experimental release data and predicted release curves derived using the models presented thus far are shown in **Fig. 3.7**. Both Peppas and Weibull models were able to predict the experimental release profile of DEET in these MICs.
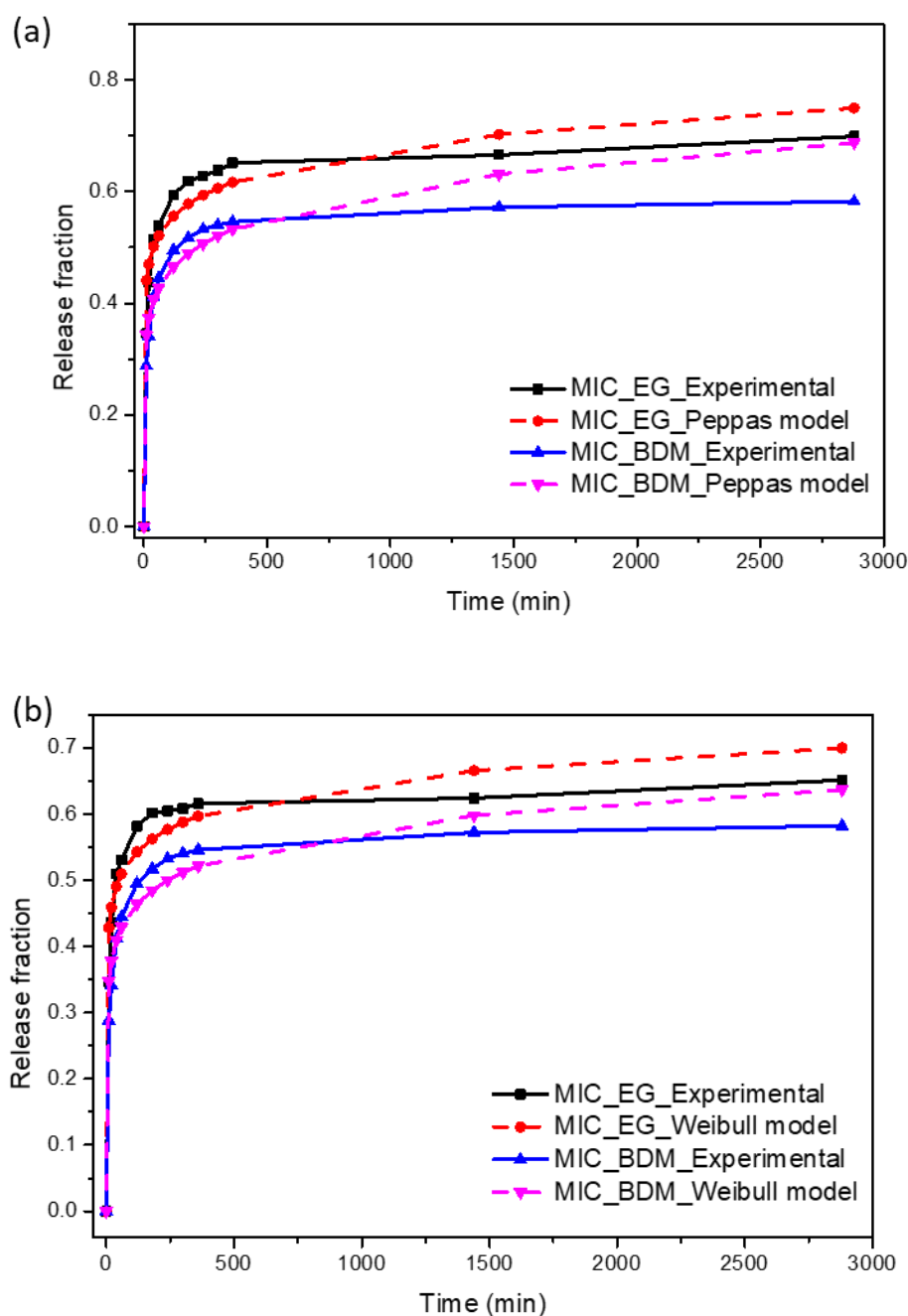


**Figure 3.7** Experimental and predicted release profiles for MIC_EG and MIC_BDM using (a) Peppas Model and (b) Weibull model.

**Table 3.2**. Parameters for mathematical models used to fit experimental release profiles.

| Model | Sample | $K$ | $n$ | $R^2$ |
|---|---|---|---|---|
| **RPM** | MIC_EG | 0.36 | 0.09 | 0.98 |
| **RPM** | MIC_BDM | 0.26 | 0.12 | 0.97 |
| | | $a$ | $b$ | $R^2$ |
| **Weibull** | MIC_EG | 0.41 | 0.14 | 0.98 |
| **Weibull** | MIC_BDM | 0.30 | 0.15 | 0.97 |

## 3.4. Conclusion

This study illustrates the use of benzene-1,4-diol, an aromatic diol, as a polyol component in the interfacial polycondensation process for making polyurea-urethane (PUU) microcapsules. Polyurethanes have been synthesized using aromatic diols, but due to their low solubility and reactivity, they have never been used in microencapsulation. We report a method for synthesizing microcapsules employing aromatic diol as a polyol component and forming a PUU shell encapsulating DMP, resulting in a high encapsulation efficiency of about 92%. The microcapsules produced were spherical and in the form of a free-flowing powder, with sizes ranging from 1 to 20 µm. Thermogravimetric analysis suggests a good correlation of encapsulation efficiency with the extraction studies and delayed decomposition of DMP upon encapsulation. Release studies suggest improvements in barrier properties with the introduction of the aromatic diol component compared to aliphatic ethylene glycol. Mathematical interpretation of the release profile using the Ritger-Peppas model, and the Weibull model suggests a non-Fickian diffusion mechanism for the release of DMP from MICs. The reduction in release rate constant $K$ with the introduction of aromatic diol implies enhanced permeation resistance.

## 3.5. References

1. Yao M., Xie J., Du H., Mc Clements D. J., Xiao H., Li L. Progress in microencapsulation of probiotics: A review. *Compr. Rev. Food Sci. Food Saf.* **2020**, *19,* 857– 874.

2. Yang X. L., Ju X. J., Mu X. T., Wang W., Xie R., Liu Z, Chu l. Y. Core−shell chitosan microcapsules for programmed sequential drug release. *ACS Appl. Mater. Interfaces* **2016**, *8,* 10524−10534.

3. Koh E., Kim N. K., Shin J., Kim Y. W. Polyurethane microcapsules for self-healing paint coatings. *RSC Adv.* **2014**, *4*, 16214-16223.

4. Nelson G. Application of microencapsulation in textiles. *Int. J. Pharma.* **2002**, *242*, 55-62.

5. Mohammadloo H. E., Mirabedini S. M., Pezeshk-Fallah H. Microencapsulation of quinoline and cerium-based inhibitors for smart coating application: Anti-corrosion, morphology and adhesion study. *Prog. Org. Coat.* **2019**, *137*, 105339-105347.

6. Su J. F., Wang L. X., Ren L., Huang Z., Meng X. W. Preparation and characterization of polyurethane microcapsules containing n-octadecane with styrene-maleic anhydride as a surfactant by interfacial polycondensation. *J. Appl. Polym. Sci*. **2006**, *102*, 4996-5006.

7. Yua D. G., Zhenga X. L., Yanga Y., Lia X. Y., Williams G. R., Zhao M. Immediate release of helicid from nanoparticles produced by modified coaxial electrospraying. *Appl. Surf. Sci.* **2019**, *473*, 148–155.

8. Wang K., Wen H. F., Yu D. G., Yang Y., Zhang D. F. Electrosprayed hydrophilic nanocomposites coated with shellac for colon-specific delayed drug delivery. *Mater. Des.* **2018**, *143*, 248-255.

9. Hai T., Wan X., Yu D. G., Wang K., Yang Y., Liu Z. P. Electrospun lipid-coated medicated nanocomposites for an improved drug sustained-release profile. *Mater. Des.* **2019**, *162*, 70– 79.

10. Li X. Y., Zheng Z. B., Yu D. G. Liu X. K., Qu Y. L. Li H. L. Electrosprayed sperical ethylcellulose nanoparticles for an improved sustained-release profile of anticancer drug. *Cellulose* **2017**, *24*, 5551–5564.

11. Rajam R., Anandharamakrishnan C. Microencapsulation of Lactobacillus plantarum (MTCC 5422) with fructooligosaccharide as wall material by spray drying. *LWT - Food Sci. Tech.* **2015**, *60*, 2, 773-780.

12. Li M., Rouaud O., Poncelet D. Microencapsulation by solvent evaporation: State of the art for process engineering approaches. *Int. J. Pharma.* **2008**, *363*, 26-39.

13. Tong W., Songa X., Gao C. Layer-by-layer assembly of microcapsules and their biomedical applications. *Chem. Soc. Rev*. **2012**, *41*, 6103-6124.

14. Moore D. G., Brignoli J. V. A., RühsOrcid P. A., Studart A. R. Functional microcapsules with hybrid shells made via sol–gel reaction within double emulsions. *Langmuir* **2017**, *33*, 36, 9007–9017.

15. Kashani, M. B., Salimi, A., Zohuriaan-Mehr, M. J., Hanifpour A. Preparation of poly (urea-formaldehyde) microcapsules for use in capsular adhesive. *J. Polym. Res.* **2019**, *26*, 270-278.

16. Yan X., Wang Y., Liu H., Li R., Qian C. Synthesis and characterization of melamine-formaldehyde microcapsules containing pyraclostrobin by in situ polymerization. *Polym. Sci. Ser. B* **2018**, *60*, 798–805.

17. Döğüşcü D. K., Altıntaş A., Sarı A., Alkan C. Polystyrene microcapsules with palmitic-capric acid eutectic mixture as building thermal energy storage materials. *Energy Build.* **2017**, *150*, 376-382.

18. Ramanathan L. S., Shukla P. G. Sivaram S. Synthesis and characterization of polyurethane microspheres. *Pure & Appl. Chem*. **1998**, *70*, 1295-1299.

19. Kulkarni S. S., Mohan M. S., Jagtap S. B., Dandage R. G., Jadhav A. S., Shukla P. G. Polyurea and polyurethane microcapsules containing mosquito repellent DEET: preparation and characterization. *Appl. Sci. Adv. Mater. Int.* **2015**, *2*, 1, 7-10.

20. Shukla P. G. Jagtap S. B. Biradar S. C. Charpe V. B., Jadhav A. S. Preparation and characterization of microcapsules containing industrially important reactive water-soluble polyamine. *Colloid Polym Sci.* **2016**, *294*, 2039–2050.

21. Shukla P. G., Kalidhass B., Shahy A., PALASKAR D. V. Preparation and characterization of microcapsules of water- soluble pesticide monocrotophos using polyurethane as carrier material. *J. Microencapsulation* **2002**, *19*, 3, 293-304.

22. Lia X., Lia L., Gonga J., Kuanga Y., Moa l., Song T. Cellulose nanocrystals (CNCs) with different crystalline allomorph for oil in water Pickering emulsions. *Carbohydr. Polym.* **2018**, *183*, 303–310.

23. Kadam S. L., Yadav P., Bhutkar S., Patil V. D., Shukla P. G., Shanmuganathan K. Sustained release insect repellent microcapsules using modified cellulose nanofibers (mCNF) as pickering emulsifier. *Colloids Surf., A Physicochem Eng. Asp* **2019**, *582*, 123883-123891.

24. Lukaszczyk J., Urbas P. Influence of the parameters of encapsulation process and of the structure of diisocyanates on the release of codeine from resinate encapsulated in polyurea by interfacial water promoted polyreaction. *React. Funct. Polym.* **1997**, *33*, 233-239.

25. Shukla P. G., Sivaram S. Process for the preparation of polyurethane microspheres. US 005814675 A, **1998**.

26. Kardar P. Preparation of polyurethane microcapsules with different polyols component for encapsulation of isophorone diisocyanate healing agent. *Prog. Org. Coat.* **2015**, *89*, 271-276.

27. Rogulska, M. New thermoplastic poly(carbonate-urethane)s based on diphenylethane-derivative chain extenders—the effect of chain extender structure on thermal and mechanical properties. *J. Therm. Anal. Calorim.* **2000**, *139*, 3107–3121.

28. Zhang, F., Zhao, T., Ruiz-Molina, D., Liu, Y., Roscini, C., Leng, J., Smoukov, S. K. Shape memory polyurethane microcapsules with active deformation. *ACS Appl. Mater. Interfaces* **2020**, *12*, 41, 47059–47064.

29. Patil M. D., Patil V. D., Sapre A. A., Ambone T. S., Torris A. T., Shukla P. G., Shanmuganathan K. Tuning controlled release behavior of starch granules using nanofibrillated cellulose derived from waste sugarcane bagasse. *ACS Sustainable Chem. Eng.* **2018**, *6*, 9208−9217.

30. Jonoobi, M., Harun, J., Mathew, A.P., Hussien, M. B., Oksman, K. Preparation of cellulose nonofibres with hydrophobic surface characteristics. *Cellulose* **2010**, *17*, 299–307.

31. Shukla, P. G., Rajgopalan, N., Bhaskar, C., Sivaram, S. Crosslinked starch-urea formaldehyde St-UF) as a hydrophilic matrix for encapsulation: studies in swelling and release of carbofuran. *J. Control. Release* **1991**, *15*, 153–165.

32. Shukla, P. G., Rajagopalan, N., Sivaram, S. Starch urea-formaldehyde matrix encapsulation. IV. Influence of solubility and physical state of encapsulant on rate and mechanism of release. *J. Appl. Polym. Sci.* **1993**, *48*, 1209–1222

33. Phoungtawee P., Crespy D. Shining a new light on the structure of polyurea/polyurethane materials. *Polym. Chem.* **2021**, *12*, 3893-3899.

34. Jagtap, S. B., Subramanian, M. Shukla, P. G. Improved performance of microcapsules with polymer nanocomposite wall: preparation and characterization. *Polymer* **2016**, *83*, 27–33.

35. Zhao C., Huang C., Chen Q., Ingram I. D. V., Zeng X., Ren T., Xie H. Sustainable aromatic aliphatic polyesters and polyurethanes prepared from vanillin-derived diols via green catalysis. *Polymer* **2020**, *12*, 586-600.

36. M. Bruschi, Mathematical models of drug release, in: M. Bruschi (Ed.), Strategies to Modify the Drug Release from Pharmaceutical Systems, Elsevier/Woodhead Publishing, Amsterdam, **2015**, 63–86.

37. Agnes, E. J., Gonzales Ortega, G. Mathematical models and physicochemical of diffusion, Pharmacy Book, **2003,** *19*, 9–19.

38. Korsmeyer, R. W., Gurny, R., Doelker, E. M., Buri, P., Peppas, N. A. Mechanism of solute release from porous hydrophilic polymers. *Int. J. Pharm.* **1983**, *15*, 25–35.

39. Ritger, P. L., Peppas, N. A. A simple equation for describing solute release. I. Fickian and non-Fickian release from non-swellable devices in the form of slabs, spheres, cylinders or discs. *J. Control. Release* **1987,** *5*, 23–36.

40. Huang, L., Zhang, X., Xu, M., Chen, J., Shi, Y., Huang, C., Wang, S., An, S., Li, C. Preparation and mechanical properties of modified nanocellulose/PLA composites from cassava residue. *AIP Adv*. **2018,** 8, 025116.

41. Langenbucher, F. Linearization of dissolution rate curves by the Weibull distribution. *J. Pharm. Pharmacol*. **1972**, *24*, 979–981.

42. Papadopoulou, V., Kosmidis, K., Vlachou, M., Macheras, P. On the use of the Weibull function for the discernment of drug release mechanisms. *Int. J. Pharm.* **2006**, *309,* 44–50.

# Chapter 4

# Polyurethane Microcapsules using Polycarbonate Polyol for Encapsulation of Mosquito Repellent DEET via oil-in-oil Emulsion Method

### 4.1.Introduction

Most of the commercial microcapsule products involve non-biodegradable polymers and hence they have become a source of microplastic pollution in landfills and water bodies.[1] There is a need to develop polymer microcapsules that are biodegradable and yet offer sustained release of actives. Biodegradable polymers have been used extensively in pharmaceuticals because of their non-toxicity and biocompatibility.

Various natural polymers such as polysaccharides (cellulose,[2] chitosan,[3] gelatin,[4] alginate,[5] pectin,[6] and starch[7]), polypeptides,[8] and synthetic biodegradable polymers such as aliphatic polyesters,[9] polybutylene succinate (PBS),[10] etc. have also been reported for microencapsulation. They are biodegradable or compostable, chemically stable, biocompatible, non-toxic, and can also be functionalized easily.[11] Methods for preparing microcapsules using these polymers are often solvent based, such as solvent evaporation,[12] spray drying,[13] and precipitation, and may need high temperatures to eliminate the solvents, resulting in reduced encapsulation efficiency and a porous wall membrane. Hence, there is a need to explore biodegradable polymers that can be used to prepare microcapsules with high encapsulation efficiency and improved barrier properties using techniques such as interfacial polycondensation.

Aliphatic polycarbonates, (polycarbonates without aromatic groups between the carbonate linkages), have low melting points and are highly prone to hydrolysis.[14] Hence, they were earlier considered inferior compared to aromatic polycarbonates and remained unexplored commercially until 1990s. Aliphatic polycarbonates have received increased attention owing to the demand for versatile degradable materials in medical, and packaging applications.[15,16] Commercially they are available as low molecular weight polycarbonate polyols and used as polyol component to prepare polyurethane elastomers.[17] Aliphatic polycarbonates prepared using carbon dioxide as feedstock are attractive as sustainable materials.[18]

Polycarbonates have not been explored much in microencapsulation for controlled release. Till date, there is only one report where aromatic polycarbonate was used in microencapsulation using solution casting followed by solvent evaporation technique. Hyperbranched polycarbonate polyols (PCPO), which are already used commercially to prepare polyurethane elastomers, can be employed to prepare polyurethane microcapsules via interfacial polycondensation. The addition of hyperbranched PCPO may introduce a biodegradable component between the polyurethane linkages without compromising the barrier properties of the microcapsules.

Herein, we report the use of hyperbranched polycarbonate polyol as a polyol component in preparing polyurethane microcapsules encapsulating N, N-Diethyl-m-toluamide (DEET), a mosquito repellent model active, *via* an oil-in-oil emulsion using Hypermer A70 as a surfactant. Hyperbranched aliphatic polycarbonate polyol is insoluble in water but soluble in ethylene glycol. Hence, it was used to create microcapsules by interfacial polycondensation process at the interface of oil-in-oil emulsion by substituting up to 50% of conventional ethylene glycol. MICs obtained as a free-flowing powder were spherical, and their surface was smooth.

4.2. Materials and methods

*4.2.1.* Materials

Hyperbranched PCPO was synthesized by Dr. Ambade's group at CSIR-NCL with molecular weight of 1700 g/mol and Polydispersity index (PDI) of 1.5. Dibutyltin dilaurate (DBTDL) and ethylene glycol (EG) were procured from TCI chemicals Pvt. Ltd. Toluene-2,4-diisocyanate (technical grade 80%) (TDI), N, N-Diethyl-m-toluamide (DEET) and fumed silica powder (0.007 µm) were procured from Sigma Aldrich, USA. Liquid paraffin (heavy) and pet ether (distillation range 65–70 °C; LR grade) were procured from Thomas Baker (Chemicals) Pvt. Ltd. Hypermer A70 was procured from Uniquema, UK. Whatman filter paper no. 1 was used to filter the microcapsules.

*4.2.2.  Preparation of polyurea-urethane microcapsules using DEET as active ingredient and ethylene glycol as polyol component.*

Polyurea-urethane microcapsules (MICs) were prepared using interfacial polycondensation in a non-aqueous medium. Oil-in-oil emulsion of DEET and TDI was prepared in paraffin oil and reacted interfacially with a polyol to prepare microcapsules.[19] In brief, the continuous phase was prepared by dissolving 0.3 wt.% Hypermer A70 in 20 mL paraffin oil and stirring at 900 rpm using an overhead stirrer at ambient conditions. Further, a solution of 2.105 g (0.01207 mmol) of TDI and 2.6 g of DEET (50 wt.% loading) and 0.2 g of DBTDL (1% solution in paraffin oil) was added dropwise to the continuous medium to form an emulsion at 900 rpm and left for stirring for 20 min to obtain stable emulsion which was confirmed by optical microscope images. After 20 minutes, polyol (EG, EG with 20, 30 and 50 wt.% PCPO) (0.5 g; 0.00805 mmol of EG) was added to the emulsion dropwise over a period of 30 min. After the addition of polyol, the temperature of the water bath was raised to 60 °C and stirred for 5 h at the same condition. After 5 h, the reaction was cooled down to 27 °C, and the stirring speed was reduced to 500 rpm and stirred overnight. The milky suspension was washed multiple times with pet ether using centrifugation technique to remove paraffin oil and catalyst and finally filtered using Whatman filter paper no. 1 and again washed with pet ether. The filtered product was dried in an incubator at 37 °C overnight to obtain microcapsules as a free-flowing powder.

*4.2.3.  Characterization*

Fourier transform infrared spectroscopy (FTIR) was used to confirm the polymer wall formation and presence of active ingredient. Attenuated Total Reflectance (ATR) mode was used to acquire the spectrum using a Perkin Elmer ALPHA-E spectrometer with a universal Zn-Se ATR accessory in 600-4000 cm$^{-1}$ region with 32 scans and a resolution of 4 cm$^{-1}$. Olympus BX-60 optical microscope equipped with an Olympus SC30 digital camera was used
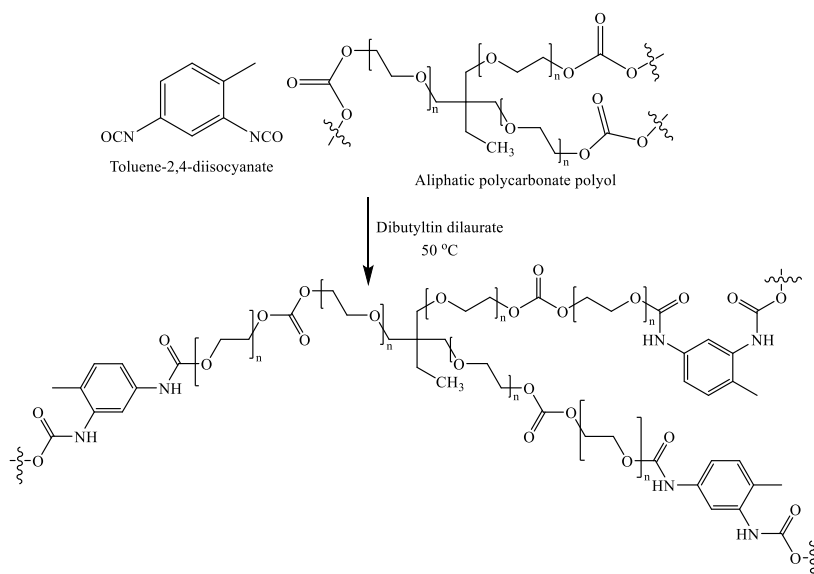
**Scheme 4.1** Preparation of polymer wall formation of MICs using TDI and aliphatic PCPO.

to evaluate the emulsion stability and MIC formation. The morphology of MICs was analyzed using a Scanning Electron Microscope (SEM) (E-SEM, Quanta 300). Before SEM imaging, samples were sputter-coated with gold to prevent charging. Thermogravimetric analysis (TGA) was carried out to assess the thermal stability of the microcapsules and quantify the active content. The TGA 550 instrument from TA instruments was used to conduct TGA analysis at a heating rate of 20 °C per minute in a nitrogen atmosphere.

*4.2.4. Extraction of active ingredient from microcapsules*

0.1 g of a dried microcapsule sample containing an active ingredient DEET was weighed accurately before being transferred to a 100 mL round-bottom flask. To this flask, 30 mL of 50% (v/v) aqueous methanol was added and refluxed for six hours. After refluxing, the mixture was cooled down to ambient temperature, filtered through a Grade-3 sintered glass crucible, and washed with 20–30 mL of aqueous methanol containing 50% v/v methanol. The filtrate was transferred to a 100 mL volumetric flask and diluted to the mark with distilled water. This solution was further diluted until the concentration of the final diluted solution fell within the calibration range. Final dilutions were made in triplicate, absorbance at 251 nm ($\lambda_{max}$ of DEET)

was measured using Hitachi 220 UV-VIS spectrophotometer, and the concentration of the active component was calculated using the following formula:[20]

$$Active\ Ingredient\ (\%)\ =\ \frac{Dilution\ Factor\ \text{x}\ Absorbance}{Calibration\ Slope\ \text{x}\ mg\ of\ sample}\ x\ 100$$

*4.2.5. Release measurements*

In a dissolution test apparatus (LABINDIA- DS8000), the release of MICs was studied. In this investigation, 100 mg of microcapsules were dispersed in 1000 mL of distilled water and stirred for 48 h at 130 RPM and 30 °C. Aliquots of 10 mL were withdrawn at regular intervals and replaced with an equal volume of fresh distilled water to keep the concentration gradient consistent. The absorbance of the aliquots was measured using a UV-vis spectrophotometer (Hitachi 220 UV-VIS spectrophotometer) at $\lambda_{max} = 251$ nm to determine the percent release of DEET from MICs. DEET levels in the reservoir never went higher than 70 parts per million (ppm), which is 70 mg. This concentration is an order of magnitude below the water solubility limit for DEET (1000 ppm). To avoid a substantial time-dependent decrease in dissolution rates due to solubility issues and subsequent inaccuracies in release data, it is recommended to use a dissolution media volume five to ten times higher than the saturation limit, i.e., maintaining perfect sink conditions.

## 4.3.  **Results and discussions**

The hyperbranched polycarbonate polyol (PCPO) was insoluble in water, but it dissolved in ethylene glycol solution to produce a clear, transparent solution. Three distinct solutions of hyperbranched PCPO in ethylene glycol were prepared by substituting ethylene glycol with PCPO by 20, 30, and 50 wt. %. Due to PCPO's insolubility in water, an oil-in-oil emulsion was made instead of an oil-in-water emulsion to prevent precipitation of PCPO in water, and this emulsion containing diisocyanate was then reacted with a solution of polyol (PCPO in EG) in continuous phase to form microcapsules.

*4.3.1. Microencapsulation of DEET via oil-in-oil emulsion*

TDI (monomer) and DEET (active ingredient) solution formed an immiscible dispersed phase in the liquid paraffin oil resulting in an oil-in-oil emulsion stabilized by Hypermer A70. The stabilized emulsion had droplet sizes in the range of 1-12 µm as shown in **Fig 4.1**. Polyol (EG and EG+PCPO) reacted with TDI at the interface of the emulsion droplet and formed a solid polymer wall around it with active ingredient DEET as the core. Good spherical and smooth microcapsules as free flowing powder were obtained with varying amounts of PCPO as polyol component.
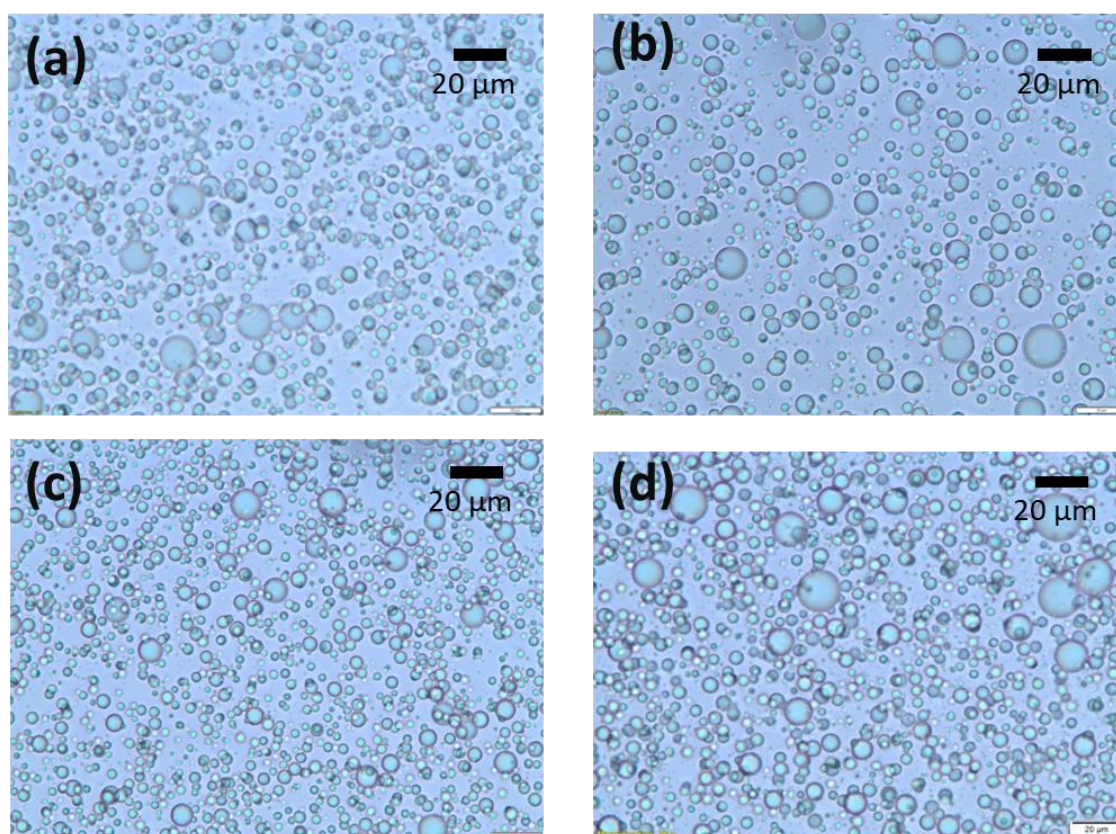


**Figure 4.1** Optical microscopic images of the emulsion for (a) MIC_DEET_EG_TDI; (b) MIC_EG+PCPO(20%); (c) MIC_EG+PCPO(30%); (d) MIC_EG+PCPO(50%).

SEM images shown in **Fig. 4.2** show prepared MICs using various proportions of PCPO. MICs are smooth and perfectly spherical with diameter in the range of 1-10 µm for MIC_DEET_EG_TDI and MIC_EG+PCPO(20%) whereas the size slightly increased to 1-12 µm with an increase in the amount of PCPO in case of MIC_EG+PCPO(30%) and
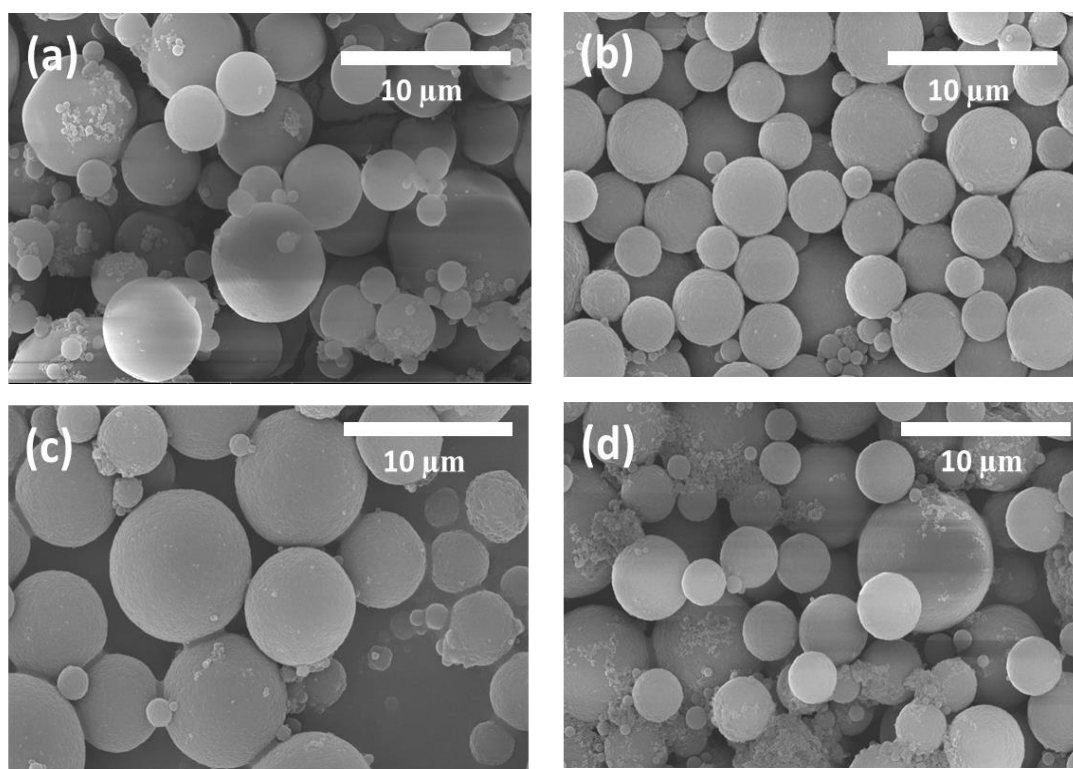
**Figure 4.2** SEM images of the emulsion for (a) MIC_DEET_EG_TDI; (b) MIC_EG+PCPO(20%);
(c) MIC_EG+PCPO(30%); (d) MIC_EG+PCPO(50%).
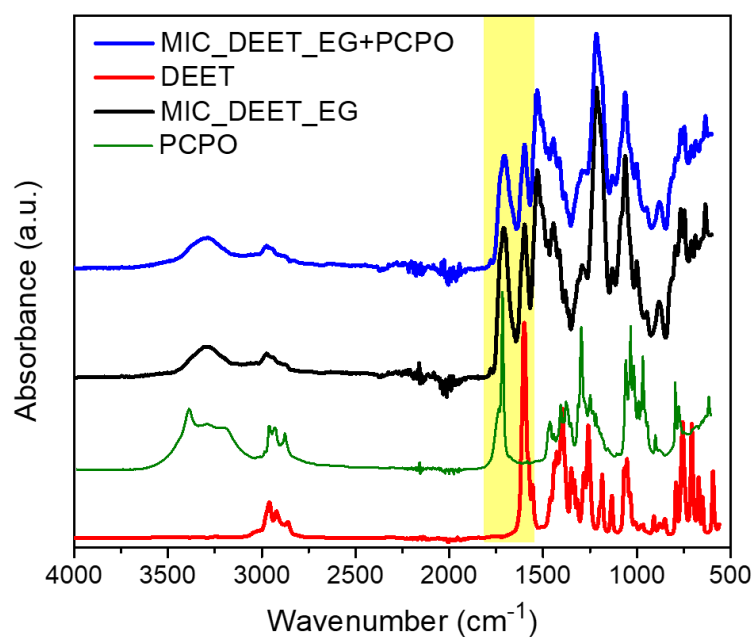


**Figure 4.3** FTIR spectrum of PCPO, DEET, MIC_DEET_EG and MIC_DEET_EG+PCPO.

MIC_EG+PCPO(50%). The size of the MICs in optical images of the emulsion and the size of MICs obtained in the end was consistent. The presence of DEET was confirmed by FTIR shown in **Fig. 4.3** where carbonyl (C=O) stretching band at 1623 cm^{-1} (band in highlighted region) can be observed. Also, an indistinguishable broader band appearing at 1714 cm^{-1} may correspond to the carbonyl (C=O) of carbonate bond and urethane linkage.[21]

*4.3.2. Encapsulation efficiency of active ingredient*

The encapsulation efficiency of the active ingredient encapsulated in PUU MICs was determined using extraction studies. Aqueous methanol 50% (v/v) was used to extract the complete active ingredient from the MICs by refluxing the capsules for six hours as described in the previous reports.[20] The slope for the active ingredient DEET was calculated from the calibration curve. Theoretical loading for the MICs was around 50% (w/w) w.r.t. polymer weight. Extraction studies reveal that the encapsulation efficiency was as high as 81% in the case of MIC_DEET_EG_TDI whereas it decreased with the incorporation of PCPO from 71% for MIC_EG+PCPO(20%) to 75% and 69% for MIC_EG+PCPO(30%) and MIC_EG+PCPO(50%), respectively as can be seen in **Table 4.1**. This can be due to the reduced diffusion of hyperbranched PCPO to the surface owing to the flexible large structure, as well as the increased flexibility affecting the reactivity and delay in wall construction, which resulted in the leaking out of active ingredient.

*4.3.3. Thermogravimetric analysis*

TGA was carried out to check the thermal stability of the MICs and determine the encapsulation efficiency. **Fig. 4.4** illustrates a thermogram of MICs prepared using only EG and with PCPO. TGA for DEET was also carried out for the reference to determine the degradation of active ingredient. DEET and microspheres show multi-step degradation. In the case of DEET, degradation starts around 100 °C and degrades completely at 200 °C whereas in case of microspheres, degradation starts at 230 °C and ends at 350 °C.[20] In the case of MICs three step

**Table 4.1** Extraction of DEET from the polyurea-urethane microcapsules.

| Sample | Theoretical Loading (%) | Loading (Extraction) (%) | EE (%) |
|---|---|---|---|
| MIC_EG_TDI | 50 | 40.5 | 81 |
| MIC_EG+PCPO 20_TDI | 50 | 35.75 | 71.5 |
| MIC_EG+PCPO 30_TDI | 50 | 37.75 | 75.5 |
| MIC_EG+PCPO 50_TDI | 50 | 34.75 | 69.5 |
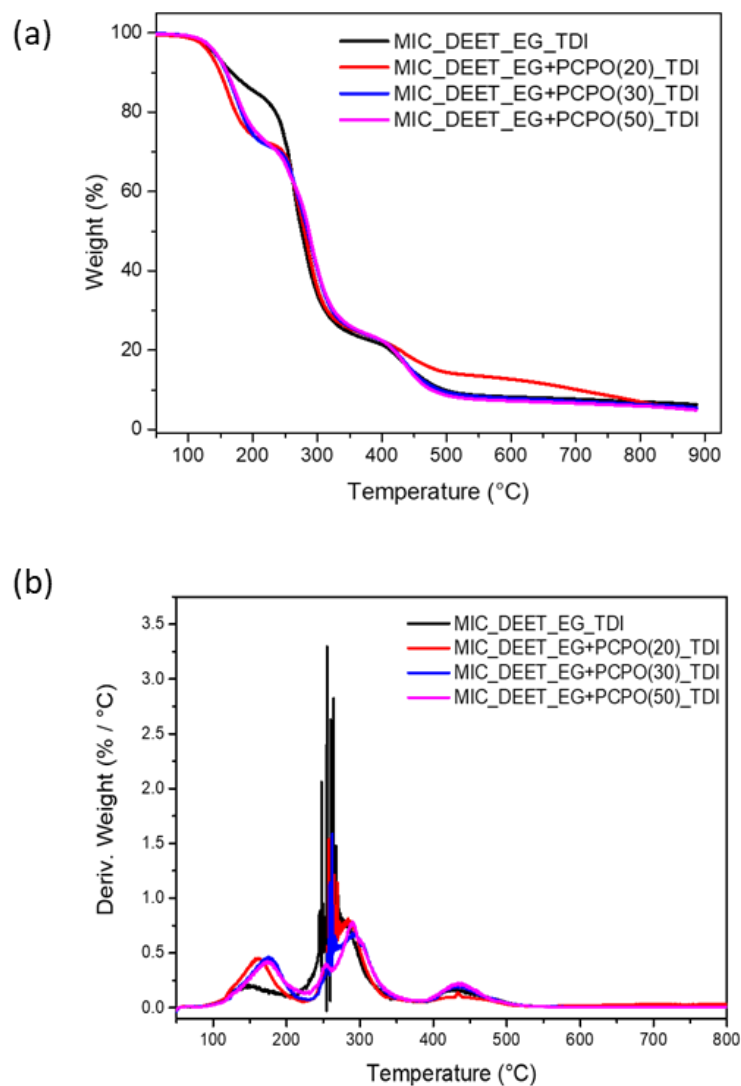


**Figure 4.4** (a) TGA and (b) differential thermogravimetry curves of DEET, MIC_DEET_EG_TDI, MIC_EG+PCPO(20%), MIC_EG+PCPO(30%), MIC_EG+PCPO(50%).

degradation was observed where first degradation starts from 110 °C until 206 °C in the case of MIC_DEET_EG whereas the degradation curve ends above 225 °C which can be ascribed to the loss of DEET from the microcapsules. The second degradation step starts at 206 °C in the case of MIC_DEET_EG and above 225 °C for MIC_DEET_EG+PCPO and is due to polymer decomposition. The same can be seen in the differential TGA thermogram. In the case of MICs, we were able to observe a change in the loss of DEET to higher temperatures, as well as an overlap between the DEET decomposition peak and the polymer decomposition peak. Consequently, it was challenging to precisely quantify the DEET concentration of the MICs using TGA. We may at least deduce that the encapsulation of DEET slows its thermal degradation.

### 4.3.4. Release study of DEET from MIC

According to the standard protocol reported elsewhere, the release of active ingredient DEET from the MICs was determined.[20] Multiple experiments were performed, and the average values have been considered in the release curves shown in **Fig. 5**. Cumulative release curve of the DEET from MICs for 48 h shows that almost all the MICs show a similar release profile. There is no significant effect of the addition of aliphatic flexible hyperbranched PCPO on the barrier properties. This could be attributed to the fact that PCPO with hyperbranched structure provides crosslinking of polymer chains which is supposed to improve the barrier properties however, this is negated by the aliphatic flexible polyol which shows plasticizing effect. Hence, there is no significant change in barrier properties. The maximum release from the MICs was around 30% after 48 h. However, we could ascertain that these formulations provide us with comparable barrier properties even after the introduction of biodegradable components in the formation of PUU MICs.
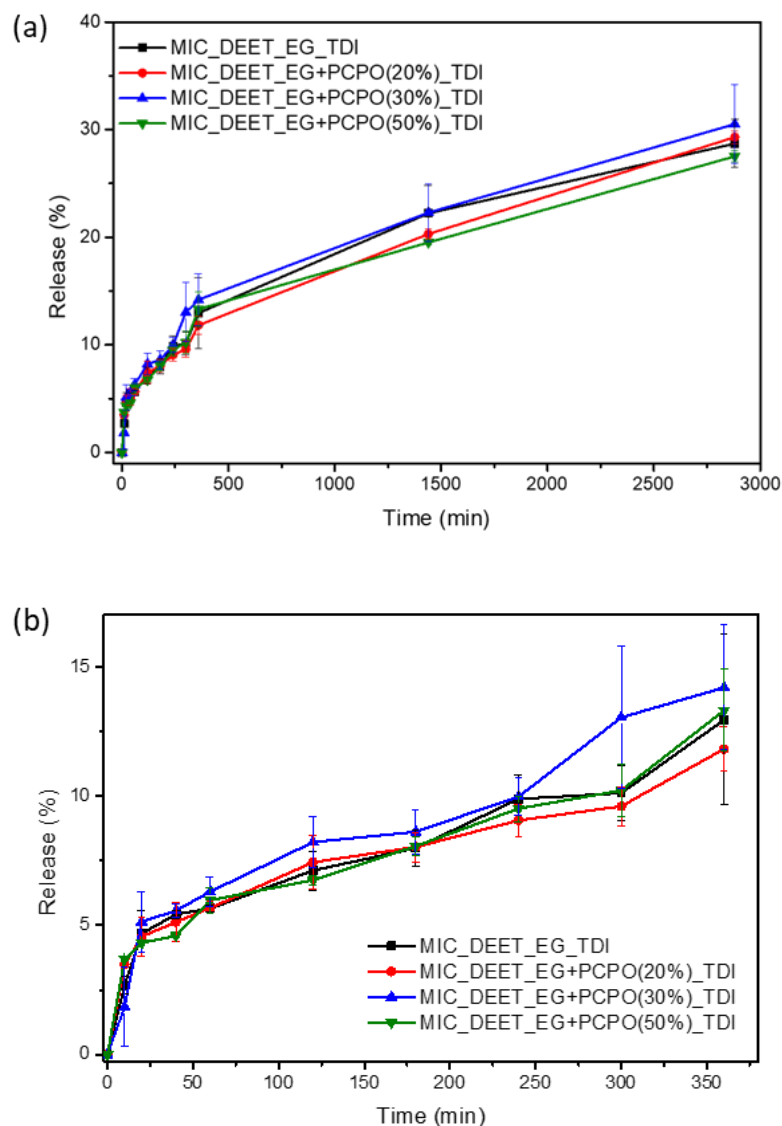
**Figure 4.5** Release profile of DEET from microcapsules in distilled water at 30 °C (a) overall release, (b) initial release.

### 4.3.5. *Mathematical interpretations*

After determining the DEET release profile from MICs, we attempted to interpret the release data using a mathematical model to get a deeper understanding of the release mechanism regulating the release of the active ingredient from MICs.[22] Diffusion is often responsible for governing the release of hydrophilic active ingredients from encapsulation, whereas swelling and matrix erosion can regulate the release of hydrophobic active ingredients. Since the

solubility of the DEET is substantial in water i.e., 1000 ppm and polyurea-urethane which forms the shell is relatively hydrophobic, we anticipated that the release is likely to be governed by diffusion mechanism. To validate this assumption, following Peppas equation was used for fitting the experimental release profile:[23,24]

$$\frac{M_i}{M_\infty} = K.t^n$$

where, $M_i/M_\infty$ corresponds to the fraction of active release at time $t$, $K$ is the release constant and $n$ represent the mechanism of release at time $t$. **Fig 4.6** displays very well fitting of the experimental release profile using this equation. **Table 4.2** reveals the values of $K$, $n$ and $R^2$ for all the prepared samples. The inclusion of PCPO as polyol into the polymer wall has no effect on the value of $K$, which correlates with the release profiles of DEET from MICs.

**Table 4.2**. Parameters for Korsmeyer–Peppas model used for experimental release profile fitting.

| Sample | $n$ | $k$ | $R^2$ |
|---|---|---|---|
| MIC_DEET_EG_TDI | 0.42 | 0.010 | 0.99 |
| MIC_DEET_EG+PCPO(20)_TDI | 0.43 | 0.009 | 0.99 |
| MIC_DEET_EG+PCPO(30)_TDI | 0.41 | 0.012 | 0.99 |
| MIC_DEET_EG+PCPO(50)_TDI | 0.40 | 0.011 | 0.99 |

The exponent '$n$' in the Korsmeyer–Peppas model is less than 0.43, indicating a deviation from the Fickian diffusion range. However, Ritger and Peppas observed values as low as 0.3 for polydisperse Fickian materials.[25] They determined that it is impossible to identify a definite range of $n$ for samples with particle size dispersion. Thus, it can be inferred that diffusion controls the release predominantly. **Fig. 4.6** depicts the experimental release data and the expected release curves derived from Korsmeyer–Peppas model.
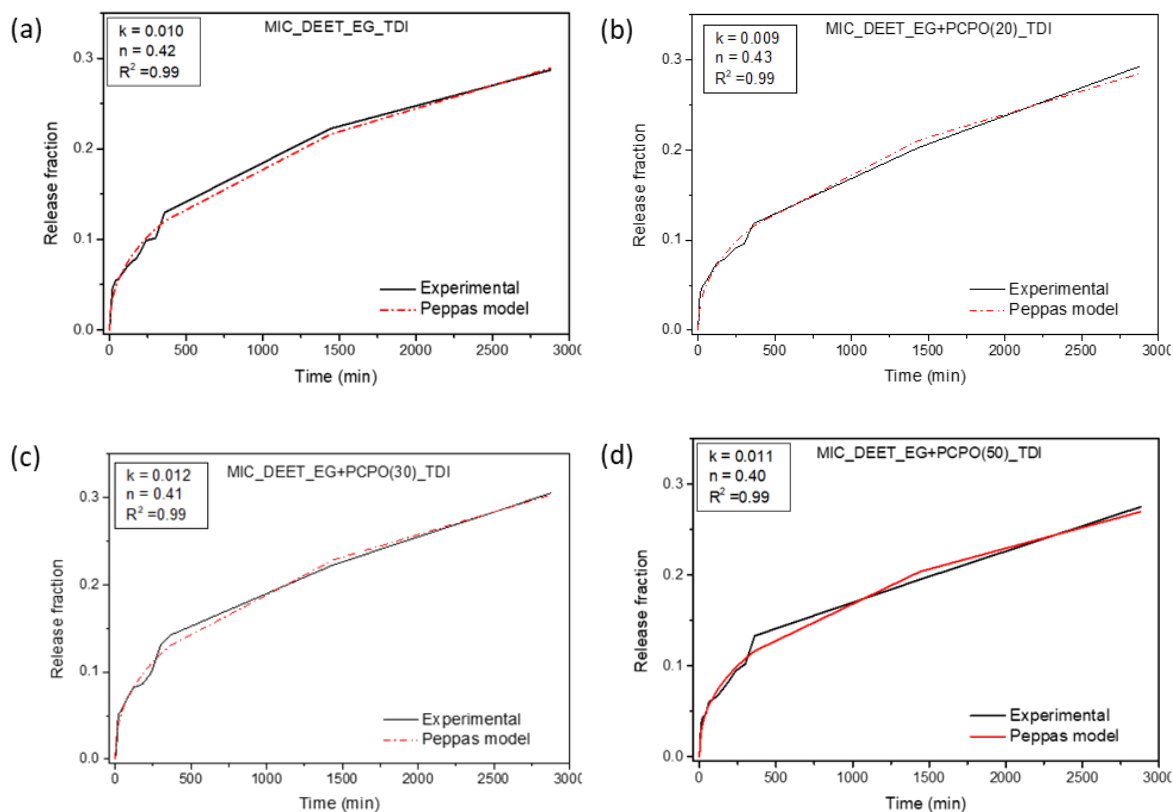
**Figure 4.6** Experimental and mathematical interpretation of release profile for (a) MIC_DEET_EG_TDI; (b) MIC_EG+PCPO(20%); (c) MIC_EG+PCPO(30%); (d) MIC_EG+PCPO(50%).

## 4.4. Conclusion

This study illustrates that aliphatic hyperbranched polycarbonate polyols (PCPO) can be used as a biodegradable polyol component to prepare polyurea-urethane microcapsules encapsulating DEET as model active ingredient. Although few reports are available on preparing polyurethanes using biodegradable substrates, they are not used in preparing PUU microcapsules using interfacial polycondensation with improved or comparable barrier properties. Here, we report on the successful encapsulation of DEET by interfacial polycondensation by replacing up to 50% of conventional ethylene glycol with hyperbranched polycarbonate polyol using oil-in-oil emulsion. The microcapsules obtained were spherical and smooth, with a size range of 1–12 µm. Encapsulation efficiency was as

high as 81% for MICs prepared using EG, however, with the incorporation of 20% (w/w) PCPO, the encapsulation efficiency was decreased to ~72%. Further increase in the PCPO concentration resulted in further decrease in the encapsulation efficiency. Thermogravimetric analysis of MICs indicates a delayed decomposition of DEET upon encapsulation. Release profile reveals that the barrier properties were not compromised with the introduction of highly flexible aliphatic hyperbranched PCPO in the wall matrix. Mathematical interpretation of release profile using Korsemayer-Ritger–Peppas model revealed that the release of DEET is governed by non-Fickian diffusion and there is no significant change in the release rate constant $K$ which correlates with the release profile of DEET from MICs.

## 4.5.  References

1.  Armentano, I., Puglia, D., Luzi, F. Nanocomposites based on biodegradable polymers. *Materials (Basel)* **2018**, *11*, 5, 795.

2.  Song, J., Babayekhorasani, F., Spice. P. T.  Soft bacterial cellulose microcapsules with adaptable shapes. *Biomacromolecules* **2019**, *20*, 12, 4437–4446.

3.  Valle, J. A., Valle, R. C. S. C., Bierhalz, A. C. K., Bezerra, F. M., Hernandez, A. L., Arias, M. J. L. Chitosan microcapsules: Methods of the production and usein the textile finishing. *J. Appl. Polym. Sci*. **2021**, *138,* e50482.

4.  Madan, P. L., Jani, R. K., Bartilucci, A. J. New method of preparing gelatin microcapsules of soluble pharmaceuticals. *J. Pharm. Sci*. **1978,** *67,* 3, 409-411.

5.  Gonzalez-Pujana, A., Orive, G., Pedraz, J.L., Santos-Vizcaino, E., Hernandez, R.M. Alginate Microcapsules for Drug Delivery. In: Rehm, B., Moradali, M. (eds) Alginates and Their Biomedical Applications. Springer Series in Biomaterials Science and Engineering, **2018**, vol 11. Springer, Singapore.

6. Noh, J., Kim, J., Kim, J. S., Chung, Y. S., Chang, S. T., Park, J. Microencapsulation by pectin for multi-components carriers bearing both hydrophobic and hydrophilic active agents. *Carbohydr. Polym*. **2018**, *182*, 172-179.

7. Tian, S., Xue, X., Wang, X., Chen, Z. Preparation of starch-based functional food nano-microcapsule delivery system and its controlled release characteristics. *Front. Nutr*. **2022**, *9*, 982370.

8. Zhi, Z., Haynie, D. T. High-capacity functional protein encapsulation in nanoengineered polypeptide microcapsules. *Chem. Commun*., **2006**, *2*, 147-149.

9. Arshady, R. Preparation of biodegradable microspheres and microcapsules: 2. Polyactides and related polyesters. *J. Control. Release*. **1991**, *17*, 1, 1-21.

10. Brunner, C. T., Baran, E. T., Pinho, E. D., Reis, R. L., Neves, N. M. Performance of biodegradable microcapsules of poly(butylene succinate), poly(butylene succinate-co-adipate) and poly(butylene terephthalate-co-adipate) as drug encapsulation systems. *Colloids Surf. B* **2011**, *84*, 498–507.

11. Parente, J. F., Sousa, V. I., Marques, J. F., Forte, M. A., Tavares, C. J. Biodegradable Polymers for Microencapsulation Systems. *Adv. Polym. Tech*. **2022**, *2022*, 1-43.

12. Li, M., Rouaud, O., Poncelet, D. Microencapsulation by solvent evaporation: state of the art for process engineering approaches. *Int. J. Pharm*. **2008**, *363*, 1-2, 26-39.

13. Halahlah, A., Piironen, V., Mikkonen, K. S., Ho, T. M. Polysaccharides as wall materials in spray-dried microencapsulation of bioactive compounds: Physicochemical properties and characterization. *Crit. Rev. Food Sci. Nutr*. **2022**, *16*, 1-33.

14. Xu, J., Feng, E., Song, J. Renaissance of aliphatic polycarbonates: new techniques and biomedical applications. *J. Appl. Polym. Sci*. **2014,** *131,* 5, 39822.

15. Thorat, S. D., Phillips, P. J., Semenov, V., Gakh, A. Physical properties of aliphatic polycarbonates made from $CO_2$ and epoxides. *J. Appl. Polym. Sci*. **2003**, *89*, 5, 1163-1176.

16. Cheng, M., Lobkovsky, E. B., Coates, G. W. Catalytic Reactions Involving C1 Feedstocks: New High-Activity Zn(II)-Based Catalysts for the Alternating Copolymerization of Carbon Dioxide and Epoxides. *J. Am. Chem. Soc*. **1998**, *120*, 42, 11018-11019.

17. Špírková, M., Pavličević, J., Strachota, A., Poreba, R., Bera, O., Kaprálková, L., Baldrian, J., Šlouf, M., Lazić, N., Budinski-Simendić, J. Novel polycarbonate-based polyurethane elastomers: Composition–property relationship. *Eur. Polym. J*. **2011**, *47*, 5, 959-972.

18. Tamura, M., Nakagawa, Y., Tomishige, K. Direct $CO_2$ Transformation to Aliphatic Polycarbonates. *Asian J. Org. Chem*. **2022**, *11*, 11, e202200445.

19. Shukla, P.G., Jadhav, A. S. Microcapsules containing water soluble amine and process for the preparation thereof. US 0325448 A1, **2017**.

20. Kadam, S. L., Yadav, P., Bhutkar, S., Patil, V. D., Shukla, P. G., Shanmuganathan, K. Sustained release insect repellent microcapsules using modified cellulose nanofibers (mCNF) as pickering emulsifier. *Colloids Surf., A Physicochem Eng. Asp*. **2019**, *582*, 123883.

21. Javidi, M., Fathabadi, H. F., Jahromi, S. A. J., Khorram, M. Investigating the interfacial synthesis of polyurethane microcapsules and optimization of the process using response surface method. *Mater. Res. Express* **2019**, *6*, 105302.

22. Agnes, E. J., Gonzales Ortega, G. Mathematical models and physicochemical of diffusion, Pharmacy Book, **2003**, *19*, 9–19.

23. Korsmeyer, R. W., Gurny, R., Doelker, E. M., Buri, P., Peppas, N. A. Mechanism of solute release from porous hydrophilic polymers. I*nt. J. Pharm*. **1983**, *15*, 25–35.

24. Ritger, P. L., Peppas, N. A. A simple equation for describing solute release. I. Fickian and non-Fickian release from non-swellable devices in the form of slabs, spheres, cylinders or discs. *J. Control. Release* **1987**, *5*, 23–36.

25. Huang, L., Zhang, X., Xu, M., Chen, J., Shi, Y., Huang, C., Wang, S., An, S., Li, C. Preparation and mechanical properties of modified nanocellulose/PLA composites from cassava residue. *AIP Adv*. **2018**, *8*, 025116.

# Chapter 5

# PCL/PLA-based microspheres using interfacial polymerization technique

## 5.1. Introduction

The physicochemical properties of polymers such as solubility, viscosity, emulsifying properties, thermal stability, and mechanical properties, are crucial for realizing higher encapsulation efficiency and microcapsule stability.[1] In addition, the particle size range of the microcapsule's compatibility between the wall and core materials, processing and economic aspects, are other factors that determine the commercial scope of developed microcapsules.[2] Various wall materials have been explored recently, including both natural and synthetic polymers and composites. In recent years, biodegradability has become a desirable property for microencapsulation due to the rising risk of microplastics in the environment and their associated health issues.[3] Natural polymers have been extensively explored owing to their biodegradability and biocompatibility (non-toxicity), but they have certain drawbacks owing to their inconsistency in molecular weight, which results in the variation of size, size distribution, shape, and release characteristics.[4] This has resulted in the use of synthetic biodegradable polymers, primarily aliphatic polyesters, polyamides, polycarbonates, polybutylene succinate, etc., where the molecular weight of the polymer may be controlled, and consistent properties can be obtained, and the presence of ester, anhydride and amide linkages provide degradability.[5,6]

Aliphatic polyesters, especially poly(lactic acid) (PLA), poly(lactic-co-glycolic acid) (PLGA), poly(caprolactone) (PCL), poly(hydroxy alkanoates) (PHAs), etc., are extensively used in diverse fields such as commodity polymers,[7] pharmaceuticals,[8] packaging,[9] etc. Polyesters derived from abundant renewable resources have certain advantages over other polymers, including, compostability, recyclability, biocompatibility, and hydrolysis *via* enzymatic and non-enzymatic processes that yield various non-harmful small molecules.[10,11] Some of the polyesters are FDA-approved, and due to their unique physical features and varying erosion

rates are desirable for biomedical applications.[12] They can be used to form films and sheets, injection-molded into various products, spun into fibers,[13] and can also be 3-D printed.[14] They have also been used to prepare biodegradable microcapsules for the sustained release of active ingredients in various applications, including drug carrier,[15] pesticide delivery,[16] and thermal energy storage systems.[17] Generally, techniques employed to prepare microcapsules of polyesters involve emulsion-solvent evaporation,[18] multiple emulsion-solvent evaporation,[19] gas/oil/water and bubble template method,[20] spray drying,[21] and electrospraying.[22] PLA microcapsules can regulate drug release rates across different time periods, ranging from a few days to several weeks to a year, based on the molecular weight of PLA, size, encapsulation efficiency, solubility, and diffusion ability.[23] Both hydrophilic and hydrophobic active ingredients can be encapsulated in the polyester matrix. Hydrophilic active ingredients are dispersed in the PLA matrix during microcapsule preparation, whereas hydrophobic active ingredients remain soluble along with polyesters. Using microencapsulation processes, good spherical microcapsules can be created; however, they are also associated with certain drawbacks, including the usage of organic solvents. The use of solvents may necessitate high temperatures for their removal and may not be appropriate for the encapsulation of a few active ingredients. In addition, the elimination of the solvent may result in the formation of pores in the wall membrane and compromise encapsulation efficiency.

Interfacial polycondensation technology is preferred over other techniques due to its simplicity, reliability, high encapsulation efficiency, high control over the mean size and membrane thickness, low cost, and scalability. In a recent report, interfacial polycondensation was used to prepare polyester-urethane microcapsules. Initially, PLA-diol was synthesized via ring-opening polymerization, which was followed by a reaction with diurethane to yield PLA-diisocyanate. Resulted PLA-diurethane forms the oil phase owing to the hydrophobicity of PLA and reacted at the interface of the emulsion droplet with diamines present in the aqueous

phase in the presence of the catalyst to yield polyester-urea-urethane microcapsules.[24,25] PLA-diurethane are susceptible to hydrolysis and may result in varying amounts of free isocyanate functional groups, resulting in reaction variability and limiting commercial scalability. Polyesters can be used to prepare microspheres and microcapsules via interfacial polycondensation using different approaches. Among various known chemistries, epoxy-amine chemistry is extensively explored for a variety of applications and can be employed to prepare microspheres as well.

In this study, we attempted to prepare polyester microspheres utilizing polyesters and epoxy amine chemistry. Initially, PLA-diol and PCL-diol were synthesized via ring-opening polymerization of L-lactide and -caprolactone on 1,4-butanediol. The prepared diols were then treated with epichlorohydrin to obtain PLA-diglycidyl ether (PLA-DGE) and PCL-diglycidyl ether (PCL-DGE). These oligomers were dissolved in chloroform to form the oil phase in oil-in-water emulsion and subsequently reacted with diamines present in the aqueous phase to form microspheres.

## 5.2. Materials and methods

### 5.2.1. Materials

PCL-diol (Mn: 530, 1250), Tin (II) octanoate, 1,8-Diazabicyclo(5.4.0)undec-7-ene (DBU), $\varepsilon$-caprolactone (CL), 4-Dimethylaminopyridine (DMAP), 1,4-diazabicyclo[2.2.2]octane (DABCO), and polyvinyl alcohol (PVA) (Mn 13,000 to 23,000) were procured from Sigma Aldrich, USA. Butane-1,4-diol (BDO) and sodium hydroxide (NaOH) were procured from Merck. Boron trifluoride etherate was procured from Spectrochem Pvt. Ltd. Mumbai. Epichlorohydrin was procured from TCI chemical Pvt. Ltd. L-lactide monomer was purchased from Purac Asia Pacific Pte Ltd. (Singapore) to prepare PLA-diols. Hexamethylenediamine (HMDA) and dichloromethane (DCM) AR grade was procured from Thomas Baker Chemicals

Pvt. Ltd. The chemicals were used as received. Distilled water was used to prepare the continuous phase and washing during microspheres preparation.

### 5.2.2. Methods

#### 5.2.2.1. *Preparation of PLA-diol*

In a round-bottomed flask, the mixture of initiator, i.e., butane-1,4-diol (BDO), L-(-)-lactide, and DBU, was heated under a nitrogen atmosphere at 130 °C for 90 min to form PLA-diol of various molecular weights.[26] The as-prepared PLA-diols were dissolved in the minimum amount of dichloromethane and reprecipitated in cold petroleum ether to remove the catalyst, followed by drying under vacuum to obtain viscous (low molecular weight PLA diol) to white solid (above 6000 molecular weights of PLA-diol).

#### 5.2.2.2. *Preparation of PCL-diol*

Similar protocol was used to prepare PCL-diol using 1,4-BDO as an initiator and $\varepsilon$-caprolactone as a monomer.

#### 5.2.2.3. *Preparation of PLA-DGE or PCL-DGE from diols*

PLA-DGE or PCL-DGE was prepared by reacting PLA-diol or PCL-diol with epichlorohydrin in the presence of boron trifluoride diethyl etherate as catalyst using previously reported method.[27] In a nutshell, the dried PLA-diol and catalyst boron trifluoride diethyl etherate were transferred to a dried round-bottomed flask and heated to 80 °C in a nitrogen atmosphere. While mechanically stirring the solution, epichlorohydrin was added to solution dropwise over 30 minutes and stirred for another 6 h. The reaction mixture was cooled to 55 °C, and 50 wt.% aqueous sodium hydroxide was added dropwise. The reaction mixture was then stirred for another 6 h and then cooled to room temperature. The suspension obtained was dissolved in DCM, precipitated in cold methanol, filtered, and dried under vacuum.

**Step 1:**
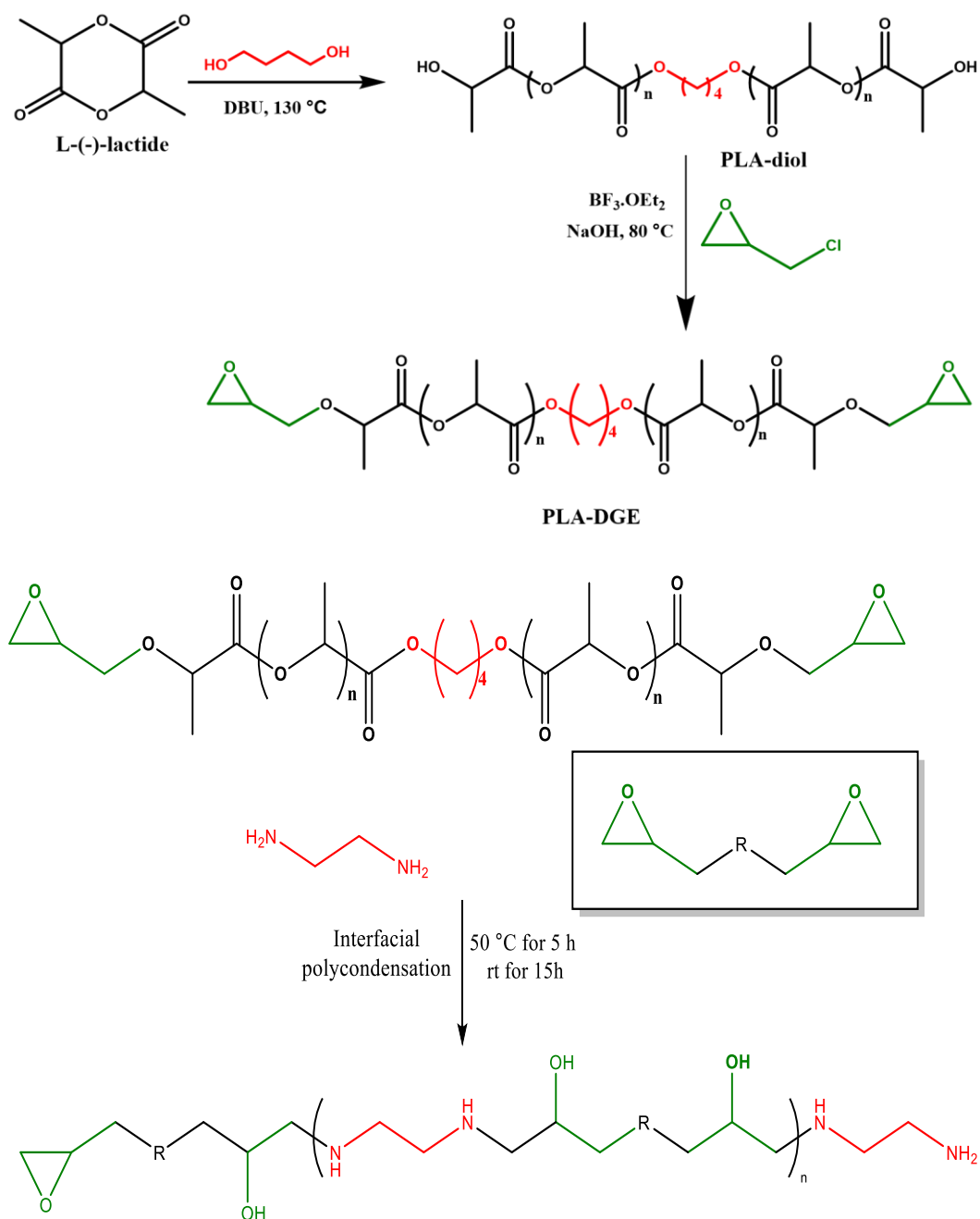


**Scheme 5.1**. Preparation of PLA-diol and PLA-DGE followed by preparation of microspheres.

5.2.2.4.    *Preparation of microspheres using interfacial polymerization*

Microcapsules were prepared by reacting DGE with diamines (1,6-hexamethylene diamine (HMDA) and ethylene diamine (EDA)) using an interfacial polymerization technique in the presence of a catalyst using a previously reported method.[28] In brief, a continuous medium was

prepared with 5 wt.% aqueous solution of PVP-K90. To the continuous medium, a PLA-DGE or PCL-DGE solution in chloroform was added to form an emulsion. The emulsion was further stirred for 15 min for stabilization. To the stable emulsion, a solution of diamine and the catalyst DABCO (mixed in a surfactant solution) was added dropwise over 30 min. The resultant reaction mixture was stirred for 5 h at 40 °C or 70 °C using a water bath before adding 2 wt.% fumed silica to prevent agglomeration and left for stirring at ambient conditions for another 15 h for the completion of the reaction. After the reaction was completed, the milky suspension was centrifuged, washed with distilled water, filtered using Whatman filter paper no. 1 and dried in an incubator at 37 °C overnight to obtain waxy solid MIS.

*5.2.2.5.    Characterization*

The synthesis of PLA-DGE and PCL-DGE was confirmed by $^1$H-NMR using JEOL 200 MHz NMR in deuterated chloroform (CDCl$_3$). Samples were prepared by dissolving 15 mg of product in 0.6 mL of CDCl$_3$ and recorded in a quartz NMR tube. Optical and scanning electron microscopy were used to examine the morphology of microcapsules. The formation of microspheres was observed using an Olympus BX-60, USA, optical microscope equipped with an Olympus SC30 digital camera. To examine the morphology of MICs, a scanning electron microscope (SEM) (E-SEM, Quanta 300) was employed. To prevent charging, samples were sputter-coated with gold before SEM imaging.

## 5.3.    Results and Discussion

PLA-diol and PCL-diol of varying molecular weights were synthesized using the organo-catalyst DBU via ring-opening polymerization using butane-1,4-diol (BDO) as an initiator. The prepared oligomers were characterized by $^1$H NMR in CDCl$_3$. PLA with low molecular weight was a pale yellowish viscous liquid whereas PLA or PCL diols with molecular weight higher than 2 kD were obtained as free flowing powder. The prepared diols and commercial diols were further reacted with epichlorohydrin to obtain diglycidyl ethers, which were again

confirmed by ^{1}H NMR. **Fig 5.1** shows the ^{1}H NMR of the PLA-diol and PLA diglycidyl ether (PLA-DGE). A multiplet appearing at 5.15–5.18 ppm corresponds to the methine of lactic acid unit, whereas the peak appearing at 4.17 ppm corresponds to the methylene protons of BDO (initiator), confirming the formation of PLA-diol. In the ^{1}H NMR of PLA-DGE, an extra resonating peak appearing at 3.62-3.74 ppm corresponds to methylene protons of the linked diglycidyl confirming the formation of PLA-DGE. Similarly, PCL-DGE was characterized by ^{1}H-NMR shown in **Fig 5.2**, where extra resonating peaks other than PCL-diol appeared around 3.47-3.53 ppm (highlighted) corresponding to methylene hydrogens of the linked oxiranylmethyl group. ^{1}H NMR of synthesized PLA/PCL diols and DGEs are shown in the appendix figures A1-A10.
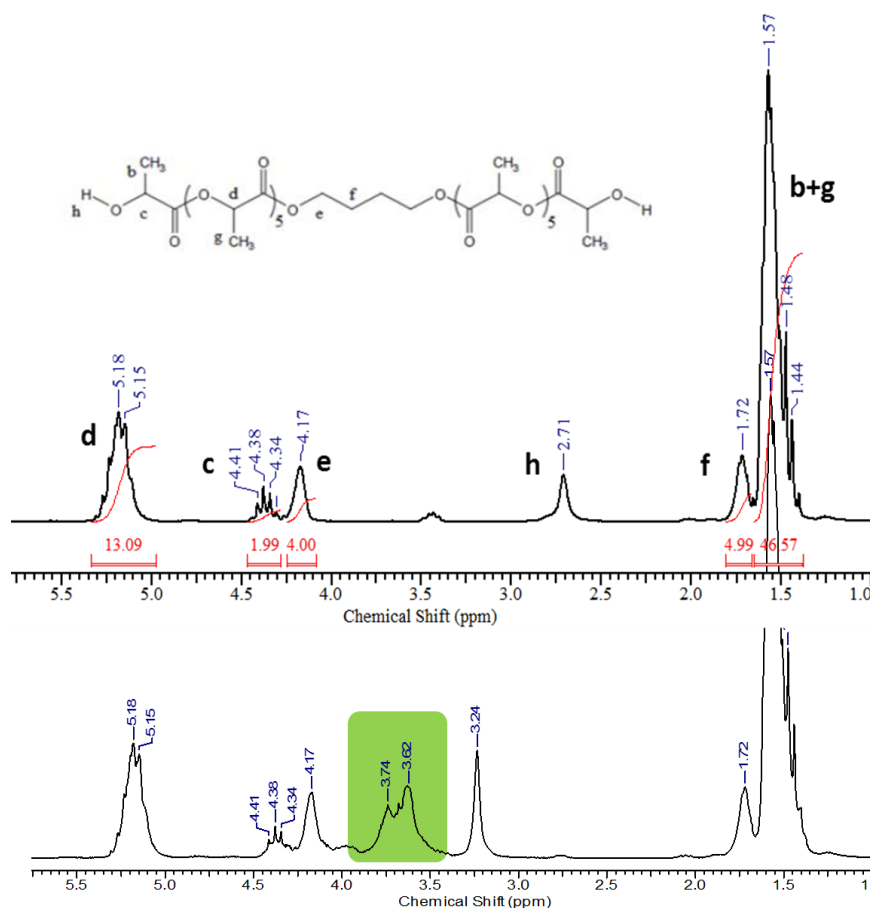


**Figure 5.1** 200 MHz ^{1}H NMR spectra of PLA-diol and PLA-DGE in CDCl$_3$.
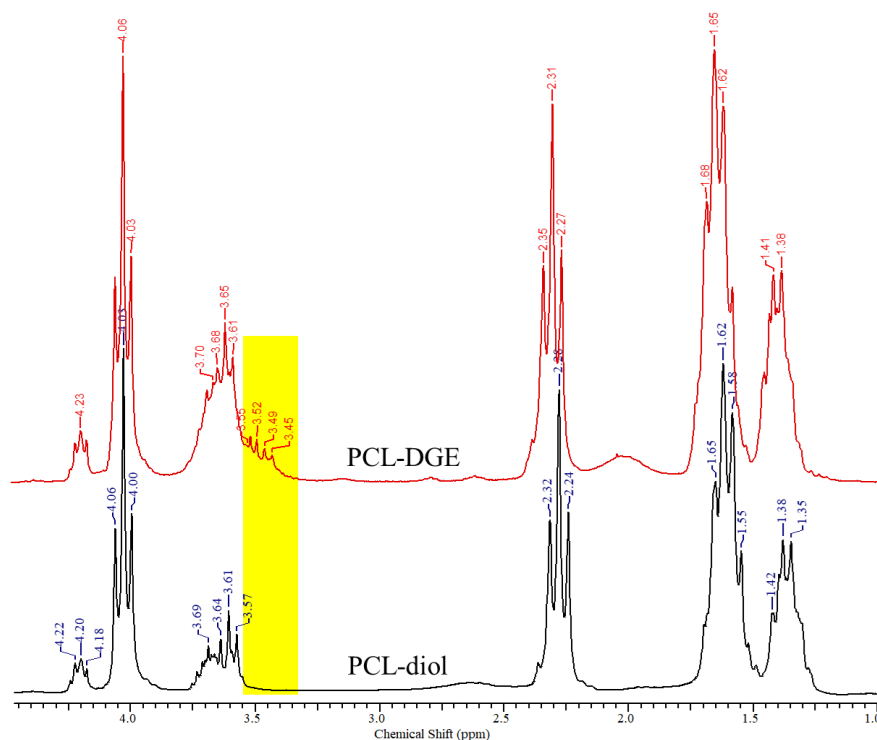
**Figure 5.2** 200 MHz $^1$H NMR spectra of PCL-diol and PCL-DGE in CDCl$_3$.

Microcapsules were prepared via an interfacial polycondensation technique where polyester diglycidyl ether was dissolved in a minimum amount of chloroform and was dispersed in an aqueous phase stabilized by PVP. Optical images given in **Fig 5.3** show the formation of oil-in-water emulsion stabilized by PVP. Further, diamines added into the continuous phase react with the DGEs at the interface. In general, the reaction between DGEs and amines is slow at room temperature but can be accelerated considerably at higher temperatures. In a report, DGEs were reacted with amines at 55 °C for two hours whereas at room temperature it takes approximately 48 hours to react.[17] Based on this report, polyester-DGE was reacted with diamines at 50 °C and 70 °C for 5 h to prepare microspheres, followed by stirring at ambient conditions for another 15 h. Microspheres obtained using the two different conditions were waxy and can be redispersed in water. Further, PEI was employed as a crosslinker to obtain solid microspheres. 10 wt.% of HMDA was replaced with PEI to prepare microspheres, but it did not show any improvement and waxy microspheres were obtained at both 50 °C and 70 °C.
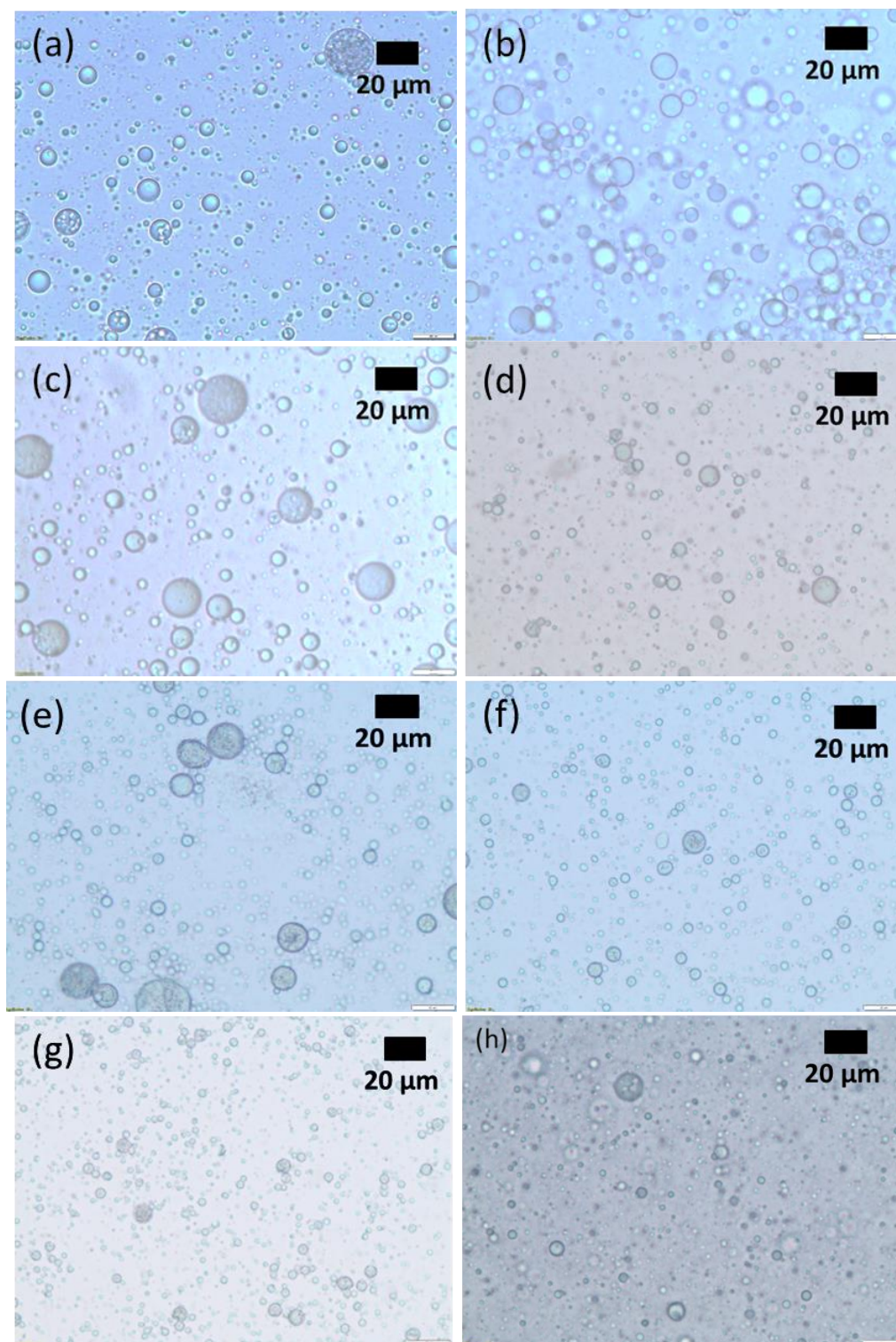
**Figure 5.3** Optical microscope images of emulsions of (a) MIS_PLADGE_HMDA (b) MIS_PCLDGE_HMDA prepared at 50 °C, (c) MIC_DMP_PCLDGE_HMDA prepared at °50 C, (d) MIS_PCLDGE_HMDA prepared at 70 °C; and redispersed microspheres (e) MIS_PLADGE_HMDA prepared at 50 °C, (f) MIS_PCLDGE_HMDA prepared at 50 °C, (g) MIS_PCLDGE_HMDA prepared at 70 °C and (h) MIS_PCLDGE_HMDA_PEI prepared at 50 °C.
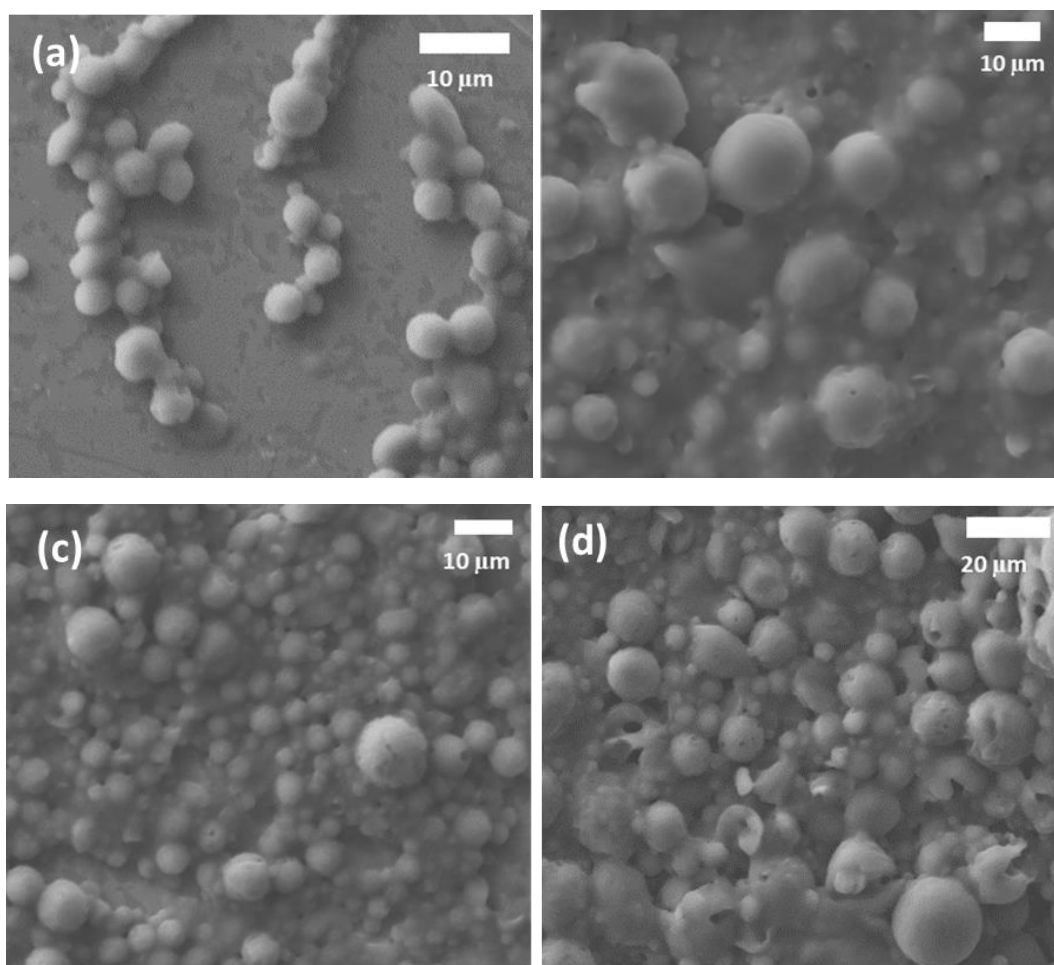
**Figure 5.4** SEM images of (a) MIS-PLA-DGE-HMDA, (b) MIS-PCLDGE-HMDA prepared at 50 °C, (c) MIS-PCLDGE-EDA-PEI(10%), (d) MIS-PCLDGE-HMDA prepared at 70 °C.

SEM images shown in **Fig. 5.4** depict spherical microspheres of sizes 1-10 µm for MIS_PLADGE_HMDA, whereas the sizes were in the range of 1-20 µm for MIS_PCLDGE_HMDA, MIS_PCLDGE_HMDA_PEI, and MIC_PCLDGE_HMDA when prepared at 70 °C.

None of the above-mentioned combinations and conditions resulted in the formation of solid microspheres. Further investigation is required to prepare solid microspheres. In future, aromatic or rigid crosslinkers can be used to make the shell robust and solid with polyester linkages which will act as degradable component. Additionally, aromatic diglycidyl ethers or poly(mandelide), which are more rigid than PLA and PCL, may be used in the future to prepare solid microspheres.

**Table 5.1** Reaction conditions, size, and observations of the microspheres prepared.

| | $M_n$ of DGE | Temperature (°C) | Size (µm) | Observation |
|---|---|---|---|---|
| MIS-PLA-DGE-HMDA (1:1.5) | 1200 | 50 | 1-10 | MIS were waxy |
| MIS-PCLDGE-HMDA (1:1.5) | 530 | 70 | 1-20 | MIS were waxy |
| MIS-PCLDGE-HMDA (1:1.5) | 530 | 50 | 1-20 | MIS were waxy |
| MIS-PCLDGE-EDA-PEI(10%) (1:1.5) | 530 | 70 | 1-20 | MIS were waxy |
| **MIC**-DMP-PCLDGE-HMDA (1:1.5) | 530 | 50 | 1-30 | Capsules cannot be separated |
| MIS-PCLDGE-EDA (1:1.5) | 1250 | 50 | 1-10 | MIS were waxy |
| MIS_PCLDGE-EDA (1:1.5) | 3000 | 50 | 1-10 | MIS were waxy |
| MIS-PCLDGE-EDA-PEI(10%) (1:1.5) | 3000 | 50 | 1-10 | MIS were waxy |

## 5.4.   Conclusion

This study demonstrates the fabrication of degradable polyester-based microspheres using epoxy-amine chemistry and the interfacial polycondensation method. Herein, PLA and PCL diols were synthesized using ring-opening polymerization with butane-1,4-diol as an initiator and catalysed by an organocatalyst such as DBU. The reaction of PLA or PCL diols with epichlorohydrin yielded PLA/PCL-DGEs, as verified by ^{1}H NMR spectroscopy analysis. PLA/PCL-DGEs were reacted interfacially with diamines catalysed by base (3° amines) at various temperatures and duration to generate microspheres. Microspheres obtained were spherical yet sticky, necessitating the employment of a crosslinker. When PEI, a polyamine, was utilized as a crosslinker and as a monomer, sticky polymeric microspheres were obtained. Further investigation is required to obtain solid microspheres and microcapsules using epoxy-amine chemistry.

## 5.5. References

1. Carneiro, H. C. F., Tonon, R. V., Grosso, C. R. F., Hubinger, M. D. Encapsulation efficiency and oxidative stability of flaxseed oil microencapsulated by spray drying using different combinations of wall materials. *J. Food Eng*. **2013**, *115*, 4, 443-451.

2. Nelson, G. Microencapsulated colourants for technical textile application, in: M.L. Gulrajani (Ed.), Advances in the Dyeing and Finishing of Technical Textiles, Woodhead publishing series in textiles, **2013**, 78-104.

3. Asghari, F., Samiei, M., Adibkia, K., Akbarzadeh, A., Davaran, S. Biodegradable and biocompatible polymers for tissue engineering application: a review. *Artif. Cells Nanomed. Biotechnol.* **2017**, *45*, 2, 185–192.

4. Bhatia, S. Natural polymer drug delivery systems: Nanoparticles, plants, and algae, Springer, **2016**.

5. Balaji, A. B., Pakalapati, H., Khalid, M., Walvekar, R., Siddiqui, H. Natural and synthetic biocompatible and biodegradable polymers, Elsevier Ltd, **2018**.

6. Yao K., Tang C. Controlled polymerization of next-generation renewable monomers and beyond. *Macromolecules.* **2013**, *46*, 1689–1712.

7. Gruber P., O'Brien M. Polylactides "NatureworksTM PLA" In: Steinbüchel A., Doi Y., editors. Biopolymers: Polyesters III—Applications and Commercial Products. Volume 4. Wiley-VCH; Weinheim, Germany: **2002**, 235–239.

8. Molavi, F., Barzegar-Jalali, M., Hamishehkar, H. Polyester based polymeric nano and microparticles for pharmaceutical purposes: A review on formulation approaches. *J. Control. Release,* **2020**, *320*, 265-282.

9. Rydz J., Zawidlak-Węgrzyńska B., Christova D. Degradable polymers. In: Mishra M.K., editor. Encyclopedia of Biomedical Polymers and Polymeric Biomaterials. CRC Press; Boca Ratón, FL, USA, **2015**.

10. Blasi, P. Poly(Lactic Acid)/Poly(Lactic-Co-Glycolic Acid)-Based Microparticles: An Overview. *J. Pharm. Investig*. **2019**, *49*, 337–346.

11. DeStefano, V., Khan, S., Tabada, A. Applications of PLA in Modern Medicine. *Eng. Regen*. **2020**, *1*, 76–87.

12. Beslikas, T., Gigis, I., Goulios, V., Christoforides, J., Papageorgiou, G.Z., Bikiaris, D. N. Crystallization study and comparative in vitro-in vivo hydrolysis of PLA reinforcement ligament. *Int. J. Mol. Sci*. **2011**, *12*, 6597–6618.

13. Gupta, B., Revagade, N., Anjum, N., Atthoff, B., Hilborn, J. Preparation of Poly(lactic acid) Fiber by Dry–Jet–Wet Spinning. II. Effect of Process Parameters on Fiber Properties. *J. Appl. Polym. Sci.* **2006***, 101,* 3774-3780*.*

14. Arefin, A. M. E., Khatri, N. R., Kulkarni, N., Egan, P. Polymer 3D Printing Review: Materials, Process, and Design Strategies for Medical Applications. *Polymers (Basel).* **2021**, *13*, 9, 1499.

15. Astuti, S. H., Rahma, W. A., Budianto, E. Biodegradable microcapsules from D,L–PLA/PCL as controlled nifedipine drug delivery carrier. *Macromol. Symp*. **2020**, *391*, 1, 1900132.

16. Liu, B., Wang, Y., Yang, F., Wang, X., Shen, H., Cui, H., Wu, D. Construction of a controlled-release delivery system for pesticides using biodegradable PLA-based microcapsules. *Colloids Surf. B*. **2016**, *144*, 38-45.

17. Zhang, S., Liu, P., Chen, Y., Campagne, C., Salaun, F. Electrospraying poly(lactic acid) microcapsules loaded with n-hexadecane for thermal energy storage systems. *Mater. Today Commun*. **2022**, *33*, 104443.

18. Kemala, T., Budianto, E., Soegiyono, B. Preparation and characterization of microspheres based on blend of poly(lactic acid) and poly(ε-caprolactone) with poly(vinyl alcohol) as emulsifier. *Arab. J. Chem.* **2012**, *5*, 1, 103-108.

19. Liu, R., Ma, G., Meng, F., Su, Z. Preparation of uniform-sized PLA microcapsules by combining Shirasu Porous Glass membrane emulsification technique and multiple emulsion-solvent evaporation method. *J. Control. Release.* **2005**, *103*, 1, 31-43.

20. Sakurai, D., Cornejo, J. J., Daiguji, H., Takemura, F. Hollow polylactic acid microcapsules fabricated by gas/oil/water and bubble template methods. *J. Mater. Chem. A*, **2013**, *1*, 14562-14568.

21. Arpagaus, C. PLA/PLGA nanoparticles prepared by nano spray drying. *J. Pharm. Investig.* **2019**, *49*, 405–426.

22. Morais, A. Í. S., Vieira, E. G., Afewerki, S., Sousa, R. B., Honorio, L. M. C., Cambrussi, A. N. C. O., Santos, J. A., Bezerra, R. D. S., Furtini, J. A. O., Silva-Filho, E. C. Fabrication of polymeric microparticles by electrospray: The impact of experimental parameters. *J. Funct. Biomater.* **2020**, *11*, 4.

23. Xu, Y., Kim, C. S., Saylor, D. M., Koo, D. Polymer degradation and drug delivery in PLGA-based drug–polymer applications: A review of experiments and theories. *J. Biomed. Mater. Res.-Part B Appl. Biomater.* **2017**, *105*, 1692–1716.

24. Fuchs, Y., Witteler, H., Bratz, M. Microcapsule comprising a polyester-urethane shell and a hydrophobic core material. European patent, EP3380225B1, **2015**.

25. Fuchs, Y., Witteler, H., Bratz, M. Microcapsule comprising a polyester-urethane shell and a hydrophilic core material. European patent, EP3380224B1, **2015**.

26. Li, H., Gu, L. Controllable synthesis of bio-based polylactide diols using an organocatalyst in solvent free conditions. *J. Polym. Sci. Part A: Polym. Chem.*, **2008**, *56*, 968-976.

27. Nanclares, J., Petrovic, Z. S., Javni, I., Ionescu, M., Jaramilo, F. Segmented polyurethane elastomers by nonisocyanate route. *J. Appl. Polym. Sci.* **2015,** 132, 36, 42492-42502.

28. Vasylieva, N., Sabac, A., Marinesco, S., Barbier, D. Simple and non-toxic enzyme immobilization onto platinum electrodes for detection of metabolic molecules in the rat brain using silicon micro-needles. *Procedia Eng*. **2011**, *25*, 1361-1364.

# Chapter 6

# Summary and Future Outlook

## Summary

This thesis addressed two problems related to two types of microspheres: i) dual-responsive functional microspheres for anti-counterfeiting/bioimaging applications and ii) sustained-release microcapsules with improved barrier properties or biodegradability. The preparation of functional microspheres involved precipitation followed by ball milling, whereas microcapsules were prepared using the interfacial polycondensation technique. In the first part, dual responsive cellulose functional microspheres were prepared with high fluorescence emission, overcoming the fluorescence quenching due to the presence of heavy metals and aggregation-induced solid-state fluorescence quenching. In the case of sustained-release microcapsules, polyurea-urethane capsules were prepared using an aromatic diol component to improve barrier properties. Later, aliphatic polycarbonate polyol was employed as a polyol component to introduce degradable segments without compromising the barrier properties. Finally, epoxy-amine chemistry was employed to prepare biodegradable polyester-based microspheres. Various characterization techniques were employed to characterize microspheres and microcapsules, such as optical microscopy for emulsion stability, scanning electron microscopy (SEM) for surface morphology and size, and attenuated total reflectance–Fourier transformed infrared (ATR–FTIR) spectroscopy for structural characterization. Major outcome of each chapter are as follows:

**Chapter 1** of this thesis presents an overview of microparticles and their classification. It also discusses current literature on the preparation techniques used to prepare solid microparticles, hollow or porous microparticles, and microcapsules. It also describes the matrix materials used

to prepare them, the evaluation of prepared microparticles using various characterization techniques, and their applications.

**Chapter 2** describes the facile synthesis of cellulose microspheres with dual responsive behavior, i.e., magnetic, and fluorescent. Tetrabutylammonium hydroxide, an environmentally benign solvent, was used to dissolve and process cellulose into microspheres. Pyrenebutyric acid (PBA) was covalently linked to cellulose microspheres to give them durable fluorescent properties, whereas iron oxide nanoparticles ($Fe_3O_4$ NPs) were incorporated into a cellulose matrix to offer magnetic properties. By varying the amount of $Fe_3O_4$ nanoparticles and fluorophore in microspheres, effect of heavy metal quenching and solid-state aggregation induced fluorescence quenching was studied. A saturation magnetization range of 2.85 to 8.54 emu/g, which is sufficient for magnetic responsiveness and a fluorescence quantum yield as high as 0.57 were realized. Covalent bonding restricted the fluorophore's mobility, preventing aggregation-induced fluorescence quenching thus resulting in strong solid-state fluorescence emission. Such a high fluorescence quantum yield for dual-responsive fluorescence microspheres has not previously been reported. These materials might be used in security features as well as medical diagnostics.

**Chapter 3** focuses on the preparation of polyurea-urethane microcapsules using an aromatic polyol (benzene-1,4-dimethanol) component. Microcapsules were prepared by performing an interfacial polycondensation reaction at the interface of an oil-in-water emulsion droplet. Benzene-1,4-dimethanol, with limited solubility and reactivity, was employed as a polyol component in the aqueous phase, which reacted with the 2,4-toluenediisocyante (2,4-TDI) present in the oil phase at the interface to create microcapsules with sizes ranging from 1 to 20 µm and an encapsulation efficiency of about 92%, which is comparable to the conventional aliphatic polyol component ethylene glycol. The addition of aromatic diol increases the $T_g$ values determined using differential scanning calorimetry (DSC), improves the shell rigidity,

and hence the barrier characteristics by around 10%. The mathematical interpretation of the release profile using the Weibull and Korsmeyer-Ritger-Peppas models suggests that the release of the active is primarily controlled by a non-fickian diffusion mechanism and that the addition of an aromatic diol improves the permeation resistance.

**Chapter 4** discusses the preparation of polyurea-urethane microcapsules to encapsulate DEET, an oil-soluble insect repellent, employing aliphatic hyperbranched polycarbonate polyol (PCPO) as a degradable polyol component. Aliphatic polycarbonates, which are often used in the synthesis of polyurethane elastomers, have never been used in the production of microcapsules. Hyperbranched PCPO formed a miscible solution with ethylene glycol to form a polyol component that reacted with the 2,4-TDI at the oil-in-oil interface to form a polyurea-urethane shell with a degradable component between urethane linkages. The encapsulation efficiency of the resulting microcapsules was about 81% when ethylene glycol was used, but it decreased to 72% when 20% PCPO was added. Thermogravimetric analysis reveals a delay in the degradation of DEET upon encapsulation. Release studies suggested that with the introduction of the biodegradable polyol component PCPO in MICs, barrier properties were not compromised. The Korsemayer-Ritger-Peppas model fits well with the release profile, suggesting that non-fickian diffusion regulates the release of DEET from MICs. Values of the release rate constant K that don't change significantly suggest similar permeation resistance properties, which correlate with the release profile of DEET from MICs.

**Chapter 5** illustrates the preparation of polyester microspheres by applying epoxy-amine chemistry using the interfacial polycondensation technique. Polyester-diol has been synthesized using ring-opening polymerization followed by modification with epichlorohydrin to yield diglycidyl ether (DGE), as confirmed by 1H NMR. Synthesized polyester-DGE forms the oil phase and is reacted with diamines in the aqueous phase at the interface of an emulsion droplet at 50 °C and 70 °C. The resulting microspheres were spherical yet sticky, necessitating

the employment of a crosslinker. PEI, an aliphatic polyamine, was employed as a crosslinker, resulting in waxy microspheres. Further investigation is required to obtain solid, free-flowing microspheres and capsules using epoxy-amine chemistry.

## Future outlook

Based on the findings in chapter 1 of this thesis, where dual responsive cellulose microspheres were made with a high fluorescence quantum yield, dual or multiple responsive biodegradable functional microspheres can be made using up-conversion nanoparticles, organic dyes or quantum dots, superparamagnetic nanoparticles, etc.

Based on the findings obtained in the study of PUU MICs using aromatic diols, we may use naturally occurring aromatic/aliphatic polyols such as sugars (fructose, mannitol, maltose, and sucrose) or biodegradable synthetic polyols such as polyester polyols as a monomer to generate bio-based or biodegradable MICs. Water-soluble lignin may also be used as a polyol component in PUU MICs.

The microspheres prepared using epoxy amine chemistry were sticky. Aromatic polyester diols could be explored in place of PLA and PCL diols to obtain rigid microspheres.

# Appendix

A.1.   FTIR spectrum of 1-pyrenebutyric acid (PBA), cellulose and PBA modified cellulose bead (FMB411). IR band appearing at 1687 cm$^{-1}$ in 1-pyrenebutyric acid shifts to 1704 cm$^{-1}$ in FMB411 confirms the formation of ester. Also, IR band appearing at 1628 cm$^{-1}$ in FMB411 corresponds to the aromatic ring stretching which also confirms the presence of 1-pyrenebutyric acid in FMB411.
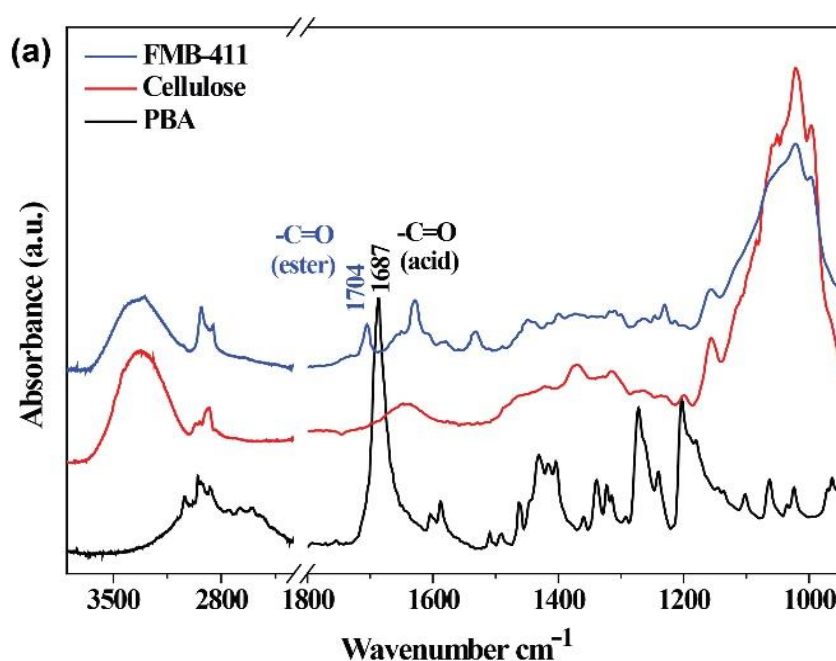


**Figure A.1** FTIR spectrum of 1-pyrenebutyric acid, Cellulose and FMB411.

**A.2. Method used for calculation of solid-state fluorescent quantum yield**.

The fluorescence quantum yield does not have a theoretical or calculated value. Fluorescence quantum yield is an experimentally measured quantity, where the quantum yield is defined as the photons emitted to photons absorbed. An 'integrating sphere', which is a hollow sphere whose inner surface is coated with an all-reflective material (typically barium sulfate) is used to determine the thin film quantum efficiencies (PLQY or photoluminescence quantum yield). Thin film samples or powder samples have anisotropic distribution of chromophores leading to anisotropic angular distribution of emission. With the integrating sphere technique, when a

light source is placed inside, the light is redistributed isotropically over the sphere interior surface regardless of the angular dependence of emission. The theory and calculation details for determining PLQY using the integrating sphere is explained in the following references, which is adopted by HORIBA Jobin Yvon for its Quanta-ϕ integrating sphere, used with the Fluorolog 3 spectrophotometer[A1-A2].
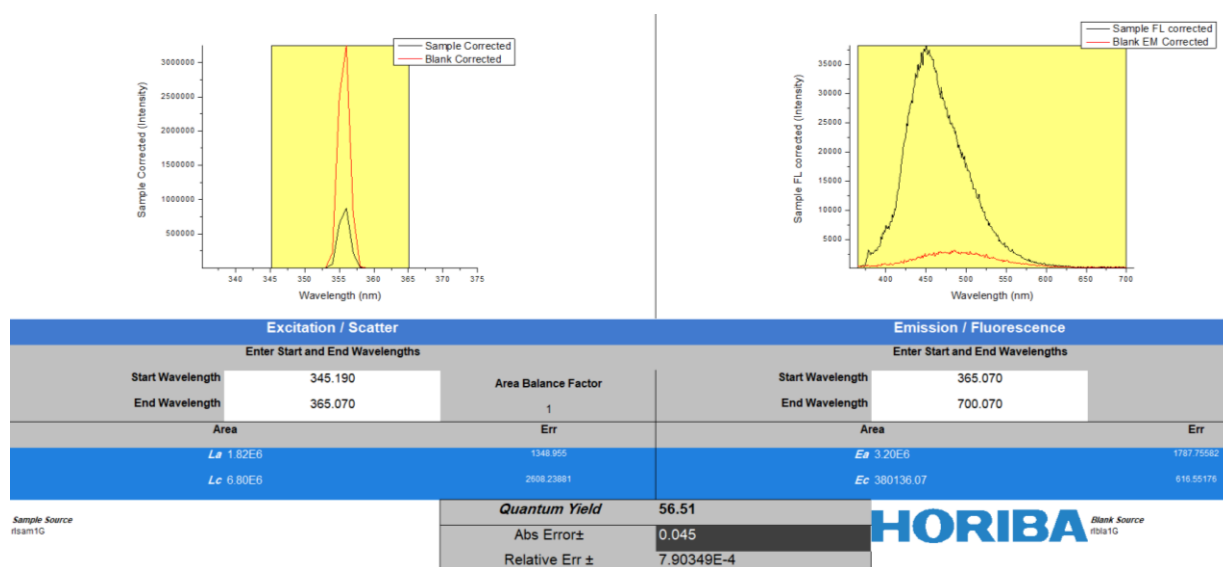
For the experimental determination of fluorescence quantum efficiency, three measurements are made: 1) the sphere is empty and laser light alone is detected by the spectrometer. 2) for the second measurement, the sample is placed inside the sphere and the laser beam is directed on to the sphere wall. 3) the third measurement is similar to the second except that the laser beam is directed to the sample.

The total amount of laser light falling on the sample has two contributions – one direct incident laser beam and second is the diffuse laser light scattered from the wall of the sphere. The equations developed for determining the PLQY takes these into account and is given as

$$\phi = \frac{[E_c - (1 - A).E_b]}{L_a.A} = \frac{E_c - E_a}{L_a - L_c}$$

Where, $E_c$ is the integrated luminescence of the film caused by direct excitation and $E_a$ is the integrated emission from an empty integrating sphere (only a blank). $L_a$ is the integrated excitation profile from an empty integrating sphere (only a blank). Similarly, $L_c$ is the integrated excitation profile from the film.

A typical sample calculation is given below for **FMB011** as example.

| Excitation / Scatter | | | Emission / Fluorescence | |
|---|---|---|---|---|
| Enter Start and End Wavelengths | | | Enter Start and End Wavelengths | |
| Start Wavelength | 345.190 | Area Balance Factor | Start Wavelength | 365.070 |
| End Wavelength | 365.070 | 1 | End Wavelength | 700.070 |
| Area | | Err | Area | Err |
| $L_a$ 1.82E6 | | 1348.955 | $E_a$ 3.20E6 | 1787.75582 |
| $L_c$ 6.80E6 | | 2608.23881 | $E_c$ 380136.07 | 616.55176 |
| | | Quantum Yield | 56.51 | |
| | | Abs Error± | 0.045 | |
| | | Relative Err ± | 7.90349E-4 | |

Sample Source rlsam1G

HORIBA *Blank Source* rlbla1G

**Figure A.2** Screen shot of the raw data from the software.

Here, the sharp peak at ~ 355 nm is the laser excitation. The area under the curve is proportional to the amount of unabsorbed light, which is denoted by the plot on the left side $L_a$ and $L_c$ for blank and sample respectively. The plot on the right side corresponds to the emission and the area is proportional to the amount of emitted light denoted as $E_a$ and $E_c$ for blank and sample respectively.

The ϕ for sample FMB011 is determined as 0.565.

These detailed calculations are carried out by the software of the Quanta-ϕ integrating sphere of HORIBA Jobin Yvon and it is understood and universally accepted that it follows the theory demonstrated in the above-mentioned publications. For instance, some of the literature examples citing PLQY measurements using the Quanta-ϕ integrating sphere of HORIBA Jobin Yvon is listed below[A3-A7].

**A.3. Scheme A1** shows the procedure for preparing polycarprolactone-diol (PCL-diol) and polycaprolactone diglycidylether (PCL-DGE). PCL-diol is produced by polymerizing caprolactone using a butane-1,4-diol initiator by ring opening polymerization (ROP). PCL-DGE is then produced by reacting PCL-diol with epichlorohydrin in the presence of boron
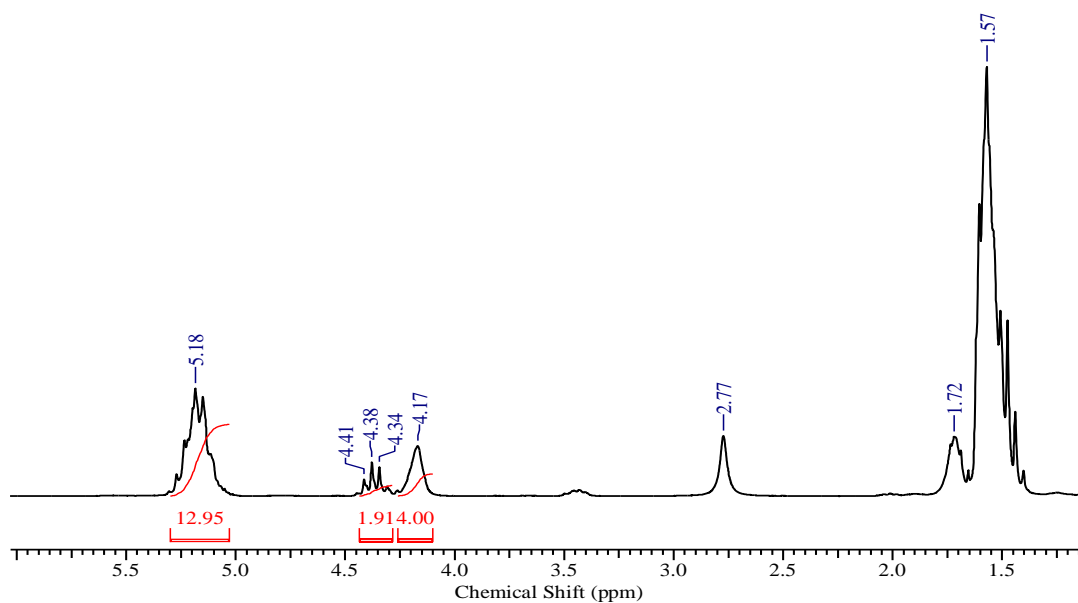
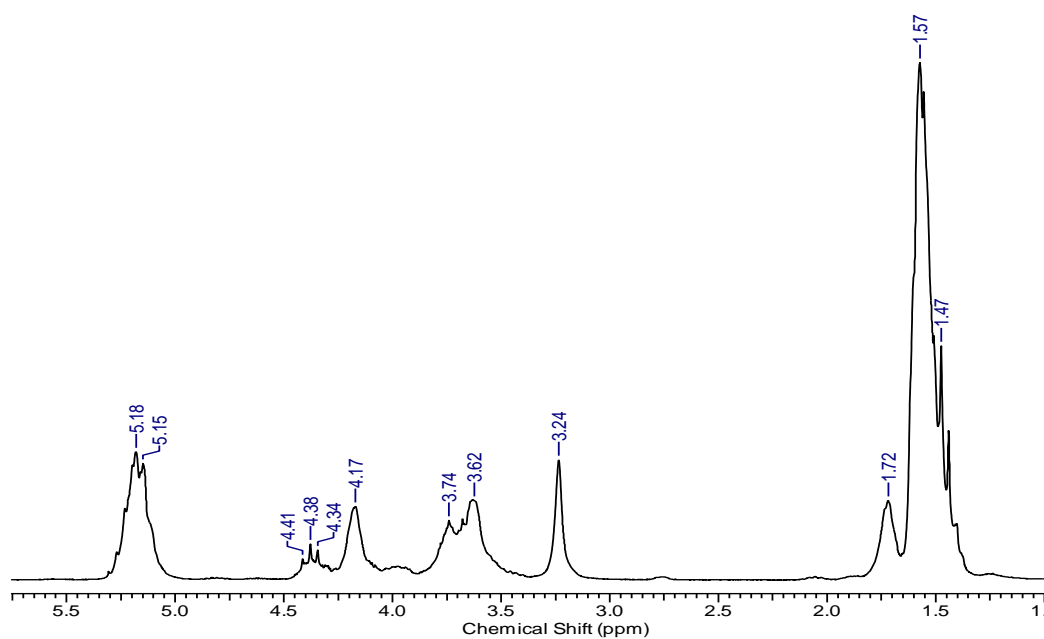trifluoro etherate catalyst. The products were validated by the 1H NMR depicted in figures A3 through A12.
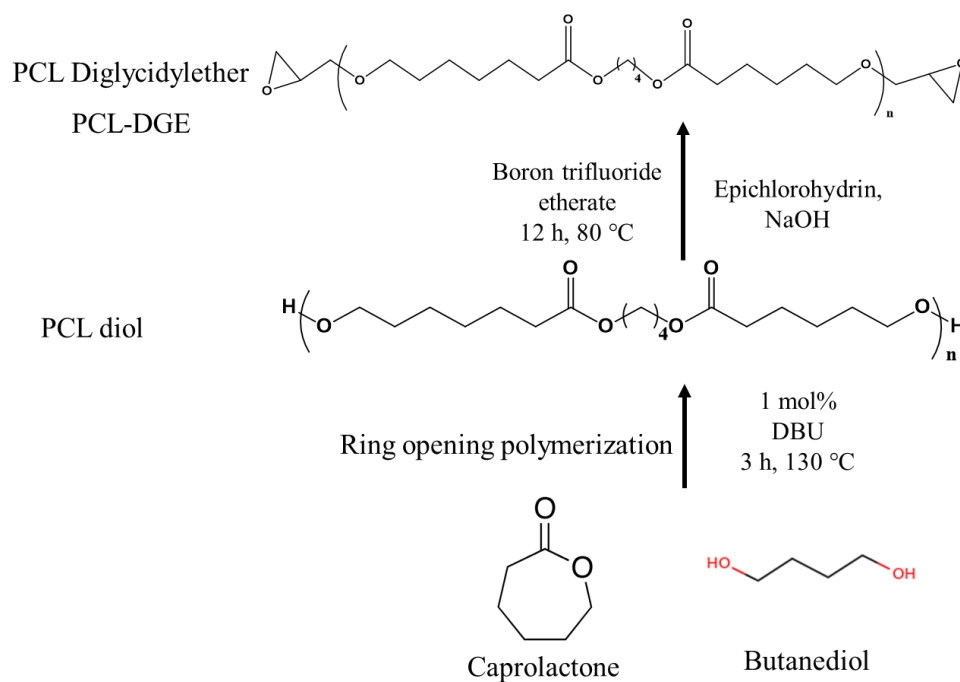


**Scheme A.1** Preparation of PCL-diol followed by preparation of PCL-DGE.
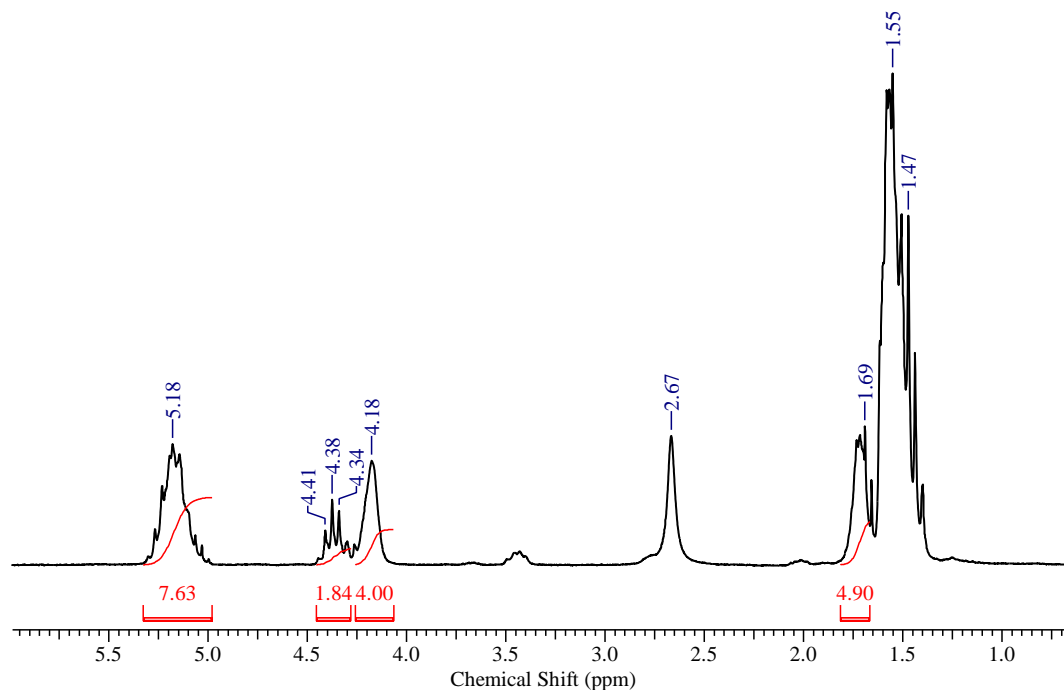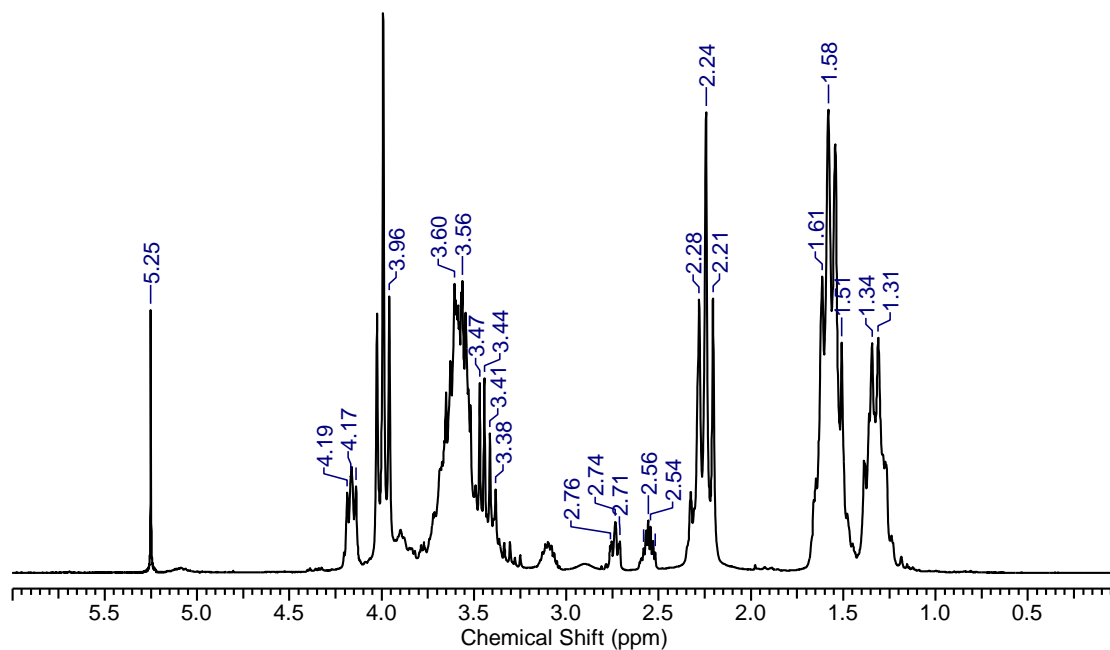


**Figure A.3** 200 MHz $^1$H NMR spectrum of PLA-diol (molecular weight: 720) in CDCl$_3$.

**Figure A.4** 200 MHz $^1$H NMR spectrum $^1$H NMR of PLA-diol (molecular weight: 1080) in CDCl$_3$.



**Figure A.5** 200 MHz $^1$H NMR spectrum $^1$H NMR of PLA-DGE (molecular weight: 1200) in CDCl$_3$.

**Figure A.6** 200 MHz $^1$H NMR spectrum $^1$H NMR of PCL-DGE (molecular weight: 530) using commercially available PCL diol in CDCl$_3$.



**Figure A.7** 200 MHz $^1$H NMR spectrum $^1$H NMR of PCL-diol (molecular weight: 3000) in CDCl$_3$.

**Figure A.8** 200 MHz ${}^{1}$H NMR spectrum ${}^{1}$H NMR of PCL-diol (molecular weight: 4800) in CDCl$_3$.

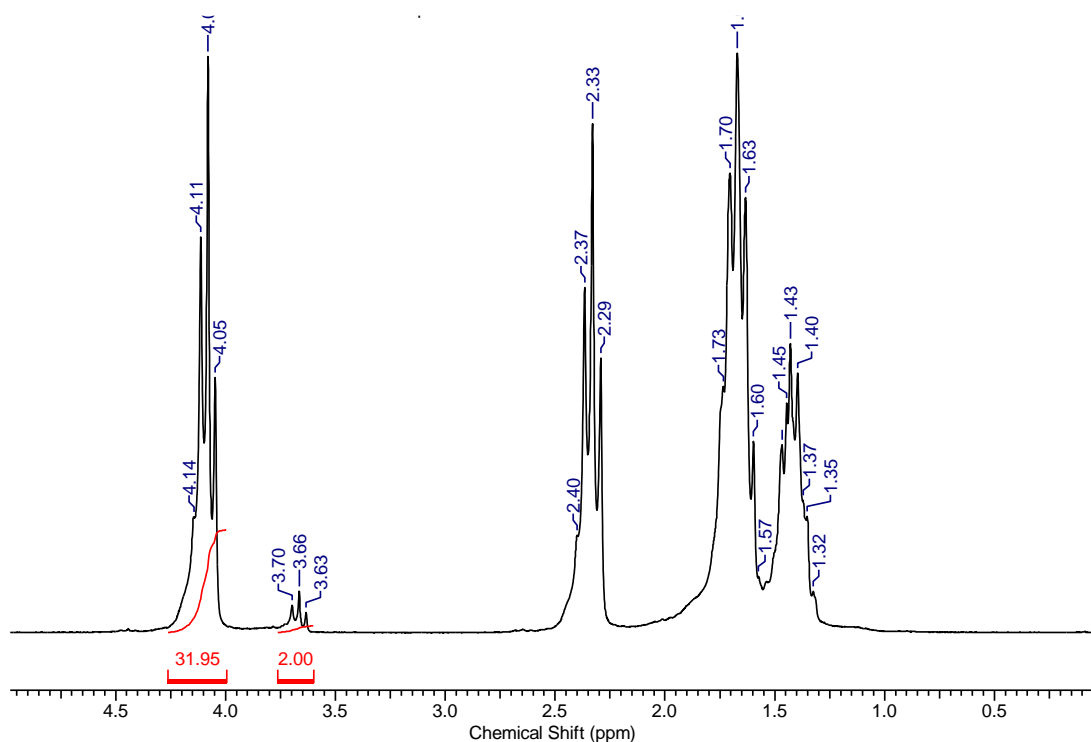

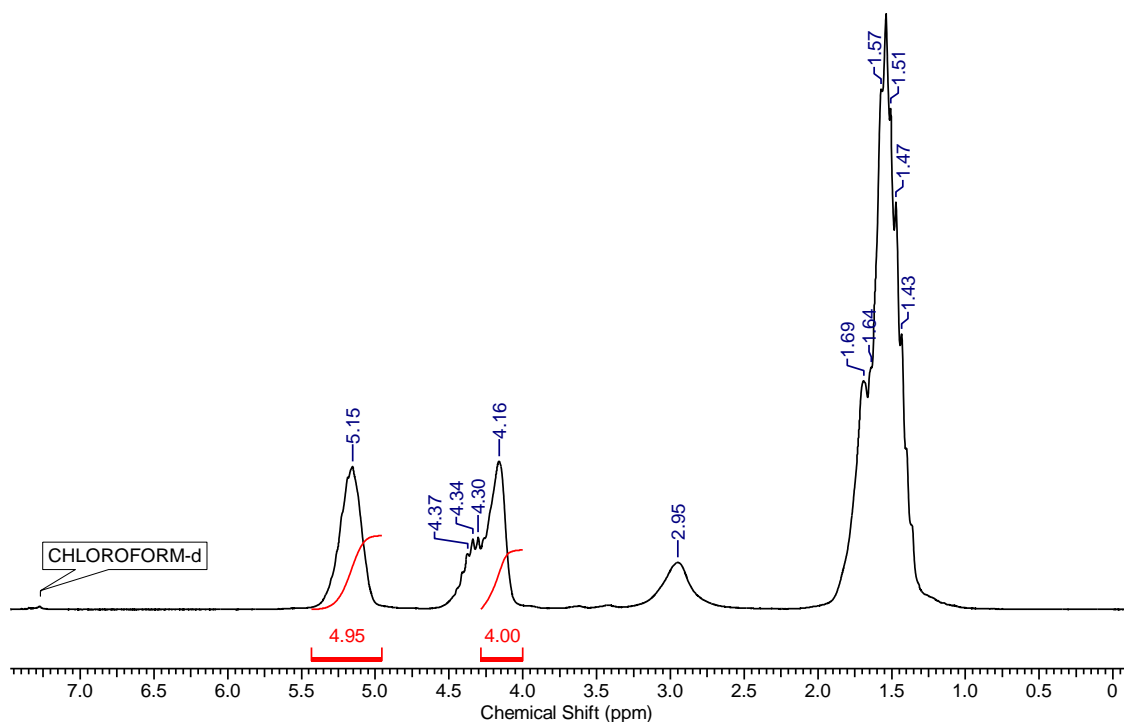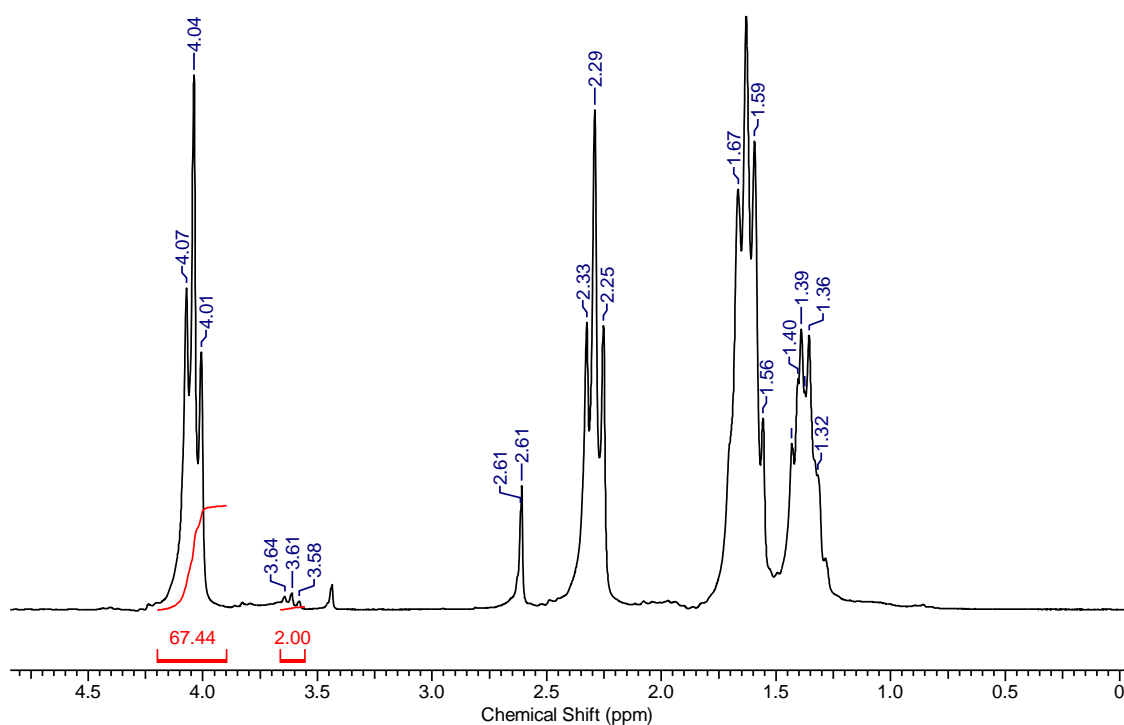**Figure A.9** 200 MHz ${}^{1}$H NMR spectrum ${}^{1}$H NMR of PCL-diol (molecular weight: 8000) in CDCl$_3$.

**Figure A.10** 200 MHz $^1$H NMR spectrum $^1$H NMR of PCL-DGE (molecular weight: 3000) in CDCl$_3$.
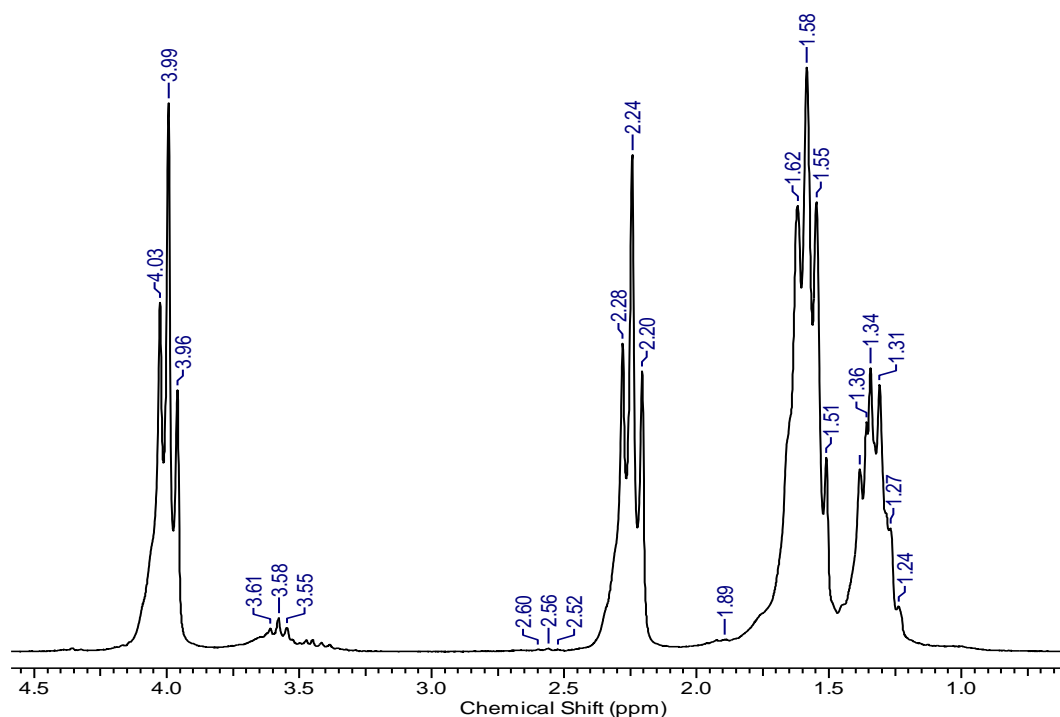


**Figure A.11** 200 MHz $^1$H NMR spectrum $^1$H NMR of PCL-DGE (molecular weight: 5000) in CDCl$_3$.

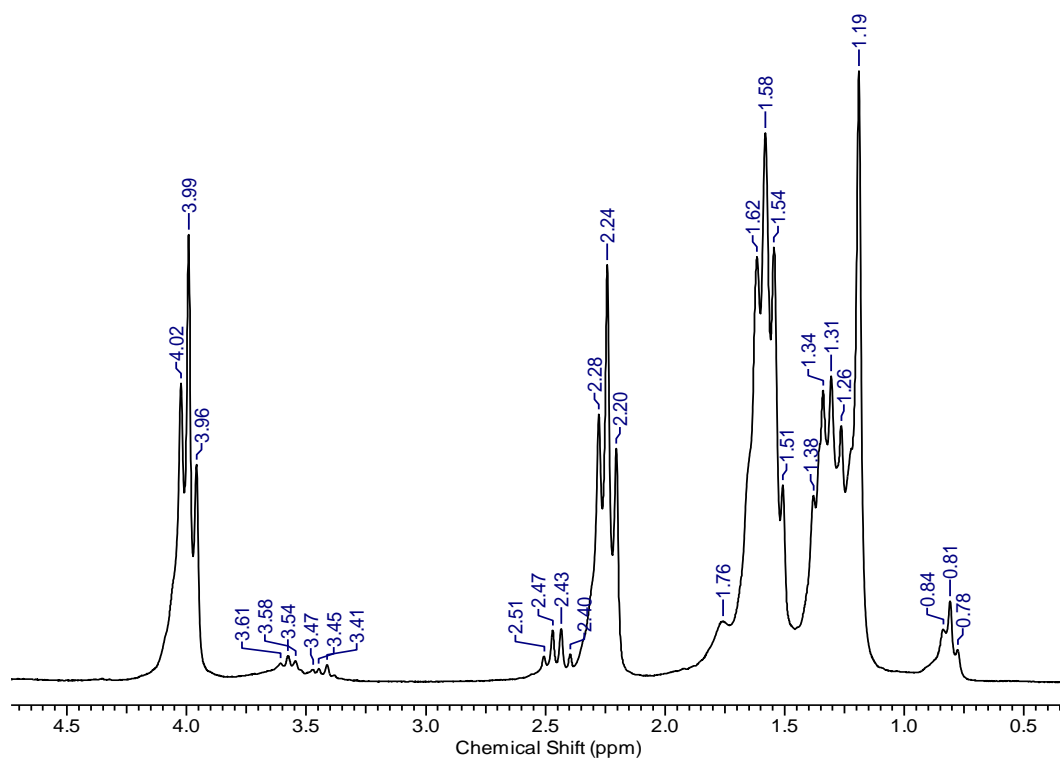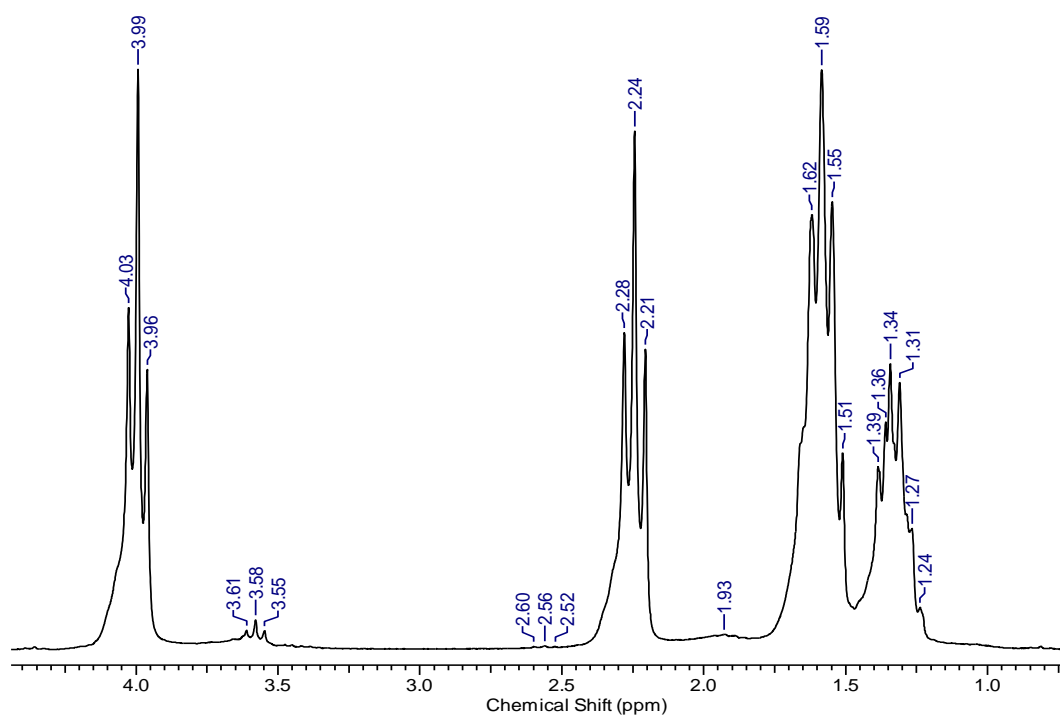**Figure A.12** 200 MHz ^{1}H NMR spectrum ^{1}H NMR of PCL-DGE (molecular weight: 8000) in CDCl$_3$.

## A.4. References

A1. deMello, J. C., Wittmann, H. F., Friend R. H. An improved experimental determination of external photoluminescence quantum efficiency. *Adv. Mater.* **1997,** *9*, 230.

A2. Pålsson, L.-O., Monkman, A. P. Measurement of Solid-State Photoluminescence Quantum Yields of Films using a Fluorimeter. *Adv. Mater.* **2002**, *14*, 10, 757–758.

A3. Suresh, C., Nagabhushana, H., Basavaraj, R. B., Darshan, G. P., Kavyashree, D., Daruka Prasad, B., Sharma, S. C., Vanithamani, R. SiO2@LaOF:Eu3+core-shell functional nanomaterials for sensitive visualization of latent fingerprints and WLED applications. *J. Colloid Interface Sci.* **2018,** *518*, 200-215.

A4. Sahoo, P. R., Kumar, A., Kumar, A., Kumar, S. Synthesis and optical properties of copper(II) and nickel(II) complexes of a highly fluorescent morpholine-derivative. *Polyhedron* **2019**, *171*, 559–570.

A5.Costa, B. B. A., Souza, P. D. C., Gontijo, R. N., Jardim, G. A. M., Moreira, R. L., da Silva, E. N., Cury, L. A. Vibronic singlet and triplet steady-state interplay emissions inphenazine-based 1,2,3-triazole films. *Chem. Phys. Lett.* **2018**, *695*, 176–182.

A6.Upadhyay, P. K., Marpu, S. B., Benton, E. N., Williams, C. L., Telang, A., Omary, M. A. A phosphorescent trinuclear gold(I) pyrazolate chemosensor for silver ion detection and remediation in aqueous media. *Anal. Chem.* **2018**, *90*, 4999−5006.

A7.Zhu, X-. D., Tian, Q- S., Zheng, Q., Tao, X- C., Yuan, Y., Yu, Y- J., Li. Y., Jiang, Z- Q., Liao, L- S. A sky-blue thermally activated delayed fluorescence emitter based on multi-modified carbazole donor for efficient organic light-emitting diodes. *Org. Electron.* **2019,** *68*, 113–120.

# Abstract

**Name of the student**: Prashant Yadav                    **Registration No**.: 10CC16J26003

**Faculty of Study**: Chemical Sciences                    **Year of submission**: 2023

**AcSIR academic centre/CSIR Lab**: National Chemical Laboratory, Pune

**Name of Supervisor**: Dr. Kadhiravan Shanmuganathan

**Name of Co-supervisor:** Dr. Ashootosh V. Ambade

**Title of the thesis**:  Functional Microparticles and Microcapsules for Advanced Applications

Microparticles have piqued interest as a result of their wide range of applications owing to their large specific surface areas, high mobility, and easy recovery from dispersion. This thesis investigates functional solid microparticles and microcapsules for sustained release. Functional materials that respond to multiple stimuli like light and magnetic fields are appealing for security and medical diagnostic applications. One of the biggest issues with dual-functional microspheres is quenching of fluorescence emission, which can occur both through the presence of magnetic nanoparticles and due to the aggregation of a fluorophores. Fluorescence quenching effects due to the presence of $Fe_3O_4$ nanoparticles and solid-state aggregation of fluorophore were examined systematically. By optimizing the reaction conditions, microspheres with a detectable magnetic response and a fluorescence quantum yield as high as 0.57 (FMB 414) were produced. Microcapsules for sustained release (MICs) with improved barrier properties and biodegradability are desirable. Polyurea-urethane and polyester MICs were prepared to improve the barrier properties or to introduce degradability. Initially, by combining aromatic polyols, benzene-1,4-diol (BDM), with aromatic diisocyanates, Polyurea-urethane MICs were synthesized using interfacial polycondensation. MICs shell obtained had a higher Tg value compared to MICs with aliphatic polyol that offered high rigidity and enhanced barrier properties. Further, aliphatic hyperbranched polycarbonate polyol (PCPO), a biodegradable material, was employed as polyol components to make PUU MICs to add biodegradable segments between the polyurethane linkages. MICs encapsulating DEET by substituting up to 50 wt.% of ethylene glycol with PCPO were produced with a marginal loss of encapsulation efficiency yet comparable barrier properties. Finally, aliphatic polyester diols were synthesized and then modified into diglycidyl ether (DGE). Using epoxy-amine chemistry, these DGEs were reacted with amines interfacially to produce degradable microspheres (MIS). This process resulted in waxy and spherical microspheres, and further investigation is required to prepare the solid, free-flowing MIS.

# List of Publications

## Research Articles

Publications from thesis work

1. **Prashant Yadav**, K P Prajitha, Vinita Dhaware, Mohan Subramani, Pattayil Joy, Asha S K, Kadhiravan Shanmuganathan. Dual responsive cellulose microspheres with high solid-state fluorescence emission. *Colloids Surf., A Physicochem Eng. Asp.* **2020**, *591*, 124510−124519.

2. **Prashant Yadav**, Swapna Kudal, Ashootosh V. Ambade, Kadhiravan Shanmuganathan. Preparation of polyurea-urethane microcapsules using aromatic diol component for encapsulation of model active dimethyl phthalate. (Manuscript under preparation).

3. **Prashant Yadav**, Shakeb Choudhari, Ashootosh V. Ambade, Kadhiravan Shanmuganathan. Polyurea-urethane microcapsules using polycarbonate polyol for encapsulation of mosquito repellent DEET via oil-in-oil emulsion method. (Manuscript under preparation).

Publications from other work

4. Farsa Ram, **Prashant Yadav**, Kadhiravan Shanmuganathan. Nanocellulose/melanin-based composites for multifunctional applications: a review. *J Mater Sci.* **2022**, *57*, 14188−14216.

5. Premkumar Anil Kothavade, **Prashant Yadav**, Aakash D. Nidhankar, Arun Torris, Harshawardhan Pol, Abdullah Kafi, Stuart Bateman, Santosh Babu Sukumaran, Kadhiravan Shanmuganathan. Luminescent 3D printed PLA nanocomposites with enhanced mechanical properties. (Under review, Addit. Manuf.)

6. Sandip L. Kadam, **Prashant Yadav**, Siddhant Bhutkar, Vishal D. Patil, Parshuram G. Shukla, Kadhiravan Shanmuganathan. Sustained release insect repellent microcapsules using modified cellulose nanofibers (mCNF) as pickering emulsifier. *Colloids Surf., A Physicochem Eng. Asp.* **2019**, *582*, 123883.

7. Sandeep Yadav, Rohit Kumar, K. Vipin Raj, **Prashant Yadav**, Kumar Vanka, Sakya S. Sen, Amidinato Germylene-Zinc complexes: Synthesis, bonding, and reactivity. *Chem. Asian J*. **2020**, *15*, 3116−3121.

8. Saurabh Usgaonkar, Subrajeet Deshmukh, Bipul Biswas, **Prashant Yadav**, Jayaraj Nithyanandhan, Guruswamy Kumaraswamy. Light-triggered, spatially localized chemistry by photoinduced electron transfer. *Angew. Chem. Int. Ed*. **2019**, *58*, 1−6.

9. Bhawana Pandey, Soumyajyoti Chatterjee, Nimisha Parekh, **Prashant Yadav**, Anuya Nisal, and Sayam Sen Gupta. Silk-mesoporous silica-based hybrid macroporous scaffolds using ice- templating method: mechanical, release, and biological studies. *ACS Appl. Bio Mater.* **2018**, 1, 6, 2082−2093.

## Patents

1. Kadhiravan Shanmuganathan, **Prashant Yadav**. A process for the preparation of essential oils modified nanocellulose and application thereof. (US Patent granted: US 20210054104 A1).

2. Kadhiravan Shanmuganathan, Ashootosh V. Ambade, **Prashant Yadav**, Sandip L. Kadam. A water miscible ester containing polyol, process for preparation of biodegradable microcapsules and use thereof. (Patent published; Application id 201911045021).

# Conferences, Awards and Affiliations

1. Awarded "DST SERB travel grant" and "CSIR travel grant" to attend a international conference APME 2023 in Paris.

2. Poster presentation "Dual responsive cellulose microspheres with high solid state fluorescence emission" at SPSI MACRO, 2022, CSIR-NCL, Pune, India.

3. Scientific talk "Dual responsive cellulose microspheres with high solid state fluorescence emission" at MACRO-MEET, Dec 2021, CSIR-NCL, Pune, India.

4. Poster presentation "Functionalized Nanocellulose for Anti- bacterial surface Coatings" APSRT-2019 at IIT Kharagpur, West Bengal, India.

5. Poster presentation "Functionalized Nanocellulose for Anti- bacterial surface Coatings" SuCHEM YUVA-2019 at IICT, Hyderabad, India.

6. Poster presentation "Functionalized Nanocellulose for Anti- bacterial surface Coatings" NSAPST-2019 at Sardar Patel University, Anand, Gujarat, India.

7. Best oral presentation "Dual responsive cellulose microspheres with high solid state fluorescence emission" at NCL-RF Annual Students conference, 2019 at CSIR-NCL, Pune, India.

8. RSC Best poster award "Surface Modified Nanocellulose for Functional Coatings" at SPSI-MACRO, Pune chapter, 2018.

9. Life member, Electron Microscopy Society of India (Since 2016).
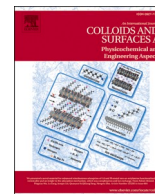
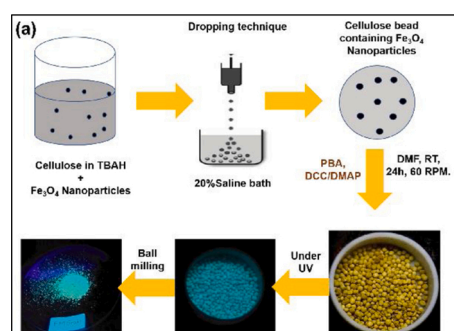# Dual responsive cellulose microspheres with high solid-state fluorescence emission

Prashant Yadav [a,b], K P Prajitha [a,b], Vinita Dhaware [a,b], Mohan Subramani [c,b], Pattayil Joy [c,b], Asha S K [a,b], Kadhiravan Shanmuganathan [a,b,*]

[a] Polymer Science and Engineering Division, CSIR-National Chemical Laboratory, Dr. Homi Bhabha Road, Pune, 411008, Maharashtra, India
[b] Academy of Scientific and Innovative Research (AcSIR), Ghaziabad- 201002, India
[c] Physical and Materials Chemistry Division, CSIR-National Chemical Laboratory, Dr. Homi Bhabha Road, Pune, 411008, Maharashtra, India

GRAPHICAL ABSTRACT



ARTICLE INFO

ABSTRACT

Materials that respond to multiple stimuli such as magnetic field and light are attractive for security and medical diagnostic applications. One of the major challenges in dual functional microspheres is that the presence of magnetic nanoparticles can quench fluorescence emission. Also, there is a probability of solid-state quenching due to the proximity of the fluorophore. We report here a facile approach to prepare cellulose microspheres with high solid-state fluorescence using 40 % tetrabutylammonium hydroxide (TBAH). The fluorescence quenching effect due to the presence of $Fe_3O_4$ nanoparticles and solid-state quenching due to aggregation of fluorophore was systematically investigated. Microspheres with the detectable magnetic response and fluorescence quantum yield as high as 0.57 (FMB 414) was obtained by optimizing the reaction conditions. Such a high quantum yield has not been reported before for dual stimuli-responsive fluorescent microspheres. The magnetic and fluorescent properties were found to be durable even after multiple washing cycles. These dual responsive cellulose microspheres can be added as security features to authenticate documents such as passports, degree certificates, currency notes, financial documents etc.

* Corresponding author at: Polymer Science and Engineering Division, CSIR-National Chemical Laboratory, Dr. Homi Bhabha Road, Pune, 411008, Maharashtra, India.
E-mail address: k.shanmuganathan@ncl.res.in (K. Shanmuganathan).

## 1. Introduction

Functional microspheres or microbeads have attracted significant interest due to their broad applications in the fields of chromatography [1], water treatment [2], protein/enzyme immobilization [3,4], solid-phase synthesis support [5], drug loading, drug release [6], magnetic resonance imaging [7], cell labeling and separation [8], biosensors [9], etc. Various polymer matrices have been used to form these beads including poly(styrene) [10], poly(ethylene) [11], poly(propylene) [12], chitosan [13], poly(ethylene glycol dimethacrylate-n-vinyl imidazole) [14], cellulose and its derivatives. These beads have been doped with various organic as well as inorganic dopants such as iron oxide nanoparticles [15,16], quantum dots [17,18], tungsten carbide [19], nickel powder [20], titanium oxide ($TiO_2$) [21], etc. Due to the added functionality brought by dopant they are termed as "functional beads" [22].

Among various polymers used for the preparation of microspheres, polysaccharides offer excellent chemical and mechanical properties along with properties such as non-toxicity, low cost, renewability, biodegradability, and natural abundance. Cellulose is preferred over other synthetic non-biodegradable polymers such as poly(ethylene), poly(styrene), poly(propylene), etc. Further, the presence of multiple hydroxyl groups makes cellulose amenable to functionalization. Almost all reports on cellulose-based microbeads involve dissolving a cellulose derivative such as cellulose acetate [23], cellulose stearate [24], cellulose xanthate (via viscose method) [25], 2,3-dialdehyde cellulose [26], etc. The difficulty in dissolving and processing native cellulose arises from its strong intra- as well as inter-molecular hydrogen bonding [27]. Various specific solvents have been used for cellulose dissolution such as DMAc/LiCl [28], NMMO [29], acetone/DMSO [25], Cuprammonium hydroxide (cuoxam) [30], NaOH/Urea [31], $NaOH/CS_2$ (Cellulose xanthate) [32]. These solvents either involve high temperature (as high as 100 °C) or cryogenic conditions (as low as -20 °C) making the processes energy intensive. Recently, Abe et al. [33] have reported dissolution of cellulose at room temperature using 40 % tetrabutylammonium hydroxide (TBAH) and tetrabutylphosphonium hydroxide (TBPH). The fact that cellulose can be dissolved at ambient conditions and TBAH can be recovered and reused makes TBAH a greener solvent for cellulose processing. Herein, we made an attempt to prepare cellulose microspheres having dual functionality, viz. magnetic and fluorescent property using 40 % aqueous TBAH solution. Independently, either the magnetic nanoparticles or the fluorophore could be loaded/incorporated into the cellulose material to a larger extent. Larger incorporation of the magnetic material could in principle impart larger magnetic properties to the modified cellulose. As far as the fluorophore is concerned, there could be a higher limit of incorporation beyond which the emission would start to decrease due to solid-state quenching effects arising from the proximity of the fluorophore. In presence of a metal nanoparticle, this upper limit would be reached much earlier due to the added quenching effect introduced by the presence of the heavy metal. Despite such constraints, through our systematic investigations, the current work demonstrates a workable loading of magnetic nanoparticles along with covalent incorporation of the fluorophore pyrene which has imparted the highest reported solid-state fluorescence quantum yields. Dual functional microspheres are more preferred as security features to authenticate documents for example passports, degree certificates, currency notes, financial documents etc. as it increases the counterfeit resistance compared to monofunctional microspheres. In earlier reports, the fluorescent molecules such as rhodamine B dye [24] or quantum dots [34] have been physically blended in the magnetic microspheres to prepare dual functional cellulose nanospheres or nanoparticles making them susceptible to leaching. In other reports (listed in table below), cellulose is either physically linked or covalently linked with fluorescent molecules to prepare monofunctional cellulose microbeads but the solid-state quantum yield is not reported and only solution based quantum yield is reported. In this work, fluorescent molecule pyrene has been covalently linked to the microspheres making them more stable. Pyrene is a well-studied fluorophore with long fluorescence lifetimes, large quantum yield and formation of excimers [35–40]. In Table 1, current work is compared with the previously reported work and distinguishes the novelty of the work. To the best of our knowledge, this is the first report demonstrating a facile approach to prepare dual functional i.e., fluorescent magnetic cellulose microspheres with high solid-state fluorescence and significant magnetization.

## 2. Materials and methods

Sigmacell cellulose Type 50 (50 μm) (MCC), Iron (II, III) oxide nanoparticles (50−100 nm particle size), 40 wt% tetrabutylammonium hydroxide (TBAH), 1-pyrenebutyric acid (PBA), 4-dimethylaminopyridine (DMAP), N, N'-Dicyclohexylcarbodiimide (DCC) were all purchased from Sigma-Aldrich Chemicals Co. LLC and used without further purification. Sodium chloride (LR Grade) and methanol (AR Grade) were acquired from Leonid Chemicals Pvt. Ltd. and used without further purification. Dimethylformamide (DMF) was purchased from Leonid Chemicals Pvt. Ltd. and was dried using standard procedure and kept over molecular sieves (4 Å × 1.5 mm).
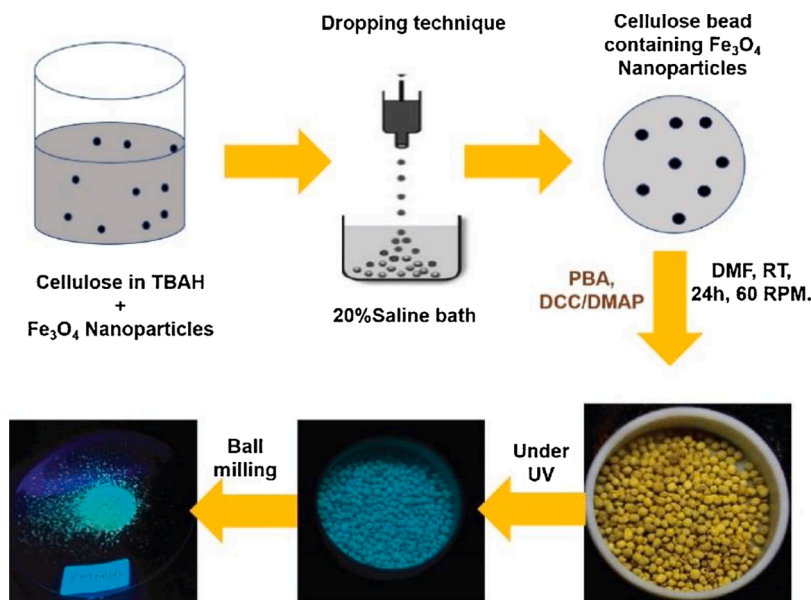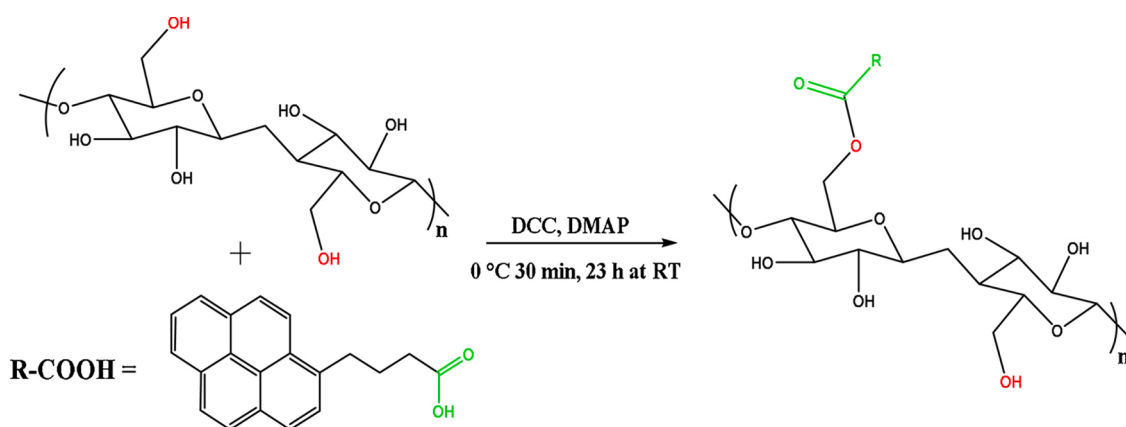
### 2.1. Preparation of magnetic cellulose beads (MB)

In a vial, 4, 8 and 12 wt% $Fe_3O_4$ NPs (with respect to the weight of cellulose) were uniformly dispersed in 40 % aqueous TBAH using vortex mixer and sonication for 10 min. In the above dispersion, MCC was dissolved to obtain a pale-yellow solution with a final concentration of 7 wt%. This solution was degassed and ejected dropwise using 5 ml syringe with 18-gauge (0.838 mm inner diameter) needle placed at a height of 8−10 cm from a 250 ml beaker containing 20 % saline as coagulation bath. As the droplets contacted the anti-solvent coagulation

**Table 1**

Comparison of reports on functionalized cellulose from literature.

| System | Process | Magnetic property | Fluorescence property | Solid-state Quantum Yield (Φ) | Leaching resistance | Ref. |
|---|---|---|---|---|---|---|
| Cellulose nanofibers | Spray drying | No | Yes (water-soluble CdTe QDs) | Not reported | No (physical blends) | [18] |
| Cellulose stearate | Nanoprecipitation | Yes ($Fe_3O_4$) | Yes (Stearoylaminoethyl rhodamine B) | Not reported | No (physical blends) | [24] |
| Surface adsorbed quantum dots ethyl cellulose nanospheres | Spray drying | Yes (oleic acid capped $Fe_3O_4$) | Yes (Cysteamine-capped CdTe QDs) | Not reported | No (physical blends) | [34] |
| Pyrene labelled hydroxypropyl cellulose | Microbeads were not prepared | No | Yes (Covalently linked pyrene butyric acid) | Not reported Methanol: 0.6 $H_2O$: 0.5 | Yes | [41] |
| Allyl cellulose derivative | Microbeads were not prepared | No | Yes | Not reported. DMSO: 0.38 | Yes (Covalently linked) | [42] |
| Microcrystalline cellulose | Precipitation and ball milling | Yes ($Fe_3O_4$ NPs) | Yes (PBA) | Yes. $\Phi_{max}$ 0.57 | Yes | This Work |

**Table 2**
Sample coding with different stoichiometry.

| | FMB011 | FMB411 | FMB811 | FMB1211 | FMB412 | FMB414 |
|---|---|---|---|---|---|---|
| % Iron oxide NPs | 0 | 4 | 8 | 12 | 4 | 4 |
| Molar ratio of glucopyranose units to PBA. | 1:1 | 1:1 | 1:1 | 1:1 | 1:2 | 1:4 |



**Scheme 1.** Reaction of cellulose beads with pyrene butyric acid (PBA).



**Scheme 2.** Scheme of preparation of fluorescent magnetic beads (FMB).

bath, they precipitated into spherical beads. Beads were washed with deionized water three times and were lyophilized using Labconco make Freeze Dryer.

### 2.2. Preparation of fluorescent magnetic cellulose micro-beads (FMB)

The as-prepared MB was reacted with PBA using a previously reported procedure with slight modifications [43]. In brief, in a two-neck round-bottomed flask containing MB (1 g, 6.17 mmol glucopyranose units), 50 ml dry DMF was added under nitrogen atmosphere. In separate two-neck round-bottomed flasks varying equivalents of PBA (1.76 g, 6.17 mmol; 3.55 g, 12.34 mmol; 7.1 g, 24.68 mmol), and DMAP (0.75 g, 6.17 mmol; 1.5 g, 12.34 mmol; 3.0 g, 24.68 mmol) were added to DMF.

Each of this mixture was combined separately with separate flasks containing MB using a glass syringe. The reaction mixture was stirred for another 10 min and cooled to 0 °C. Finally, DCC (1.27 g, 12.34 mmol; 2.54 g, 24.68 mmol; 5.08 g, 49.36 mmol) was added as per the amount of PBA and the mixture stirred for another 30 min at 0 °C. The reaction mixture was stirred for another 24 h at ~25 °C. After 24 h, these fluorescence magnetic cellulose beads (FMB) were recovered by centrifugation, washed with deionized water three times and air dried at ambient conditions. After complete drying, these beads were crushed using a ball mill (Retsch Mixer Mill MM 400) for 45 min at a frequency of $25 \text{ s}^{-1}$ to obtain a free-flowing powder and was further characterized using various techniques. The samples were coded as shown in Table 2. For example, in FMB411 FMB denotes fluorescent magnetic beads, the
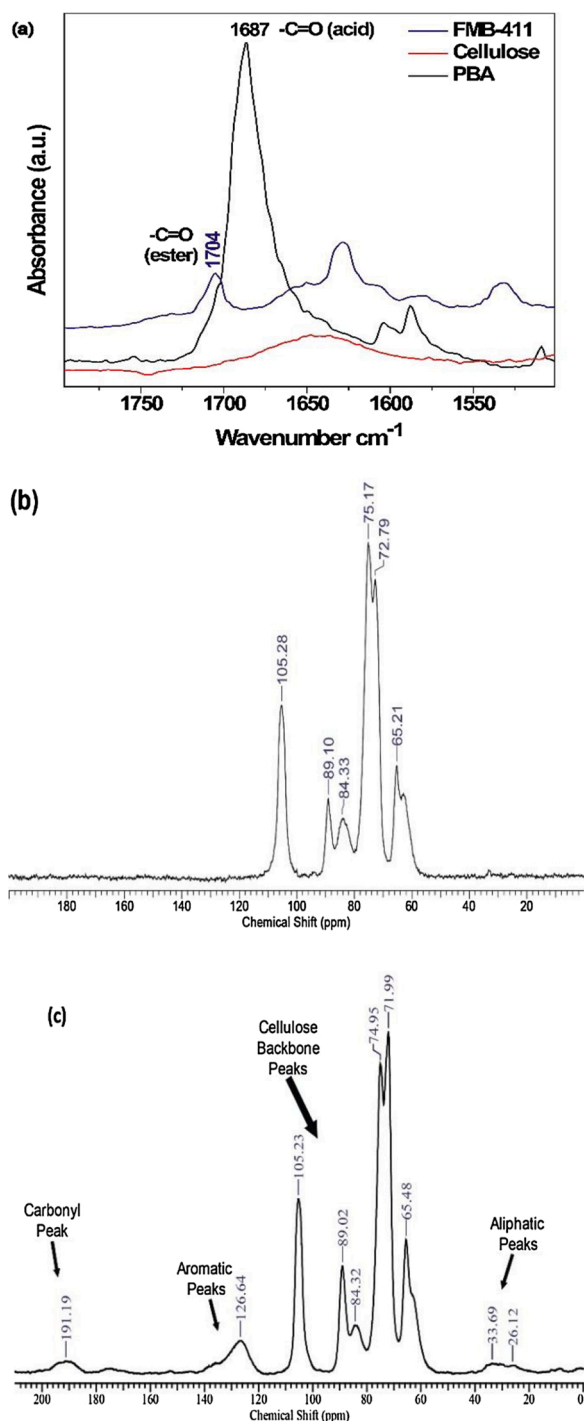
**Fig. 1.** (a) FTIR spectrum of FMB411, $^{13}$C CPMAS solid-state NMR of (b) cellulose and (c) FMB011.

last two digits signifies the ratio of no. of equivalents of glucopyranose units in beads to pyrene butyric acid and preceding number indicates iron oxide NPs content in the beads in wt % w.r.t cellulose, i.e., FMB411 implies 4 wt% iron nanoparticles, and 1:1 ratio of glucopyranose units to pyrene butyric acid.

### 2.3. Characterization

FTIR was used to confirm the reaction between pyrene butyric acid and magnetic cellulose beads. KBr pellets were prepared using the standard procedure, and FTIR spectrum was acquired using Perkin

Elmer Q5000 GX IR instrument with 32 scans and resolution of 4 cm$^{-1}$. The reaction of magnetic beads with pyrenebutyric acid was also confirmed using solid-state $^{13}$C Cross polarization/Magic Angle Spinning (CP/MAS) NMR. For this purpose, beads were prepared without iron oxide NPs, and this powder (FMB011) was analyzed using Bruker Spectrometer (200 MHz) broad band 4 mm CP/MAS probe. Scanning electron microscope (SEM) with tungsten filament as electron source (FEI, QUANTA 200 3D) was used at 15 kV to obtain images of magnetic beads. FMB411 was dispersed in acetone at a concentration of 1 mg/ml and was drop casted on silicon wafers. The solvent was allowed to evaporate at room temperature (~25 °C) in air for 12 h. The samples were sputter-coated with gold to dissipate charge. Energy dispersive X-ray spectroscopy (EDX) was used along with SEM for the elemental mapping. XPS analysis was performed using ThermoScientific K-Alpha (+). FMB411 sample was used for this analysis. The free-flowing powder was compressed to form a pellet of diameter 10 mm and data was recorded using this pellet. Magnetic measurements were made on an EG&G PAR 4500 vibrating sample magnetometer (VSM). Magnetization (M) as a function of magnetic field (H) was measured in the field range ±15 kOe. Thermogravimetric analysis was performed to quantify the amount of Fe$_3$O$_4$ NPs in the cellulose beads using Perkin Elmer thermal analyzer STA 6000 by heating the samples from 40 °C to 800 °C at a heating rate of 10 °C/min under nitrogen. Solid-state UV-VIS spectra were recorded using Agilent Cary 5000 series UV-VIS-NIR spectrophotometer, and the measurements were performed using a solid sample holder. Solid-state quantum yield ($\Phi_{Solid\text{-}state}$) was determined using integrating sphere Quanta Horiba Jobin Yvon Fluorolog 3 spectrophotometer attachment using Tris-(8-hydroxyquinolinato) aluminium as a standard sample. Quantum yield ($\Phi$) is defined by the number of photons emitted divided by the number of photons absorbed. It is the emission efficiency of the fluorophore. The sample was inserted into the chamber and was excited at $\lambda_{max}$ =355 nm, and the emission spectrum was obtained in the range $\lambda_{excitation}$ = 365−700 nm. Steady-state fluorescence studies were performed using Horiba Jobin Yvon Fluorolog 3 having a Xenon lamp of 450 W. The emission and excitation slit was maintained at 1 nm throughout the experiments, and the data was obtained in "S1″ mode and both emission and excitation spectrums were recorded. Fluorescence microscopic images were acquired using Carl Zeiss Fluorescence microscope using filter Alexa Fluor 350. A well-dispersed solution of FMB obtained by sonication was drop casted on a glass slide and then covered with a coverslip. The slide was examined using 10X objective with a 346 nm excitation light and 442 nm emission light under Carl Zeiss Axio Observer Z1 microscope.

## 3. Results and discussion

Fluorescent magnetic beads (FMB) were synthesized as per Scheme 1 by optimizing the process variables. We found that 7 wt% MCC in aqueous TBAH provides the required viscosity to form beads consistently. Above this concentration, higher viscosity leads to the formation of a continuous stream of fluid when ejected through a syringe pump. In the regeneration process, saline disrupts the strong ionic interaction between cellulose and TBAH and allows the formation of stronger intra- and intermolecular hydrogen bonding between the cellulose chains resulting in precipitated beads [44] Scheme 2.

In order to impart dual responsive behavior, the magnetic cellulose beads were reacted with PBA. This esterification reaction was confirmed by FTIR and solid-state NMR. The stretching band appearing at 1687 cm$^{-1}$ [45,46] (Fig. 1a) corresponding to (C=O) stretching is shifted to 1704 cm$^{-1}$ due to esterification of the carboxyl group of PBA with cellulose hydroxyl group. Full FTIR spectra is provided in supporting information (**Figure S1**). The reaction was also confirmed by $^{13}$C CP/MAS solid-state NMR (Fig. 1c) where the peaks appearing at 126.6 ppm and 191.19 ppm correspond to aromatic and carbonyl carbons of PBA respectively. Also, peaks appearing at 105.2, 89.02, 84.3, 75.0, 72.0 and 65.5 ppm corresponds to the cellulose backbone peaks
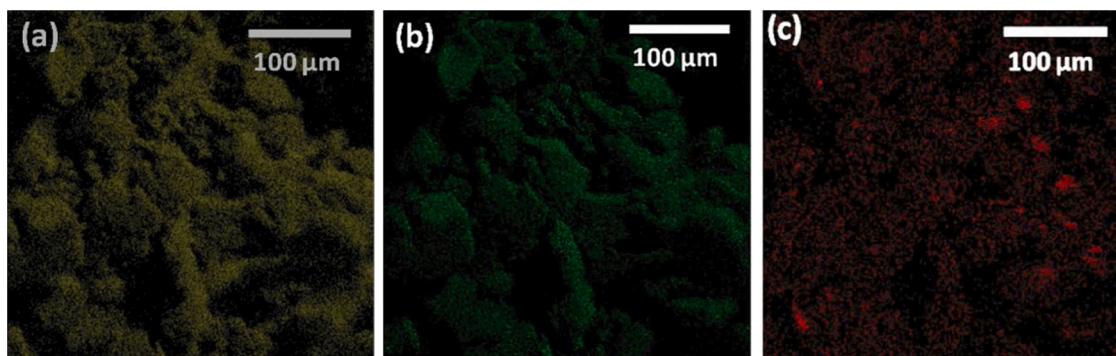
**Fig. 2.** Elemental mapping of FMB 411 (a) for carbon (yellow) (b) for oxygen (green) and (c) $Fe_3O_4$ NPs (Red).
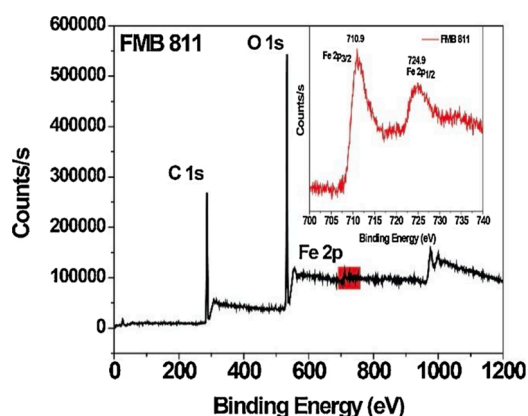


**Fig. 3.** XPS data of FMB 811 and zoomed plot for Fe 2 P (inset red color).
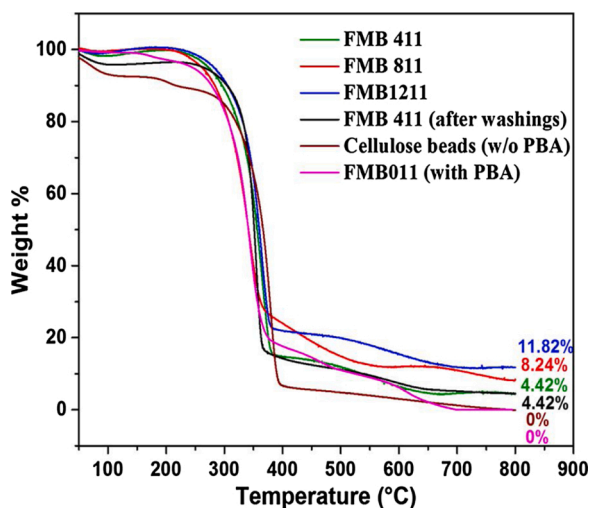


**Fig. 4.** Thermogravimetric analysis data for FMB411, FMB811, FMB1211, FMB 411 (after washing), cellulose beads without PBA and FMB011 (with PBA).

(Fig. 1b) and peaks appearing in Fig. 1**c** at 33.7 ppm and 26.1 ppm corresponds to the methylene groups of pyrenebutyric acid.

Presence of $Fe_3O_4$ NPs in the beads was confirmed by elemental mapping using EDX as shown in Fig. 2, where it is observed that the iron oxide NPs, shown in red color, were homogeneously dispersed throughout the matrix in fluorescent magnetic microspheres. [47]

XPS analysis was used to probe the surface of FMB811. In the spectra (Fig. 3), in addition to C 1s and O 1s signals (located at about 284.8 and 532 eV, respectively) two peaks appearing at binding energies of 710.9

and 724.19 eV (Fig. 3 **(inset)**) could be attributed to Fe 2p3/2 and Fe 2p1/2 respectively [48,49] due to the presence of $Fe_3O_4$ NPs.

Thermogravimetric analysis was performed to quantify the amount of $Fe_3O_4$ NPs in the fluorescent magnetic beads. The inorganic $Fe_3O_4$ NPs remained as a residue after heating the sample to 800 °C, whereas no residue was obtained in case of cellulose beads without $Fe_3O_4$ NPs. Samples FMB011 (contains no $Fe_3O_4$ NPs), FMB411, FMB811 and FMB1211 yielded a residue approximately 0 %, 4.42 %, 8.24 %, and 11.82 % respectively as shown in Fig. 4. This serves to confirm the successful incorporation of $Fe_3O_4$ in the cellulose matrix without much loss during the precipitation. The beads were also subjected to multiple washing cycles with deionized water to check the stability of $Fe_3O_4$ NPs. The amount of $Fe_3O_4$ NPs in the beads remained same even after washing.

Scanning Electron Microscopy (SEM) of FMB (Fig. 5a) revealed beads of spherical shape of around 1000 μm or more in size, which after ball milling yielded irregular shaped particles with size ranging between 1−10 μm (Fig. 5c). The magnetic beads were porous which could be due to the lyophilization process, where the water present in the beads crystallize and sublimate leaving behind pores ranging from 0.5 μm to 2 μm (Fig. 5b).

Magnetization versus field curves of the $Fe_3O_4$ NPs, FMB411, FMB811, and FMB1211 were measured at room temperature, using a VSM, up to a maximum field strength of 15 kOe (Fig. 6). A small magnetic hysteresis loop is observed for $Fe_3O_4$ with a coercivity of ~70 Oe (inset in Fig. 6), suggesting that the $Fe_3O_4$ nanoparticles are not superparamagnetic. The iron oxide nanoparticles show a magnetization of ~71 emu/g at high fields which is less than the saturation magnetization for bulk $Fe_3O_4$ (~80 emu/g). The reduced magnetization is due to the smaller size of the nanoparticles. The magnetizations of FMB411, FMB811, and FMB1211 at 15 kOe are obtained as 1.54 emu/g, 5.37 emu/g, and 6.08 emu/g, respectively. The large reduction in the magnetization of the microspheres with respect to that of the $Fe_3O_4$ NPs is due to the incorporation of the particles in the non-magnetic cellulose matrix. The experimental magnetizations are comparable to the expected values of 2.85, 5.70, and 8.54 emu/g for 4, 8, and 12 wt% of $Fe_3O_4$ in FMB 411, FMB 811, and FMB 1211, respectively. Such lower saturation magnetization of magnetic beads as compared to that of bare magnetic nanoparticles has been reported in the literature, where incorporation of magnetic particles in cellulose or other non-magnetic matrix results in reduced magnetization due to the low concentration of the magnetic nanoparticles such as $MnFe_2O_4$ or $Fe_3O_4$ in the final matrix [50–52]. Although the FMB samples have low magnetization, they exhibit sensitive magnetic responsiveness and therefore, the magnetization is still sufficient enough for security and diagnostic applications as can be compared with the previous report by Xie et al. [34], where the saturation magnetization of fluorescent magnetic nanospheres exhibit 0.025 emu/g of saturation magnetization for the applications in security and anti-counterfeiting. In another report by Wu et al. [53], they have synthesized magnetic cellulose composites for

**Fig. 5.** SEM images of (a) magnetic bead, (b) magnified image of the magnetic bead, (c) FMB411, and (d) histogram plot of the particle size distribution of the ball-milled FMB411.
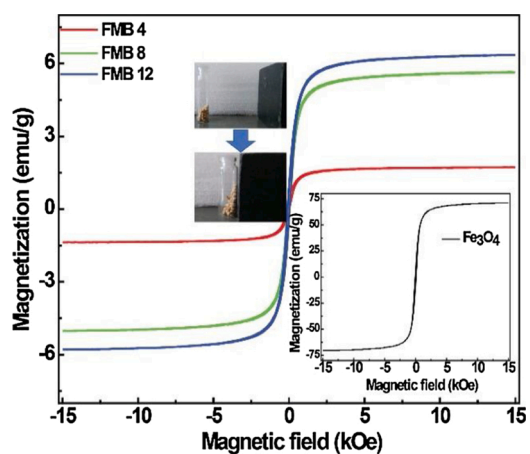


**Fig. 6.** VSM MH Hysteresis of FMB411, FMB811, FMB 1211 and $Fe_3O_4$ NPs (inset) and an image showing magnetic responsiveness of the beads (inset).



**Fig. 7.** Solid-state UV-VIS spectrum of FMB 411 and FMB 011.

applications in packaging, security paper, and information storage by using citric acid modified $Fe_3O_4$ nanoparticles exhibiting 8.00–9.60 emu/g of saturation magnetization where the loading of iron oxide nanoparticles is 7.5 wt% and 13.2 wt%. In another report by Luo et al. (2009) [15], where they have synthesized $Fe_3O_4$/cellulose
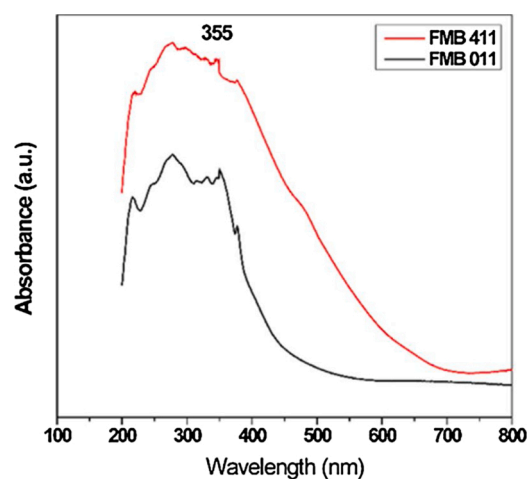
microspheres for magnetic induced protein delivery. These microspheres exhibit 5.16–8.36 emu/g of saturation magnetization upon loading 10.2–19.6 wt% $Fe_3O_4$ nanoparticles.

In Fig. 7, the solid-state UV-VIS absorption spectra of two of the fluorescent magnetic beads – FMB011 (no iron content, only pyrene

**Fig. 8.** Steady-state fluorescent spectrum (a) emission spectrum & (b) excitation spectrum.



**Fig. 9.** Solid-state quantum yield with (a) varying PBA equivalents and (b) varying Iron NPs.

incorporation) and FMB 411 (both pyrene and iron incorporated) is compared. The sharp peak observed for FMB011 at 355 nm wavelength corresponds to the absorbance of PBA covale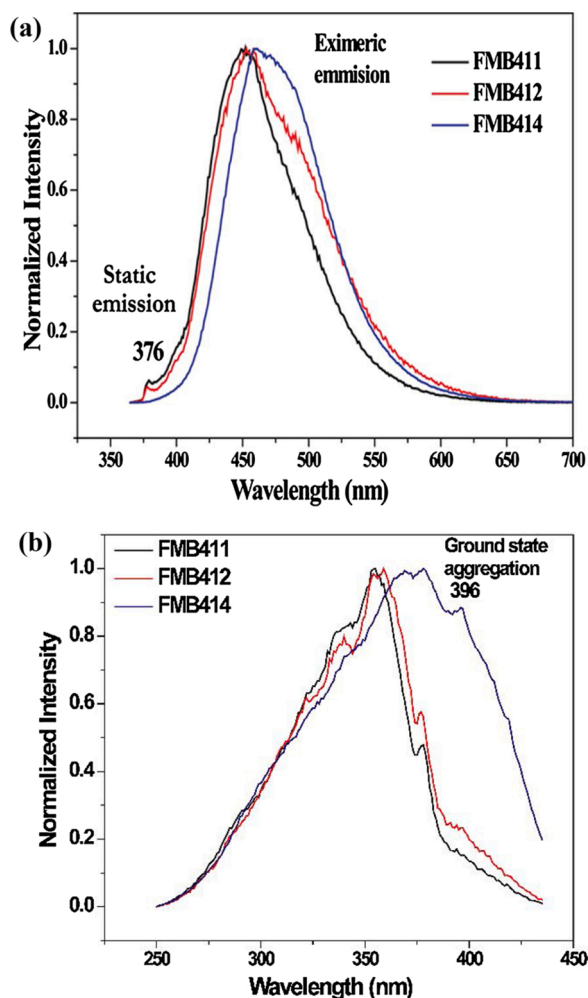ntly linked to cellulose beads. The samples were irradiated at 355 nm, and their emission spectra were recorded between 365–700 nm.

Fluorescence quantum efficiency is not exactly equal to fluorescence intensity but related to the fluorescence intensity; greater the intensity greater is the emission quantum yield. The absolute quantum yield is defined as the ratio of the number of photons absorbed, to the number of photons emitted by a material. The fluorescence intensity F is proportional to the amount of light absorbed and $F = \Phi(I_0 - I)$, where $\Phi$ is the emission quantum yield, $I_0$ and $I$ are intensity of incident and transmitted light respectively. As per Beer-Lambert law, $I/I_0 = 10^{-\varepsilon l c}$ where $\varepsilon$ is molar extinction coefficient, $l$ is the optical path length, and $c$ is the concentration. Combining these two, we get $F = \Phi I_0(1 - 10^{-\varepsilon l c})$. Thus the fluorescent intensity is linear with concentration and quantum yield at low concentration of the fluorophore. The absolute emission quantum yield measurements in the solid-state are carried out by preparing the sample as a fine powder and similar quantities are used as far as possible for every sample and measured under identical experimental conditions. The calculation of the absolute emission quantum yield takes into account the excitation profile of the sample (absorption), which automatically accounts for the actual amount of fluorescent dye present in the sample. [54]

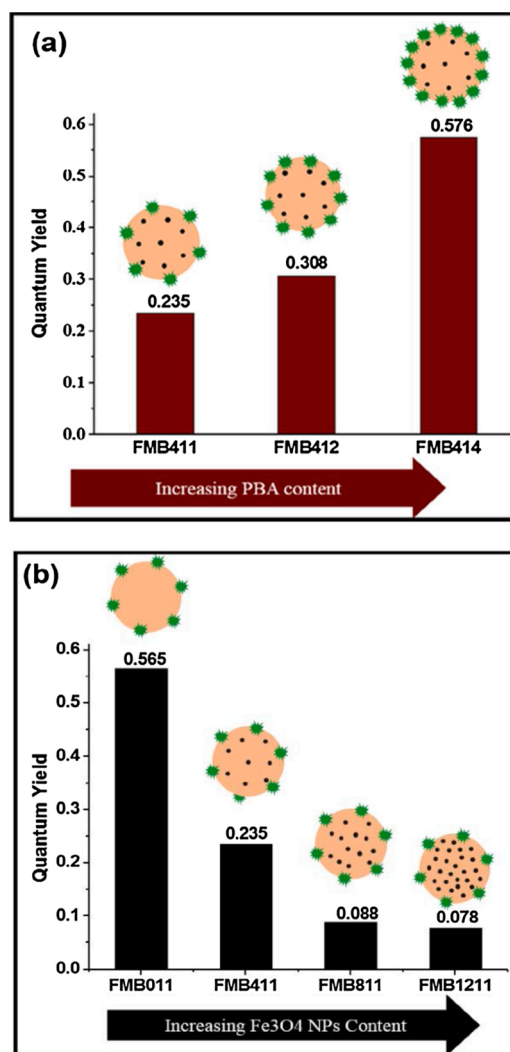Fig. 8(a) shows the normalized emission spectra of fluorescent magnetic microbeads containing both pyrene and iron with the iron content kept constant at 4 % and pyrene incorporation varied from 1 to 4 equivalents. The fluorescent magnetic microbeads exhibited broad emission characteristic of pyrene excimer emission. Generally, pyrene solutions at low concentrations ($< 10^{-5}$ M) are characterized by emission with vibronic fine structures in the 370–390 nm range. As concentration increases above $10^{-5}$ M, the monomeric emission decreases and a broad, featureless emission appears beyond 390 nm, known as the pyrene excimer emission, which is due to the aromatic π-π interaction of the pyrene moieties. In the present work, even at the lowest pyrene incorporation i.e., FMB011 the emission spectra was characterized by noticeable excimeric characteristic. For all samples, the pyrene monomeric emission which is usually observed at 377 nm and 398 nm was almost negligible with only a small shoulder peak observed at 377 nm for FMB411 and FMB412. It could be speculated that the covalent binding of the pyrene on to the cellulose surface enables the π-π interaction among the pyrene units leading to the excimeric emission. It is quite interesting to note that the excimeric emission was observed with peak maxima at 440 nm and not at 480 nm, which usually recognized as the typical pyrene excimeric emission. Pyrene as a fluorophore is greatly influenced by its environment, and the excimeric emission observed around 440 nm is usually associated with the pyrene in a constrained surrounding such as embedded in films, adsorbed on surfaces or in solids where they are not oriented favorably with respect to one another [55]. With increase in pyrene content, we could observe the emergence of the
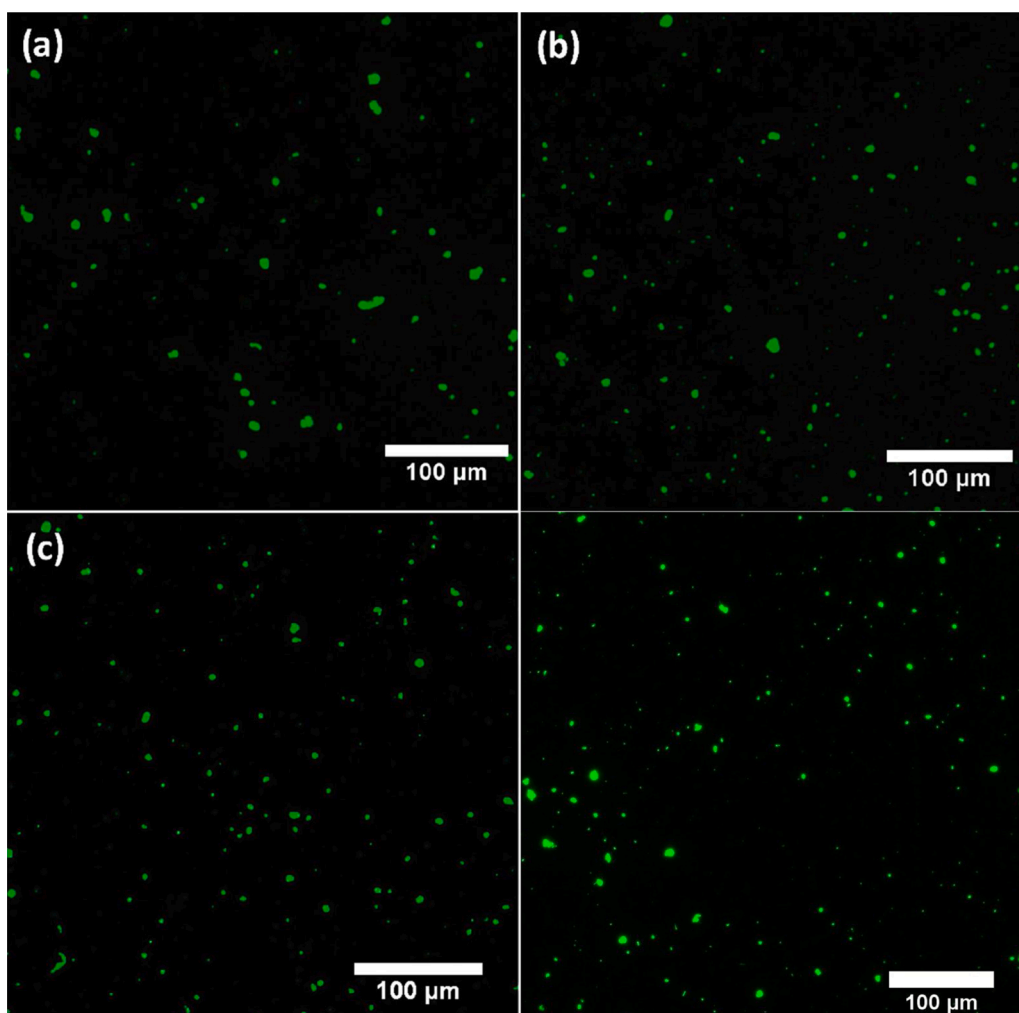
**Fig. 10.** Fluorescent microscope images of (a) FMB011 (b) FMB 411 (c) FMB1211 and (d) FMB414 using a green filter.

characteristic pyrene excimer emission band at 480 nm as a shoulder peak in FMB412 and FMB414. Fig. 8**b** shows the excitation spectra collected at 450 nm for the three samples. The excitation spectra of FMB411 and FMB412 were very similar with vibronic fine structures as well as a prominent $S_1 \longleftarrow S_0$ absorption band at 375 nm. The excitation spectrum of FMB414, on the other hand, was distinct with a prominent shoulder peak at 396 nm, which is usually associated with static excimer [56]. The static excimer has its origin in pre-arranged pyrene moieties in the ground state. FMB414 with the highest pyrene incorporation has pre-arranged pyrene moieties in close proximity in the ground state. The emission quantum yield in the solid-state was also measured using the integrated sphere set up, and the results are shown in Fig. 9a.

As expected, a steady increase in the emission quantum yield was observed with increasing pyrene incorporation in samples FMB411, FMB412, and FMB414 (Fig. 9a). On the other hand, a clear reduction in emission quantum yield was observed in samples FMB411, FMB811 and FMB1211 having similar pyrene incorporation but with increasing iron oxide content (Fig. 9b) as $Fe^{3+}$ is an effective quencher of pyrene emission. [57–59] Highest solid-state fluorescence of 0.57 is achieved with an FMB414 sample containing both pyrene and iron oxide. FMB414 has 4 wt % $Fe_3O_4$ incorporation and has been surface modified by reacting with 4 equivalents of pyrene to the glucopyranose units. It is a known fact that the environment of a dye can affect its optical properties. Unlike in solution, the dyes in a microsphere (whether encapsulated or covalently bound) are screened from oxygen or other impurities that can quench its emission. The covalent incorporation not only prevents

dye leakage but it also restricts the mobility of the dye thereby limiting aggregation induced emission quenching.

This could form the theoretical basis for the high emission quantum yield in the solid-state. The solid-state fluorescence quantum yield that has been reported for polymeric polystyrene beads containing fluorescent active oligo(p-phenylenevinylene)-based cross-linker (OPV) is as high as 0.72 [60]. In another report, pyrene labelled hydroxypropyl cellulose has shown solution state fluorescence quantum yield of 0.6 in water-methanol mixture [41]. The above two reports reveal high quantum yield with mono-functionalization only i.e., it does not contain any other functionality other than fluorescence. In this report, we have shown dual functionality with high quantum yield which is the significant advancement over existing materials.

The microspheres were observed under epifluorescence microscope (Fig. 10). All the compositions exhibited green fluorescence under microscope. One can tune the amount of fluorophore and magnetic particle and the dual responsive microspheres can be used in inks for creating special tags or features in security documents such as passports, degree certificates, currency notes, financial documents etc. according to the desired application. These can be used as overt security feature (detectable with UV light source) for authenticating security documents. Having both magnetic and fluorescent characteristics would enhance counterfeit resistance of these security documents. Therapeutic protein molecules can be adsorbed on the magnetic microbeads, wherein the magnetic property can be used for targeted drug delivery, and the fluorescence property can aid in bioimaging. [61,62]

## 4. Conclusions

This work establishes the preparation of dual responsive cellulose beads containing an optimum loading of magnetic nanoparticles along with covalent incorporation of pyrene with high solid state fluorescence quantum yield. A simple and facile process has been developed to prepare dual responsive cellulose micro-beads. A greener solvent, i.e., 40 % aqueous TBAH, was used to dissolve and process native cellulose into functional microspheres. Microspheres exhibit a saturation magnetization of 2.85–8.54 emu/g, which has sufficient responsiveness. The fluorophore $\gamma$-pyrenebutyric acid has been covalently linked to the cellulose beads to provide durable fluorescence effect even after subjecting to multiple washing cycles. Quenching effect of $Fe_3O_4$ nanoparticles on fluorophore and solid-state quenching due to aggregation of PBA was studied systematically using solid-state quantum yield experiments and quantum yield as high as 0.57 has been achieved. Such a high quantum yield has not been reported in solid state for dual responsive fluorescent microspheres based on cellulose. These materials could have potential applications in security features and medical diagnostics.

## Author contributions

The manuscript was written through contributions of all authors. All authors have given approval to the final version of the manuscript.

## CRediT authorship contribution statement

**Prashant Yadav:** Methodology, Investigation, Formal analysis, Writing - original draft. **K P Prajitha:** Methodology, Investigation. **Vinita Dhaware:** Methodology, Investigation. **Mohan Subramani:** Methodology, Investigation. **Pattayil Joy:** Methodology, Formal analysis, Writing - review & editing. **Asha S K:** Methodology, Formal analysis, Writing - review & editing. **Kadhiravan Shanmuganathan:** Conceptualization, Methodology, Formal analysis, Visualization, Writing - review & editing, Supervision.

## Declaration of Competing Interest

The authors declare that they have no known competing financial interests or personal relationships that could have appeared to influence the work reported in this paper.

## Acknowledgments

## Appendix A. Supplementary data

Supplementary material related to this article can be found, in the online version, at doi:https://doi.org/10.1016/j.colsurfa.2020.124510.

## References

[1] W.D. Oliveira, W.G. Glasser, Hydrogels from polysaccharides. I. Cellulose beads for chromatographic support, J. Appl. Polym. 60 (1996) 63–73.
[2] J. Peška, J. Štamberg, J. Hradil, Chemical transformations of polymers. XIX. Ion exchange derivatives of bead cellulose, Angew. Macromol. Chem. 53 (1976) 73–80.
[3] H. Chen, M. Kaminski, X. Liu, M. Torno, A novel human detoxification system based on nanoscale bioengineering and magnetic separation techniques, Med. Hypotheses 68 (2007) 1071–1079.
[4] R.A. Sheldon, Enzyme immobilization: the quest for optimum performance, Adv. Syn. & Cat. 349 (2007) 1289.
[5] L.D. Luca, G. Giacomelli, A. Porcheddu, M. Salaris, M. Taddei, Cellulose beads: a new versatile solid support for microwave-assisted synthesis. Preparation of pyrazole and isoxazole libraries, J. Comb. Chem. 5 (2003) 465–471.
[6] J. Trygg, E. Yildir, R. Kolalovic, Anionic cellulose beads for drug encapsulation and release, Cellulose 21 (2014) 1945–1955.
[7] T. Iscan, Z. Dokur, T. Olmez, Tumor detection by using Zernike moments on segmented magnetic resonance brain images, Expert Syst. Appl. 37 (3) (2010) 2540–2549.
[8] W. Piotr, R.-C. Jesus, A.K. Dorota, A.G. Assaf, L. Sopo, B. Bradley, Q. Lu, L. Hyam, W.M.B. Jeff, Magnetoelectroporation: improved labeling of neural stem cells and leukocytes for cellular magnetic resonance imaging using a single FDA-approved agent, Nanomed. Nanotechnol. Biol. Med. 2 (2006) 89–94.
[9] M. Cui, Z. Shao, Z. Li, D. Lu, A kind of composite fluorescence biosensor, its preparation method and application, China Patent (2018), 107632002 A.
[10] S.L. Sonawane, S.K. Asha, Fluorescent polystyrene microbeads as invisible security ink and optical vapor sensor for 4-nitrotoluene, ACS Appl. Mater. Interfaces 8 (2016) 10590–10599.
[11] J.W. Kim, H.S. Choi, Surface crosslinking of high-density polyethylene beads in a modified plasma reactor, J. Appl. Polym. Sci. 83 (2002) 2921–2929.
[12] R. Sipheira, A.S. Chawla, T.M.S. Chang, Enhanced albumin binding to polypropylene beads via anhydrous ammonia gaseous plasma, Biomaterials 7 (1986) 471–473.
[13] R.B. Iglesias, R. Coronilla, A. Concheiro, C. Alvarez-Lorenzo, Preparation of chitosan beads by simultaneous cross-linking/insolubilisation in basic pH: rheological optimization and drug loading/release behavior, Eur. J. Pharm. Sci. 24 (2005) 77–84.
[14] A. Kara, L. Uzun, N. Besirli, A. Denizli, Poly(ethylene glycol dimethacrylate-n-vinyl imidazole) beads for heavy metal removal, J. Hazard. Mater. 106 (2004) 93–99.
[15] X. Luo, L. Zhang, High effective adsorption of organic dyes on magnetic cellulose beads entrapping activated carbon, J. Hazard. Mater. 171 (2009) 340–347.
[16] X. Luo, L. Zhang, Immobilization of penicillin g acylase in epoxy-activated magnetic cellulose microspheres for improvement of biocatalytic stability and activities, Biomacromolecules 11 (2010) 2896–2903.
[17] T.R. Sathe, A. Agrawal, S. Nie, Mesoporous silica beads embedded with semiconductor quantum dots and iron oxide nanocrystals: dual-function microcarriers for optical encoding and magnetic separation, Anal. Chem. 78 (2006) 5627–5632.
[18] Q. Guan, R. Song, W. Wu, L. Zhang, Y. Jing, H. Dai, G. Fang, Fluorescent CdTe-QD-encoded nanocellulose microspheres by green spraying method, Cellulose 25 (2018) 7017–7029.
[19] W. Phottraithip, D.-Q. Lin, F. Shi, S.-J. Yao, A novel method for the preparation of spherical cellulose-tungsten carbide composite matrix with NMMO as non-derivatizing solvent, J. Appl. Polym. Sci. 121 (2011) 2985–2992.
[20] H.-F. Xia, D.-Q. Lin, S.-J. Yao, Spherical cellulose–nickel powder composite matrix customized for expanded bed application, J. Appl. Polym. Sci. 104 (2007) 740–747.
[21] Y.-L. Lei, D.-Q. Lin, S.-J. Yao, Z.-Q. Zhu, Preparation and characterization of titanium oxide-densified cellulose beads for expanded bed adsorption, J. Appl. Polym. Sci. 90 (2003) 2848–2854.
[22] M. Gericke, J. Trygg, P. Fardim, Functional cellulose beads: preparation, characterization and applications, Chem. Rev. 113 (2013), 4812-2836.
[23] Y. Takeda, M. Ohba, M. Ueno, A.R. Saniabadi, I. Wakabayashi, Cellulose acetate beads activate the complement system but inactivate the anaphylatoxins generated, Artif. Organs 34 (2010) 1144–1149.
[24] A. Geissler, D. Scheid, W. Li, M. Gallei, K. Zhang, Facile formation of stimuli-responsive, fluorescent and magnetic nanoparticles based on cellulose stearoyl ester via nanoprecipitation, Cellulose 21 (2014) 4181–4194.
[25] T. Heinze, T. Liebert, Unconventional methods in cellulose functionalization, Prog. Polym. Sci. 26 (2001) 1689–1762.
[26] J. Lindh, D.O. Carlsson, M. Stromme, A. Mihranyan, Convenient one-pot formation of 2,3-dialdehyde cellulose beads via periodate oxidation of cellulose in water, Biomacromolecules 15 (2014) 1928–1932.
[27] J.D. Holbrey, J. Chen, M.B. Tumer, R.P. Swatloski, S.K. Spear, R.D. Rogers, Applying ionic liquids for controlled processing of polymer materials, in: C. S. Brazel, R.D. Rogers (Eds.), Ionic Liquids in Polymer Systems: Solvents, Additives, and Novel Applications. ACS Symposium Series 913, American Chemical Society, Washington DC, 2005, pp. 71–87.
[28] A.L. Dupont, Cellulose in lithium chloride/N, N-dimethylacetamide, optimization of a dissolution method using paper substrates and stability of the solutions, Polymer 44 (2003) 4117–4126.
[29] H.-P. Fink, P. Weigel, H.J. Purz, J. Ganster, Structure formation of regenerated cellulose materials from NMMO-solutions, Prog. Polym. Sci. 26 (2001) 1473–1524.
[30] E.J. Courtney, Method of making a cuprammonium cellulose solution, US Patent 2651582 (1952).
[31] J. Cai, L. Zhang, J. Zhou, H. Li, H. Chen, H. Jin, Novel fibers prepared from cellulose in NaOH/urea aqueous solution, Macromol. Rapid Commun. 25 (2004) 1558–1562.
[32] H. Sihtola, B. Nizovsky, Process for manufacturing cellulose xanthate and viscose prepared from said cellulose xanthate, US Patent (1971), 3728330 A.
[33] M. Abe, Y. Fukaya, H. Ohno, Fast and facile dissolution of cellulose with tetrabutylphosphonium hydroxide containing 40 wt% water, Chem. Commun. (Camb.) 48 (2012) 1808–1810.
[34] Y. Xie, Y. Wu, M. Chub, X. Yub, Q. Wu, A highly efficient route for preparing porous magnetic nanospheres with surface-adsorbed quantum dots, J. Exp. Nanosci. 8 (2013) 752–761.
[35] J.B. Birks, Photophysics of Aromatic Molecules, Wiley/ Interscience, New York, 1970.
[36] J.R. Lakowicz, Principles of Fluorescence Spectroscopy, 3rd ed., Kluwer Academics/Plenum, New York, 2006.

[37] I.B. Berlman, Handbook of Fluorescence Spectra of Aromatic Molecules, Academic Press, New York, 1971.

[38] F.M. Winnik, Photophysics of preassociated pyrenes in aqueous polymer solutions and in other organized media, Chem. Rev. 93 (1993) 587–614.

[39] P. Conlon, C.J. Yang, Y. Wu, Y. Chen, K. Martinez, Y. Kim, N. Stevens, A.A. Marti, S. Jockusch, N.J. Turro, W. Tan, Pyrene excimer signaling molecular beacons for probing nucleic acids, J. Am. Chem. Soc. 130 (2008) 336–342.

[40] J.B. Birks, D.J. Dyson, I.H. Munro, The relations between the fluorescence and absorption properties of organic molecules, Proc. R. Soc. London, Ser. A 275 (1963) 135–148.

[41] F.M. Winnick, M.A. Winnick, S. Tazuke, Synthesis and characterization of pyrene-labeled (hydroxypropyl)cellulose and its fluorescence in solution, Macromolecules 20 (1987) 38–44.

[42] H. Hu, F. Wang, L. Yu, K. Sugimura, J. Zhou, Y. Nishio, Synthesis of novel fluorescent cellulose derivatives and their applications in detection of nitroaromatic compounds, ACS Sustainable Chem Eng. 6 (2018) 1436–1445.

[43] B. Neises, W. Steglich, Simple method for the esterification of carboxylic acids, Angew. Chem., Int. Ed. 17 (1978) 522–524.

[44] L. Alves, B. Medronho, F.E. Antunes, M.G. Miguel, B. Lindman, A. Romano, On the role of hydrophobic interactions in cellulose dissolution and regeneration: colloidal and molecular solutions, Colloids Surf. A Physicochem. Eng. Asp. 483 (2015) 257–263.

[45] S. Majeed, V. Filiz, S. Shishatskiy, J. Wind, C. Abetz, V. Abetz, Pyrene-POSS nanohybrid as a dispersant for carbon nanotubes in solvents of various polarities: its synthesis and application in the preparation of a composite membrane, Nanoscale Res. Lett. 7 (2012) 296–306.

[46] S. Yang, X. Wu, X. Wang, L.A. Samuelson, A.L. Cholli, J. Kumar, Synthesis and characterization of fluorescent cellulose, J. Macromol. Sci. A 40 (2003) 1275–1282.

[47] S.T. Shah, W.A. Yehye, O. Saad, K. Simrani, Z.Z. Chowdhury, A.A. Alhadi, L.A. Al-Ani, Surface functionalization of iron oxide nanoparticles with gallic acid as potential antioxidant and antimicrobial agents, Nanomaterials 7 (2017) 306–322.

[48] W. Lu, M. Ling, M. Jia, P. Huang, C. Li, B. Yan, Facile synthesis and characterization of polyethyleneimine-coated Fe3O4 superparamagnetic nanoparticles for cancer cell separation, Mol. Med. Rep. 9 (2014) 1080–1084.

[49] X. Yu, D. Kansg, Y. Hu, S. Tong, M. Ge, C. Cao, W. Song, One-pot synthesis of porous magnetic cellulose beads for the removal of metal ions, RSC Adv. 4 (2014) 31362–31369.

[50] D. Fragouli, L.S. Bayer, R.D. Corato, R. Brescia, G. Bertoni, C. Innocenti, D. Gatteschi, T. Pellegrino, R. Cingolani, A. Athanassiou, Superparamagnetic cellulose fiber networks via nanocomposite Functionalization, J. Mater. Chem. 22 (2012) 1662.

[51] H. Huang, X. Wang, H. Ge, M. Xu, Multifunctional magnetic cellulose surface-imprinted microspheres for highly selective adsorption of artesunate, ACS Sustainable Chem. Eng. 4 (2016) 3334–3343.

[52] N. Sun, R.P. Swatloski, M.L. Maxim, M. Rahman, A.G. Harland, A. Haque, S. K. Spear, D.T. Daly, R.D. Rogers, Magnetite-embedded cellulose fibers prepared from ionic liquid, J. Mater. Chem. 18 (2008) 283–290.

[53] W.-B. Wu, Y. jing, M.-R. Gong, X.-F. Zhou, H.-Q. Dai, Preparation and properties of magnetic cellulose fiber composites, BioResources 6 (2011) 3396–3409.

[54] L.-O. Palsson, A.P. Monkman, Measurements of solid-state photoluminescence quantum yields of films using a fluorimeter, Adv. Mater. 14 (2002) 757–758.

[55] H.-S. Jang, Y. Wang, Y. Lei, M.-P. Nieh, Controllable formation of pyrene (C16H10) excimers in polystyrene/ tetrabutylammonium hexafluorophosphate films through solvent vapor and temperature annealing, J. Phys. Chem. C 117 (2013) 1428–1435.

[56] F.M. Winnik, Photophysics of preassociated pyrenes in aqueous polymer solutions and in other organized media, Chem. Rev. 93 (1993) 587–614.

[57] S.K. Mandal, N. Lequeux, B. Rotenberg, M. Tramier, J. Fattaccioli, J. Bibette, B. Dubertret, Encapsulation of magnetic and fluorescent nanoparticles in emulsion droplets, Langmuir 21 (2005) 4175–4179.

[58] X.-G. Li, Y.-W. Liu, M.-R. Huang, S. Peng, L.-Z. Gong, M.G. Moloney, Simple efficient synthesis of strongly luminescent polypyrene with intrinsic conductivity and high carbon yield by chemical oxidative polymerization of pyrene, Chem. Eur. J. 16 (2010) 4803–4813.

[59] X.-G. Li, Y. Liao, M.-R. Huang, R.B. Kaner, Interfacial chemical oxidative synthesis of multifunctional polyfluoranthene, Chem. Sci. 6 (2015) 2087–2101.

[60] S.L. Sonawane, S.K. Asha, Blue, green, and orange-red emission from polystyrene microbeads for solid-state white-light and multicolor emission, J. Phys. Chem. B 118 (2014) 9467–9475.

[61] X. Luo, S. Liu, J. Zhou, L. Zhang, In situ of Fe3O4/Cellulose microspheres with magnetic-induced protein delivery, J. Mater. Chem. 19 (2009) 3538–3545.

[62] S. Dong, M. Roman, Fluorescently labelled cellulose nanocrystal for bioimaging applications, J. Am. Chem. Soc. 129 (2007) 13810–13811.